UNIVERSITÀ DEGLI STUDI DI MILANO

GRADUATE SCHOOL IN PHARMACOLOGICAL SCIENCES/
SCUOLA DI DOTTORATO IN SCIENZE FARMACOLOGICHE

DIPARTIMENTO DI SCIENZE FARMACOLOGICHE e BIOMOLECOLARI

CORSO DI DOTTORATO IN SCIENZE FARMACOTOSSICOLOGICHE, FARMACOGNOSTICHE E BIOTECNOLOGIE FARMACOLOGICHE
XXV CICLO

TESI DI DOTTORATO DI RICERCA

Evaluation of left ventricular and atrial-appendage function in normal and ischemic mouse models by cardiac imaging techniques: a pharmacological validation

BIO/14

Laura Castiglioni
Matricola: R08633

TUTOR: Chiar.ma Prof.ssa Elena TREMOLI

COORDINATORE: Chiar.mo Prof. Guido FRANCESCHINI

ANNO ACCADEMICO 2011-2012

INTRODUCTION

1 CARDIOVASCULAR DISEASE

Cardiovascular disease (CVD), which defines a heterogeneous class of pathological conditions occurring heart and circulatory system, is among the leading causes death and disability in the world. From 1998 to 2008, the rate of death attributable to CVD declined 30.6% (Kovacic JC et al., 2011). In 2008 about 20% of death due to CVD occurred before 65 years old and 33% before 75 years old, which is well before the average life expectancy of 77.9 years (Roger VL et al., 2012).

The mortality is associated to several non-modifiable risk factors as age, family's history of cardiovascular disease, gender and race.

In particular CVD risk is higher for black than for white people and for males than for females (Roger VL et al., 2012).

The most important modifiable risk factors associated with CVD are tobacco and alcohol use, hypertension, high cholesterol, obesity, physical inactivity and unhealthy diets.

The association of two or more of these factors increase the likelihood of a CV event, so it's very important to modify the exposure to risk factors to prevent them compromising heart health.

Among CVDs, ischemic heart disease (IHD) and cerebrovascular disease (stroke) are the two most common with incidence of 43% and 33% respectively.

Ischemic heart disease is caused by an occlusion of coronary arteries due to atherosclerotic plaque fissuring. A complete blockage of an artery causes myocardial infarction, which is characterized by necrosis and damage to the tissues. IHD is one of the causes of heart failure (HF), a progressive disorder in which damage to the heart causes weakening of the cardiovascular system. It manifests by insufficient cardiac pump function, fluid congestion and inadequate blood flow to tissues.

Stroke is a pathological condition caused by disruption of blood supply to the brain. This may result from either blockage (ischemic stroke) or rupture of a blood vessel (hemorrhagic stroke). As result a rapid loss of brain function occurs which may lead to difficult or inability to move, understand or formulate speech.

The other events are indicated as minor types of CVDs, briefly described below.

Peripheral vascular disease affects the circulation in legs and arms. Patients with this disease typically complain of pain in their calves especially when walking.

Rheumatic heart disease is a major problem in many poor countries. This disease begins with a bacterial infection (commonly streptococcal bacteria) in childhood but the heart problems appear many years later. It affects joints and heart valves, which often have to be replaced by surgery. Other infections can occur attacking pericardium (pericarditis).

Congenital heart disease is a malformation of heart structures existing at birth and may be caused by

genetic factors or adverse exposures during gestation. These anatomical defects can be a small hole in one of the inside walls of the heart, abnormal valves or abnormal heart chambers. Some congenital heart problems result in death unless immediately corrected by surgical intervention.

Aortic aneurysm and Dissection is characterized by dilatation and rupture of the aorta.

Deep venous thrombosis and pulmonary embolism is a pathological condition in which blood clotted in the leg veins, can dislodge and move to the heart and lungs leading tissue infections.

Twenty years ago, a group of experts framed CVDs as a chain of events, caused by a lots of related and unrelated risk factors, and progressing through numerous physiological pathways and processes to the end-stage heart disease (Figure 1) (Dzau V et al., 1991).

Furthermore, although the original concept focused on risk factors for coronary artery disease (CAD), the CVD continuum has expanded to include other areas such as cerebrovascular disease, peripheral vascular disease, and renal disease (Dzau VJ et al., 2006).

The intervention along the chain of events leading to CVD could modify the pathophysiological process and confer cardioprotection (Dzau VJ et al., 2006).

So the development of new technologies for diagnosis, the release of new landmark and the research of novel therapeutic agents is a great goal for clinicians and researcher.

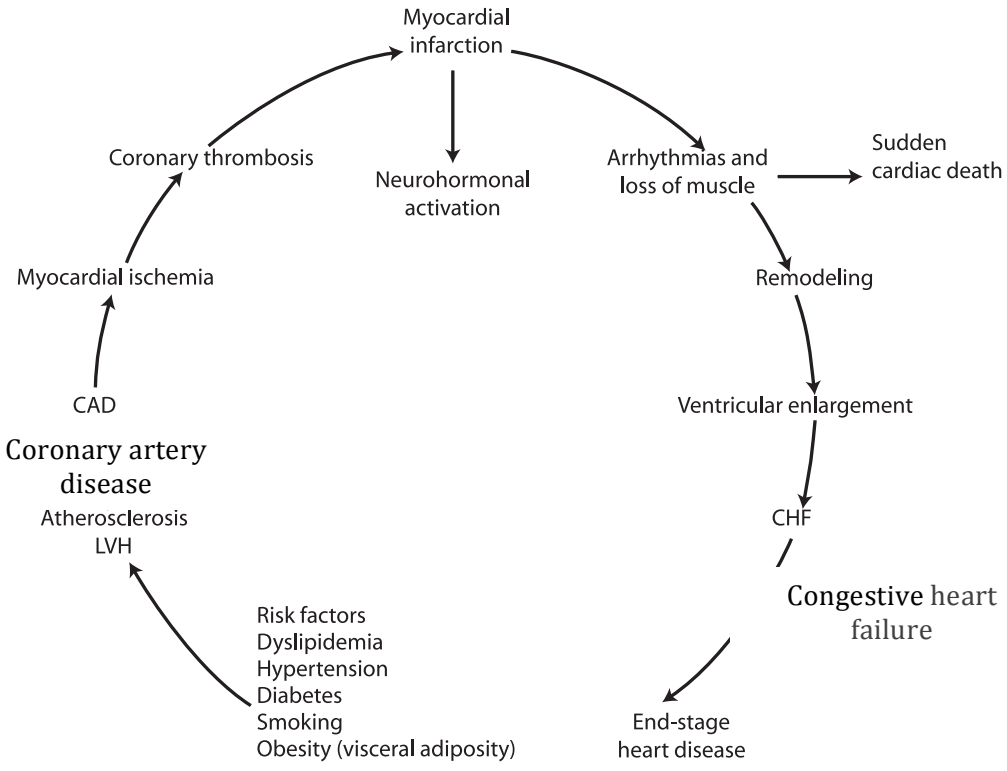

Figure 1. The cardiovascular disease continuum. Adapted from Dzau VJ et al., 2006.

2 HEART ANATOMY AND FUNCTION: IMPORTANCE OF LEFT ATRIUM

2.1 Left Ventricle

2.1.1 Anatomy And Morphology

The heart is divided into four chambers, two ventricles and two atria. Left ventricle is connected to left atrium by mitral valve, while right ventricle and atrium are connected through tricuspid valve.
Left and right ventricles are divided by septum; normally, the left ventricular free wall is thickest at the cardiac base (12-15 mm) and it gradually becomes thinner towards the apex. The endocardial aspect of the ventricle is characterized by a criss-crossing meshwork of thin muscle bundles (trabeculations) at the apical third of the ventricle. Left ventricle wall consists of three 'layers' according to the longitudinal alignment of the myocardial strands: superficial (subepicardial), middle, and deep (subendocardial) (Ho SY et al., 2002).

2.1.2 Function

The ventricles function is to pump blood into the entire body; while right ventricle receives venous blood from the right atrium and pumps it into pulmonary arteries, left ventricle (LV) receives oxygenated blood from left atrium and pumps it into the aorta.
During cardiac cycle we can recognize two phases: diastole during which left ventricle, relaxes and fills rapidly with oxygenated blood flowing from atrium, and systole when left ventricle contracts rapidly and forcibly to pump blood into the aorta, overcoming the much higher aortic pressure.
End-diastolic volume (EDV) and end-systolic volume (ESV) are respectively the volume of blood in left ventricle at the end of diastolic filling phase and at the end of contraction; ejection fraction (EF) represents the fractional volume of blood pumped into aorta for each beat. The stroke volume (SV), amount of blood ejected per each beat, is the difference between EDV and ESV and is an important determinant of cardiac output (CO), which increase or decrease in response to changes in heart rate or SV (CO is the product of SV and heart rate).
SV is ruled Frank-Starling law, which defines the ability of the heart to change its force of contraction, and therefore SV, in response to changes in venous return. Increased venous return increases EDV and, consequently, the stretching of the cardiac myocytes prior to contraction. Myocyte stretching increases the sarcomere length, which causes an increase in force generation. This mechanism enables the heart to eject the additional venous return, thereby increasing stroke volume.

2.1.3 Remodeling

In response to a transmural myocardial infarction (MI), LV undergoes significant remodeling leading to LV volume increases, ejection fraction decrease, anterior wall thinning and a loss of contractility due to fibrosis. It is believed that initially remodeling is required for maintenance of cardiac output but ultimately leads to LV dysfunction.

2.2 Left Atrium

2.2.1 Anatomy And Morphology

The left atrium (LA) receives oxygenate blood from 4 pulmonary veins (PVs) and pumps it into left ventricle through the mitral valve.

The LA presents three different structures: a venous component that receives the PVs, a vestibule and an atrial appendage (LAA). The venous component is LA's largest part, is located posteriorly and has four venous orifices, one at each corner (Ho SY et al., 2002). The vestibule is the tissue surrounding the mitral valve orifice. The LAA is a characteristic tubular small finger-like extension, its junction with the left atrium is narrow and well-defined, it has lobes that are potential sites for deposition of thrombus (Cabrera JA et al., 1999; Veinot JP et al., 1997). Venous component and vestibule are relatively smooth-walled, whereas LAA is rough with pectinate muscles.

During embryo development the primordial pulmonary vein and its branches are incorporated gradually into the LA and extend themself around the dorsal wall as the atrium grows in volume. The four pulmonary veins with separate atrial orifices are formed at about 8 weeks and LAA has formed from the primordial LA (Hara H et al., 2009) (Figure 2).

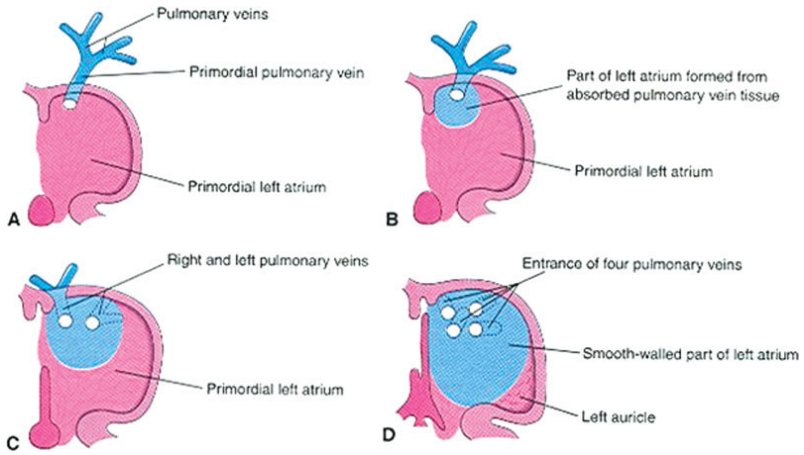

Figure 2. Illustration of absorption of the pulmonary vein into LA. A: common pulmonary vein opening into the primordial LA;B: partial absorption of the common pulmonary vein. C: the openings of two pulmonary veins into LA due to the advanced absorption of the common pulmonary vein at 6 weeks. D: four pulmonary veins with separate atrial orifices enter the LA (Hara H et al., 2009).

The atrial walls are composed of one to three (or more) overlapping layers of differently aligned myocardial fibers. From birth to third decade, there is proliferation of smooth muscle cells, elastic fibers, and collagen; by the eighth decade, there is increased infiltration of fatty tissue, as well as increased collagen and atrial amyloid deposition (Kitzman DW et al., 1990).
The atrial wall presents marked regional thickness differences (Ho SY et al., 2002) and, for example in normal adult, the superior wall is the thickest part of LA (3.5–6.5 mm), whereas the anterior (just behind the aorta) and the posterior (between the superior PVs) walls are usually the thinnest (Ho SY et al., 1999).

2.2.2 Function

Left atrium is both structurally, through mitral valve, and functionally linked to LV function (Khoo CW et al., 2011).
Functionally, the LA has been described by three phases within the cardiac cycle (Pagel PS et al., 2003) The LA area curve shows an increase in during ventricular systole (reservoir phase) followed by three diastolic stages: a rapid decrease (conduit phase), a plateau (diastasis), and a second rapid decrease occurring during atrial contraction (booster pump phase) (Spencer KT et al., 2001).
Phases:

a) reservoir or left atrial filling: during ventricular systole and isovolumic relaxation, the LA acts as a "reservoir" that receives blood from pulmonary veins and stores energy in the form of pressure.
The left atrium reservoir is an important determinant of cardiac output (Suga H, 1974) and is determined by left atrial contraction, relaxation and by the displacement of the mitral annulus during left ventricular contraction (Barbier P et al., 1999).
We can calculate LA reservoir volume as difference between LA maximum volume (just before mitral valve opening) and LA minimum volume (at mitral valve closure) (Abhayaratna WP et al., 2006).

b) conduit and diastasis or left atrial passive emptying: during early ventricular diastolic filling, the LA operates as a "conduit" for transfer (via a pressure gradient) blood from the pulmonary veins into the left ventricle (LV) after mitral valve opening (in doppler flow we observe a early wave E-wave).
Left atrial conduit function is modulate by left ventricular relaxation.
LA (passive) conduit volume is calculated as the difference between LV stroke volume and the total LA emptying volume (Abhayaratna WP et al., 2006).

c) contraction or left atrial active empying: during the "contractile" function LA works as a pump which normally allows to augment the LV stroke volume by approximately 25% (in Doppler flow we observe as active wave, A-wave) (Mitchell JH et al., 1969).

The relative contribution of this “booster pump” function becomes more dominant in the setting of LV dysfunction (Appleton CP et al., 1988; Thomas L et al., 2002).

LA active emptying (contractile) volume is calculated as the difference between pre-atrial contraction LA volume (at the onset of the P-wave on electrocardiography) and minimum LA volume (Abhayaratna WP et al., 2006).

In subjects with normal diastolic function, the relative contribution of the reservoir, conduit, and contractile function of the LA to the filling of the LV is approximately 40%, 35%, and 25%, respectively (Prioli A et al., 1998). With abnormal LV relaxation, the relative contribution of LA reservoir and contractile function increases and conduit function decreases. However, as LV filling pressure progressively increases with advancing diastolic dysfunction, the LA serves predominantly as a conduit (Prioli A et al., 1998).

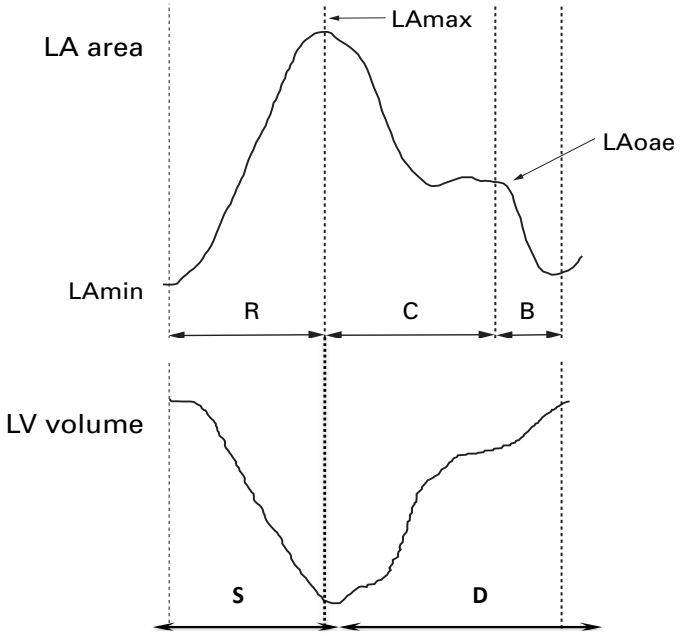

Figure 3. Schematic representation of trend of Left Atrial (LA) area and Left Ventricular (LV) volume during the cardiac cycle. Functional atrial phases are labeled: R, reservoir; C, conduit; B, booster pump; LAmin: LA minimum area; LAmax: LA maximum area; LAoae,: LA onset atrial emptying area. Left Ventricular phases are labeled: S, systole; D, diastole (adaptated from Spencer KT et al., 2003).

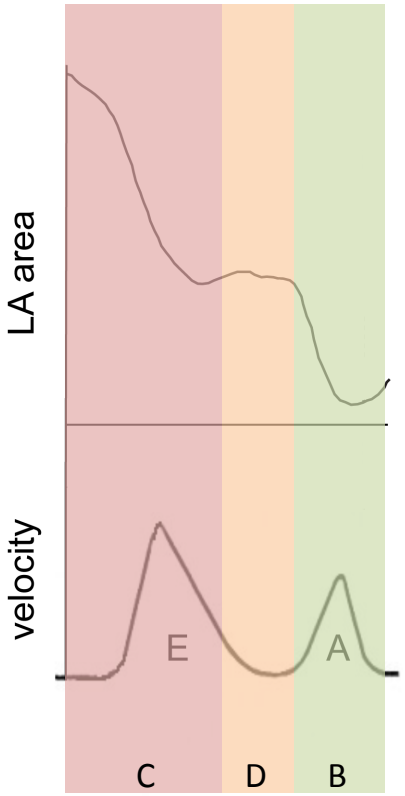

Figure 4 Schematic representation of LA emptying phase and mitral flow velocity. Functional atrial phases are labeled: C: conduit; D: diastases; B: booster pump. Mitral flow wave are labeled: E: early, A: atrial.

2.2.3 Left Atrium Appendage

Because substantial embryologic, anatomic, and functional differences exist between the LAA and the LA itself, the LAA is more than a simple 'appendage' and should be considered a unique cardiac chamber (Hara H et al., 2009). During embryo development the LAA originates from primordial atrial tissue and is formed by confined pectinate muscles without a terminal crest; it's internal surface is trabeculated. It has a narrow base, a hooked tubular apex typically pointing downward. LAA myocardial cells are visually similar to ventricular myocardial cells and resemble skeletal muscle.

Interest on LAA has grown after it has been understood that most intracardiac thrombus originates there during and after atrial fibrillation (AF), causing stroke, infarction, and emboli. Today percutaneous LAA exclusion may eventually replace anticoagulant therapy while simultaneously reducing stroke risk (Sick PB et al., 2007; Al-Saady NM et al., 1999).

The LAA differs in normal sinus rhythm compared with patients in chronic AF (Shirani J et al., 2000), those patients have marked fibrous endocardial thickening and a smoother internal LAA surface. LAA histopathology in hearts exhibiting spontaneous or congenital thrombosis and LAA infarction (Spigel J et al., 1988) showed aneurysmal dilatation with endocardial fibroelastosis (King TD et al., 1973), and

papillary fibroelastoma (Tsukube T et al., 2000), and found changes comparable with other myocytes of the heart in these disorders (Hara H et al., 2009).

2.2.4 Remodeling

In response pressure and/or volume overload caused by to diastolic dysfunction, ischemia, and valvular disease, LA responds with an adaptive (or maladaptive) process named ”LA remodeling” in order to maintain homeostasis against this external stressors.

The type and extent of remodeling depends on the strength and duration of exposure to the stressors (Casaclang-Verzosa G et al., 2008).

LA remodeling includes

- myocyte growth, hypertrophy, necrosis, and apoptosis;
- alterations in the composition of extracellular matrix;
- recalibration of energy production and expenditure;
- changes in the expression of cellular ionic channels and atrial hormones;
- reversal to a fetal gene program (Colucci WS et al., 2005).

This changes promote a cascade of reactions leading to LA remodeling with structural, functional, elettrical, metabolic and neurohormonal conseguences (Casaclang-Verzosa G et al., 2008).

In normal humans, the LA is a highly expandable chamber with relatively low pressures. In the presence of acute or chronic stress or injury, the LA stretches and stiffens (Hoit BD et al., 1998; Khan A et al., 2004).

Ultrastructural changes in heart failure-induced remodeling are marked by extensive interstitial fibrosis and myocyte hypertrophy (Li DS et al., 1999; Khan A et al., 2004; Boixel C et al., 2003).

There is strong evidence that left atrial (LA) enlargement is indicative of significant ventricular (Matsuda Y et al., 1983), atrial (Brodsky MA et al., 1989) or valvular (Vaturi M et al., 2001) disease and it is a robust predictor of cardiovascular outcomes (Abhayaratna WP et al., 2006).

2.2.4.1 effects of myocardial infarction

Myocardial infarction causes abnormal LV dilatation and a reduction in LV compliance as a consequence of altered actin–myosin interactions, increased collagen deposition and changes of cardiac viscoelastic properties (Dent CL et al., 2001).

In this condition LV end-diastolic pressure increases and LA is directly exposed to this increase. To maintain adequate LV filling, LA pressure and wall tension increase consequently (Greenberg BH et al., 1979) resulting in dilatation and stretching of atrial myocardium (Tsang TS et al., 2002).

So LA volume reflects the severity of diastolic dysfunction and the long-term exposure to abnormal LV diastolic function (Tsang TS et al., 2002).

After MI LV remodeling is accompanied by LA function changes and remodeling (Bozkurt E et al., 2007):

- in line with the increase in LV diameters and volumes, an increase in both supero-inferior and medial-lateral diameters and LA volumes (Vmax, Vmin Voae) is observed (Matsuda Y et al., 1983);
- reduced LV compliance causes LA passive emptying fraction (LAPEF) reduction and, in order to maintain almost constant LV SV, despite the dramatic fall in EF%, increase in LA active emptying function (LAAEF) (Triposkiadis F et al., 1995). This condition is evident from the beginning of the acute MI and become more significant from the first month after MI (Bozkurt E et al., 2007);
- on the basis of point 2, in patient with MI the ratio of left atrial volume to LV SV is different than in normal subject, for example the ratio of left atrium active emptying (LAAE) to LV SV is significantly higher in patients with MI than in normal subjects;
- left atrium pressure - volume relation change in MI patient, in fact LA work is significantly higher in MI patient than in normal subjects, and this correlates with the increase of the ratio LAAE to LV SV (Matsuda Y et al., 1983).

2.2.4.2 effects of age

Aging is associated with vascular and myocardial alterations that are related to the pathogenesis of cardiac dysfunction. Vascular alteration results in luminal dilation and vascular stiffening resulting in an increase of vascular load and contributing to the development of cardiac hypertrophy; moreover the deposition and cross-linking of extracellular matrix proteins in the cardiac interstitium play an important role in the pathogenesis of diastolic heart failure (Frangogiannis NG et al., 2002).

Clinical studies have reported conflicting results regarding the relationship between LA size and aging (Kitzman DW et al., 1998).

The development of LV diastolic dysfunction and relaxation impairment cause an increase in LA contractility in order to maintain LV SV (Klein AL et al., 1994).

The anatomical and hemodynamic perturbations in the LV are transmitted to the LA, promoting atrial stretch and dilatation (Redfield MM et al., 2005).

Aging is characterized by atrial morphology and function changes:

- a tendency to increase in left atrial diameters and volumes (Vmax, Vmin and Voae) (Nikitin NP et al., 2003);
- atrial reservoir function doesn't deteriorate and LA maintains its ability to dilatation to maintain cardiac output (Nikitin NP et al., 2003);

- left ventricular relaxation deteriorates with age reducing the left atrial counduit function;
- left atrial passive emptying fraction, highest in young healthy subjects, declines significantly in middle age with a further decline in the oldest subjects, confirming deterioration of left atrial conduit function with age. These changes correspond to the well-described age-related reversion in E/A ratio (Nikitin NP et al., 2003).
- left atrial active emptying volume index increases with age. This, in the presence of left atrial dilatation, is probably a consequence of the effect of the Starling mechanism. An increase in left atrial active contractile performance with age was further confirmed by a progressive increase in left atrial kinetic energy, a recently proposed non-invasive index of left atrial stroke work (Stefanadis C et al., 1998).

Other studies show that atrial size, active emptying volume and ejection force naturally increase with aging (Triposkiadis F et al., 1995), but more recent data demonstrate that with normal aging, maximum volume, minimum volume and total atrial contribution to LV SV are not significantly altered, supporting that left atrial size does not change as a function of chronologic aging alone (Thomas L et al., 2002).

3 ANIMAL MODELS IN CARDIOVASCULAR RESEARCH

Despite progress in the diagnosis and treatment of CHD, appropriate animal models are still crucial for the investigation of the mechanisms involved in the pathogenesis and the advancement of diagnosis and therapies (Gargiulo S et al., 2012).

Anatomic similarity in developmental and postnatal heart (Gargiulo S et al., 2012), structural similarities and evolutionary conservation between genomes (Scherrer-Crosbie M et al., 2008) advocate the genetically modified mouse as a model of choice for studying the human cardiovascular system (Toischer K et al., 2010; Joho S et al., 2007; James JF et al., 1998). Moreover, the recent development in microsurgical instruments and technique, compensating the smaller size, has allowed to shift most of animal surgery in cardiovascular research from the rat to the mouse (Lin MC et al., 1995). Mouse, being smaller, is easy to handle and to house, have a rapid gestation period (21 days), and a relatively low maintenance costs (Tarnavski O et al., 2004). In addition mouse genome has been extensively characterized, and gene-targeted "knockout" and transgenic overexpression experiments are currently performed using mice, rather than rats (Lin MC et al., 1995). Several mouse models of cardiovascular disease are today available: models of atherothrombotic disease, myocardial infarction by coronary ligation, pressure overload by transverse aortic constriction, genetic or pharmacological induced models of dilated cardiomyopathy

Mouse heart, despite very small (its diameter is approximately 5 mm), is deeply studied, and normal reference values have been established for left ventricle anatomy, mass and function (Gardin JM et al., 1995; Collins KA et al., 2003), in normal and also in several phatological animal models. In contrast, probably due to its smaller size, murine left atrium structure and function have never been systematically evaluated. Only a few studies evaluate left atrium anatomy in rat model of myocardial infarction assessing, for example, the enlargement of left atrium (Milliez P et al., 2005) and the effect of a pharmacological treatment on the LA dimension and fibrosis.

Recently, specialized imaging system, such as high frequency echocardiography, have undergone impressive development offering new approaches to murine heart investigation (Gardin JM et al., 1995; Collins KA et al., 2003; Zhou YQ et al., 2003), such as the systematic study of the atrium.

4 MYOCARDIAL INFARCTION

4.1 Patology

Myocardial infarction (MI) is the major cause of death and disability worldwide (Thygesen K et al., 2007). It's a result of rupture of atherosclerotic plaque which causes a coronary artery occlusion leading to a significant reduction of blood flow and oxygen supply to the portion of the myocardium subserved.

MI may be a minor, sometimes undetected, event in a lifelong chronic disease, but it can also lead to sudden death or severe haemodynamic deterioration (Thygesen K et al., 2007).

The severity of MI depends on three factors: the position of the coronary artery occlusion (proximal occlusion is more dangerous), the duration of the occlusion (longer period of vessel occlusion may cause irreversible myocardial damage) and the presence of collateral circulation (Bolooki HM et al., 2010).

From an anatomic or morphologic point we can distinguish two types of MI: transmural and nontransmural.

A transmural MI is characterized by ischemic necrosis of the total wall thickness, extending from the endocardium through the myocardium to the epicardium in contrast with a nontransmural MI. In a nontransmural MI the area of ischemic necrosis is limited to the endocardium and subendocardium because these zones are the least perfused regions of the heart and so the most vulnerable to conditions of ischemia.

Myocardial infarction is also classified by the clinical setting into various subtypes:

- spontaneous and related to ischemia from a primary coronary event (e.g., plaque rupture, thrombotic occlusion);
- secondary to ischemia from a supply-and-demand mismatch;
- resulting in sudden cardiac death;
- associated with percutaneous coronary intervention;
- associated with in-stent thrombosis;
- associated with coronary artery bypass surgery (Thygesen K et al., 2007).

A more common clinical diagnostic classification scheme is based on electrocardiographic findings as a mean of distinguishing between two types of MI, one that is marked by ST elevation (STEMI) and one that is not (NSTEMI).

STEMI is usually the result of complete coronary occlusion after plaque rupture, instead NSTEMI with greater plaque burden without complete occlusion. This difference results with higher early mortality

and morbidity seen in STEMI and the eventual equalization of mortality between STEMI and NSTEMI after 1 year (Andreson J et al., 2007).

4.2 Symptoms And Detection

The ischemic symptoms are diffuse, not localized, not positional, not affected by movement. The discomfort lasts at least 20 mins and occurs at chest, upper extremity, or epigastric at rest or exertion. Often, these principal symptoms may be accompanied by dyspnoea, diaphoresis, nausea, or syncope which are not specific to MI and can be misdiagnosed and thus attributed to gastrointestinal, neurological, pulmonary, or musculoskeletal disorders (Thygesen K et al., 2007).
Sometimes MI can be occur without symptoms and detected only by biomarkers elevations, electrocardiographic changes or cardiac imaging (Thygesen K et al., 2007).

a) biomarker evaluation

Cardiomyocytes damage and death can be recognized by the release in circulatory system of several proteins such as myoglobin, cardiac troponin T and I, Creatin Kinase-MB (CKMB) and lactate dehydrogenase (LDH) (Jaffe AS et al., 2000).
Although elevations in these biomarkers reflect myocardial necrosis, they do not indicate its mechanism and causes (Jaffe AS et al., 2000; Jaffe AS et al., 2006); in fact, in the absence of clinical evidence of ischemia, an elevated value of cardiac troponin, that is index of myocardial necrosis, should indicate other pathologies such as myocarditis, aortic dissection, pulmonary embolism, congestive heart or renal failure.
If troponin assays are not available, the best alternative is CKMB (measured by mass assay). Measurement of total CK is not recommended for the diagnosis of MI because of the large skeletal muscle distribution and the lack of specificity of this enzyme (Thygesen K et al., 2007).

b) electrocardiographic (ECG) detection

In patients with suspected MI, the ECG can be used as diagnostic system even if it's not able alone to identify an ischemic event because of confounding condition (The Joint European Society of Cardiology/American College of Cardiology Committee, 2000; Luepker RV et al., 2003; Antman EM et al., 2004, Braunwald E et al., 2002).
MI may be characterized by ECG abnormalities in PR segment, QRS complex, ST segment or T-waves (Holland RP et al., 1975; Richeson JF et al., 1978).
Increased T-wave amplitude with prominent symmetrical T-waves is an early sign that may precede the elevation of the ST segment, both typical condition of MI manifestation.

Instead, increased R-wave amplitude and width (giant R-wave with S-wave diminution) are often seen in leads exhibiting ST elevation, and tall T-waves reflecting conduction delay in the ischaemic myocardium (Ekmekci A et al., 1961).

Transient Q waves may be observed during an episode of acute ischaemia or rarely during acute MI with successful reperfusion (Matetzky S et al., 1995).

The presence of Q waves or ST segment elevation is associated with higher early mortality and morbidity; however, the absence of these two findings does not confer better long-term mortality and morbidity.

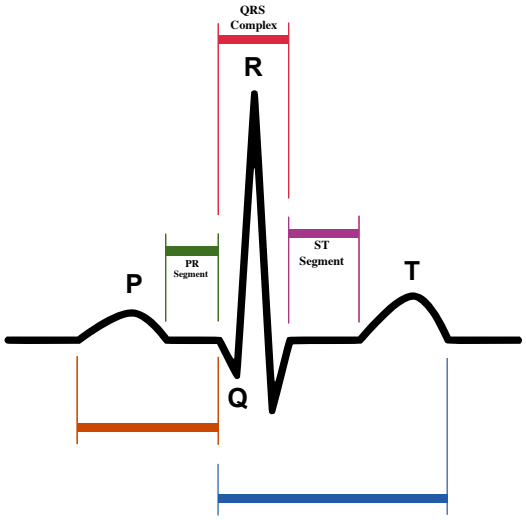

Figure 5. Chematic representation of ECG wave. P wave represents the atria depolarization; complex QRS represent the ventricular depolarization and T wave represents the repolarization of the ventricles.

4.3 Remodeling Process

During the first minutes to hours after infarction, the balance between oxygen supply and demand is a dynamic one, and the final size of the infarct can be influenced by changes in loading conditions and by pharmacologic agents (Maroko PR et al., 1971; Miura T et al., 1987). During this period the heart gradually loses its ability to generate systolic force (Holmes JW et al., 2005) and the ischemic myocardium behaves as a passive elastic material, displaying stretching and thinning during filling and isovolumic contraction, then recoiling passively during ejection and isovolumic relaxation (Tennant R et al., 1935; Tyberg JV et al., 1974; Villarreal FJ et al., 1991). Several hours after ischemic event the infarct region begins to stiffen loosing in compliance and contractility.

After infarction three different phases can be recognized: *necrotic* (myocyte death and inflammatory response), *fibrotic* (fibroblast proliferation and collagen deposition) and *remodeling* (left ventricular enlargement and thinning of infarcted region).

Depending on the species, this entire process is completed within weeks to months (Fishbein MC et al., 1978).

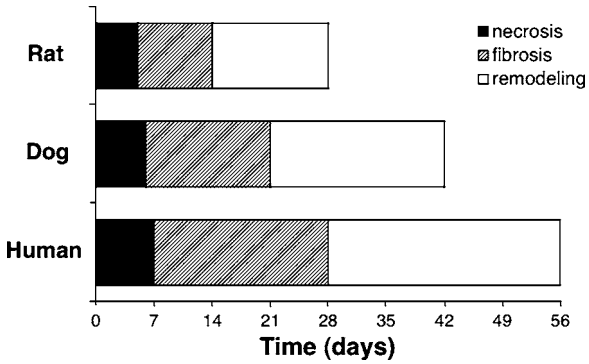

Figure 6. Comparative diagram of the temporal course of the phases of healing defined for various animal models (Holmes J.W. et al., 2005).

Necrotic phase begins within a few hours, when the infarct heart stiffens, and ends when the number of fibroblasts and amount of new collagen begin to increase rapidly in the healing infarct (approximately 7 days after infarction in the human (Fishbein MC et al., 1978) and 5 days after infarction in the rat (Fishbein MC et al., 1978).

This phase involves (Fishbein MC et al., 1978) cardiomyocyte death, degradation of normal ECM, invasion of inflammatory cells at the site of initial injury, and the induction of pro-inflammatory cytokines and chemokines, such as interleukin IL-1, IL-6, IL-8 and tumor necrosis factor α (TNFα) (Frangogiannis NG et al., 2002; Frangogiannis NG et al., 2005). Degradation of the ECM during the acute phase is considered to be an essential event that allows for the ingress of inflammatory cells as well as proliferation and maturation of macrophages and fibroblasts, and provides the necessary substructure for scar formation (Spinale FG, 2007).

Necrosis is then followed by *fibrotic phase,* that begins when the number of fibroblasts, most prevalent resident myocardial cell type (Porter KE et al., 2009; van Nieuwenhoven FA et al., 2012) and directly involved in this process, and amount of new collagen in the healing infarct rapidly increase, and ends when collagen accumulation slows. This response is essential to replace the areas devoid of cardiomyocytes and prevent rupture of the myocardial wall.

Fibrotic process is a long-term phase of proliferation and differentiation of fibroblast in myofibroblast, cells involved in deposition of new ECM components (fibronectin, laminin and collagen type IV (Knowlton AA et al., 1992; Ulrich MM et al., 1997; Morishita N et al., 1996) forming a

scaffold for new type I and III collagen which is the primary determinant of scar formation, structural and mechanical changes establishing after MI.

While historically considered a static structure, it is now becoming recognized that the myocardial ECM is a complex microenvironment containing a large portfolio of matrix proteins, signaling molecules, proteases, and cell types that play a fundamental role in the myocardial remodeling process (Spinale FG, 2007). An adequately balance in ECM degradation and accumulation is fundamental for outcome.

Post infarction remodeling and changes involve globally the left ventricle (MI region, the viable myocardium within the border zone and the remote region) with progressive ventricular architecture alterations in infarcted and non-infarcted regions. Typically, after initial inflammatory responses and scar formation, LV chamber volume increases and a distortion of ventricular shape occurs (it becomes less elliptical and more spherical) to maintain or improve cardiac output (Cohn JN et al., 2000).

In MI region the ventricular remodeling is associated with anterior wall thinning in particular at apex (Bozkurt E et al., 2007) and the slippage of myocyte fascicles (Anversa P et al., 1991; Olivetti G et al., 1990; Weisman HF et al., 1988). The late change in left ventricle dimension is due to lengthening of contractile tissue (remote region) rather than further expansion of the infarcted, non-contractile segment.

With regard to the remote region, the uncompensated mechanical overload prompt increased ECM deposition which occurs between hypertrophied, viable cardiac myocytes and fascicles (Jugdutt BI et al., 1986; McCormick RJ et al., 1994; Peterson DJ et al., 1999; Volders PG et al., 1993; Zimmerman SD et al., 2004) leading to progressive functional deterioration, including myocardial fibrosis and ventricular dilatation, and ultimately to heart failure or death if untreated (Tsuda T et al., 2012).

4.3.1 *Extracellular Matrix*

Deposition of ECM proteins and their increased gene expression after MI play critical role in MI outcome; a rat model of MI was use to describe this modifications (Stanton LW et al., 2000) and technological advances in the production of cDNA microarrays have made it possible to profile gene expression of tens of thousands of genes simultaneously (Duggan DJ et al., 1999; Brown PO et al., 1999). Stanton and colleagues studied the gene pattern expression separately in infarcted and in interventricular septum (IVS) regions showing an enhance expression both in infarcted region and in IVS over normal myocardium for a large number of genes that encode ECM proteins such as fibronectin, laminin, fibrillin, fibulin, and decorin, all proteins conferring stiffness to LV increasing ventricular dysfunction and incidence of cardiac rupture. Moreover, Shuttleworth and colleagues observed an increase expression of collagen VIII, which plays a role in organization of the other

collagens and in tissue remodeling (Shuttleworth CA, 1997). Stability and orientation of the myocardial ECM are finely regulated by balanced control of degradation and deposition of different ECM components by members of the matrix metalloproteinase (MMP) family (Spinale FG, 2007). TIMPs, metalloproteinase inhibitors, are regulators of MMPs in that they inhibit the activated enzyme and prevent proteolytic activity of MMPs and degradation of ECM.

4.4 Pharmacological Treatments

The main goals of pharmacological treatments are the restoration of normal coronary artery flow and the maximum salvage of functional myocardium (Andreson J et al., 2007). than can be reached limiting infarct size and preserving ischemic myocardium to minimize infarct expansion and ventricular dilatation, improving long-term prognosis.

Unfortunately the primary obstacles to achieving these goals are not the low efficacy of drug, but the patient's failure to recognize MI symptoms quickly and the delay in seeking medical attention (Andreson J et al., 2007).

4.4.1 *Fibrinolytics*

Coronary blood flow in MI patients can be restored pharmacologically with the use of fibrinolytic agents. The most critical variable in achieving successful clinically relevant fibrinolysis is time from symptom onset to drug administration. In fact the fibrinolytic therapy is most effective within the first hour, when the door-to-needle time is 30 minutes or less and it is indicated for patients with a STEMI within 12 hours.

In these patients the plasminogen activators have been shown to restore normal coronary blood flow in 50% to 60% of patient (Bolooki HM et al., 2010).

The successful use of fibrinolytic agents provides a definite survival benefit that is maintained for years (Antman E et al., 2008).

Absolute contraindications to fibrinolytic therapy include history of intracranial hemorrhage, ischemic stroke or head injury within the past 3 months, presence of an intracranial malignancy, signs of an aortic dissection, or active bleeding (Bolooki HM et al., 2010).

4.4.2 *Antiplatelet Agents*

The rupture of an atherosclerotic plaque and the persistent thrombotic occlusion may result in acute MI, so antiplatelet agents can play pivotal role as drugs of first choice. Relevantly aspirin alone has been shown to reduce dramatically MI mortality (Andreson et al., 2007; Antman et al., 2008).

Aspirin irreversibly interferes with function of cyclooxygenase and inhibits the formation of

thromboxane A2. Within minutes, aspirin prevents additional platelet activation and interferes with their adhesion and cohesion. Its beneficial effect is observed early in therapy and persists for years with continued use. Accordingly to the ACC/AHA 2007 guidelines, aspirin in a dose of 325 mg should be administered immediately on recognition of MI signs and symptoms and the long-term benefit is sustained, even at doses as low as 75 mg/day (Andreson et al., 2007; Antman et al., 2008).

Clopidogrel, a drug of a different class of oral antiplatelet agents, blocks the P2Y12 component of the adenosine diphosphate receptor, inhibiting platelet activation and aggregation (Quinn MJ et al., 1993). Clopidogrel reduces the risk of death and cardiovascular complications in patients with symptomatic atherosclerotic disease, in the setting of percutaneous coronary intervention (PCI), and in patients with unstable angina or NSTEMI (CAPRIE Steering Committee, 1996; Steinhubl SR et al., 2002; Yusuf S et al., 2001).

The CLARITY-TIMI 28 study (Clopidogrel as Adjunctive Reperfusion Therapy—Thrombolysis in Myocardial Infarction 28) showed a benefit in favor of clopidogrel respect to placebo(in patients receiving fibrinolytics within 12 hours of STEMI). Clopidogrel was most effective in reducing the rate of occluded infarct-related artery and recurrent myocardial infarction, but had no significant effect on all-cause mortality (Sabatine MS, 2006).

Clopidogrel also increased the odds of achieving optimal epicardial flow and optimal myocardial reperfusion and reduced the odds of intracoronary thrombus (Sabatine MS, 2006).

4.4.3 *Nitrates*

Nitrates treatment in patients with myocardial infarction limits infarct size, left ventricular remodeling, infarct expansion, infarct related-complications and reduce mortality for up to 1 year.

Intravenous nitrates should be administered to patients with acute coronary syndromes, congestive heart failure, persistent ischemia, or large anterior wall MI (Andreson et al., 2007; Antman et al., 2008).

Also when administered sublingually, nitroglycerin has a rapid onset of action and some clinical trial data have supported the initial use of nitroglycerin for up to 48 hours in MI.

Nitrates are metabolized in the vascular to nitric oxide, which is active relaxing vascular smooth muscle producing a vasodilatation effect.

As response occurred a dilatation of large coronary arteries and arterioles, which may lead to increased perfusion of ischemic myocardium and a dilatation of the venous and arterial system, reducing respectively cardiac preload and afterload and decreasing the myocardial oxygen requirements needed for circulation at a fixed flow rate. Vasodilatation of the coronary arteries improves blood flow through the partially obstructed vessels as well as through collateral vessels. Nitrates can reverse the vasoconstriction associated with thrombosis and coronary occlusion (Bolooki

HM et al., 2010).

Despite these positive results, the large GISSI-3 trial (Gruppo Italiano per lo Studio della Sopravvivenza nell'infarto Miocardico) and ISIS 4 (Fourth International Study of Infarct Survival) failed to show a significant mortality benefit in patients treated with nitrates after acute myocardial infarction. This may have been due to a null bias related to extensive use of non-study nitrates and also to the limited efficacy of the nitrate regimens used. However, there may be a true lack of additionally efficacy of routine nitrate therapy when used concurrently with thrombolysis, aspirin, ACE inhibitors, and ß-blockers. Although routine intravenous nitroglycerin may be used during the first 24 hours after myocardial infarction, nitrates are not recommended routinely beyond this time except for specific indications, which include persistent ischemia, hypertension, or heart failure.

Low blood pressure, headache, and tachyphylaxis limit the use of nitroglycerin. Nitrate tolerance can be overcome by increasing the dose or by providing a daily nitrate-free interval of 8 to 12 hours. Nitrates must be avoided in patients who have taken a phosphodiesterase inhibitor within the previous 24 hours (Andreson et al., 2007).

4.4.4 *Beta-Blockers*

Beta-blockers are beta-adrenergic antagonist drugs with different actions on heart, slowing the heart rate, reducing myocardial contractility and lowering the systemic blood pressure. In MI conditions these effects may be beneficial reducing myocardial workload, contraction and oxygen demand minimizing myocardial injury and death. Furthermore, beta-blockers may reduce the incidence of ventricular recurrent ischemia, re-infarction, and, if given early enough, infarct size and short-term mortality (Andreson et al., 2007; Antman et al., 2008).

Administration of intravenous beta-blockers within 12 to 24 hours of infarction, followed by oral therapy, has been found to reduce the mortality rate approximately 13 percent within the first week of infarction. Studies indicate that the most marked reduction (25 %) occurs in the first two days after infarction (Yusuf S et al., 1988).

Use of beta-blocker within days to weeks after infarction and continuation of therapy for periods ranging from several months to three years was found in randomized trials to reduce total mortality, nonfatal myocardial infarction and sudden death by approximately 20 to 30 percent (Yusuf S et al., 1985).

The use of a beta -blocker has a number of recognized adverse effects. The most serious are heart failure, bradycardia, and bronchospasm. During the acute phase of an MI, beta-blocker therapy may be initiated intravenously; later, patients can switch to oral therapy for long-term treatment. The COMMIT-CCS 2 trial raised safety concerns about the use of early intravenous beta-blockers in high-risk patients (Second Chinese Cardiac Study Collaborative Group, 2009).

4.4.5 *Renin-Angiotensin-Aldosterone System (RAAS)*

The renin-angiotensin-aldosterone system (RAAS) has a central role in regulating systemic pressure working on vascular resistance and fluid and electrolyte balance.

RAAS is activated in response to a decrease in renal perfusion pressure (hypotension condition) salt depletion, and ß1 adrenergic stimulation, and in particular, renin, a protease produced by the kidney juxtaglomerular cells, is released in the blood. Renin cleaves, in a rate-limited process, angiotensinogen, which is a circulating protein, synthesized by liver, to form angiotensin I (Ang I) which is relatively inactive. Ang I activity is increased 100-fold when it is converted to angiotensin II (Ang II) by the angiotensin-converting enzyme (ACE) (Cheung BM, 2002). Non-ACE pathways also exist and modulate the production of Ang II. Ang II inhibits renin secretion, via a negative feedback loop (Campbell DJ, 1987).

Ang II is a potent stimulant for the contraction of vascular smooth muscle and stimulates the synthesis and release of aldosterone from the adrenal cortex. Aldosterone increases the absorption of sodium and excretion of potassium in the distal tubules and collecting ducts of nephrons in the kidney, increasing volemia, cardiac pre-loading and also systemic pressure (Cheung BM, 2002).

Moreover, increased serum levels of Ang II are seen in patients with cardiovascular diseases associated with myocardial fibrosis, including atherosclerosis, hypertension, cardiac hypertrophy and heart failure (Kim S et al., 2000; Brasier AR et al., 2002; Zhao Q et al., 2004).

The cardiac effects of prolonged Ang II stimulation have been well documented and include marked cardiac hypertrophy and interstitial fibrosis (Iwai N et al., 1995).

Some experimental studies investigated the role of Ang II in cardiac hypertrophy and fibrosis. In particular Ang II given exogenously to rodents has been shown to result in cellular changes within the myocardium, hypertrophy and eventual fibrosis, similar to that seen in humans (Billet S et al., 2008; Harada K et al., 1998; Li HL et al., 2007; Liu J et al., 2003).

Ang II activity is mediate by two major receptor subtypes, AT1 and AT2 G-coupled receptor, both of which are expressed in the heart, kidney, SNCs and brains (Ozono R et al., 2000).

It has been suggested that AT1 receptor signaling mediates vasoconstriction, aldosterone secretion and promotes cardiomyocyte hypertrophy, upregulates TGFb1, which stimulates the expression and deposition of collagen type I and type III, and induces fibrosis through its action on cardiac fibroblasts proliferation and matrix metalloproteinase (Casaclang-Verzosa et al., 2008). All these evidences suggest AT1 receptor as a mediator of the progression of LV remodeling.

Experimental studies showed that AT1 knockout mice have severe cardiac developmental defects and increased mortality (Tsuchida S et al., 1998). Interestingly, isolated AT1A knockout mice have been shown to display less remodelling and increased survival following acute MI (Haranwaki M et

al., 1998). Animals overexpressing AT1-receptors exhibit marked cardiac hypertrophy and fibrosis (Sadoshima J et al., 1993).

Clinical studies have also demonstrated that the AT1-receptor (particularly AT1A) is largely responsible for many of the pathological effects of Ang II (Studer R et al., 1994). These findings exemplify the importance of AT1-receptors in mediating cellular growth and in causing hypertrophy and fibrosis during remodeling.

The AT2-receptor is currently regarded as having opposite effects to the AT1-receptor. Animal studies have revealed that stimulation of the AT2-receptor results in suppression of myocardial hypertrophy (Booz GW et al., 1996), fibroblast proliferation (Tsutsumi Y et al., 1998) and vascular cell hyperplasia (Jin XQ et al., 2002*).*

In addition, genetically engineered mice with selective deletion of the AT2 subtype demonstrated enhanced interstitial fibrosis and left ventricular hypertrophy (LVH); the converse was the case with selective up-regulation of this receptor.

Modulation of RAAS has long been acknowledged as a target of pharmacologic treatment for primary and secondary prevention of cardiovascular outcomes (Unger T, 2002; Brown B et al., 2005; Schmieder R et al., 2007; Chu KY et al., 2009). The two most widely used classes of agents that target the RAAS are angiotensin-converting enzyme inhibitors (ACEIs) and angiotensin receptor blockers (ARBs), which activity improves cardiac remodeling and outcomes (Pfeffer MA et al., 1990; Pfeffer MA et al., 1992; White HD et al., 2004).

4.4.6 Angiotensin-Converting-Enzyme Inhibitor

Angiotensin-converting-enzyme inhibitor (ACE inhibitor) is a class of drug for the treatment of hypertension and congestive heart failure. Clinical studies have demonstrated that ACE-I, when compared with placebo, reduce left ventricular (LV) volumes, retard the progression of LV dilatation and hypertrophy and increase systolic function. This may partially explain their proven clinical efficacy in reducing CV events post-MI and in the management of heart failure (St John Sutton et al., 2003). The gross beneficial effects of these compounds are multifactorial and include transient reductions in Ang II and aldosterone levels (both of which have direct vasoconstrictive and smooth muscle proliferative effects) and reduced degradation of bradykinin (an established vasorelaxant). Despite transient reductions in Ang II formation, chronic ACE inhibition is associated with persistent morbidity and mortality benefits even beginning treatment 1 week after MI.

Contraindications to ACE inhibitor use include the increase of bradikynin levels and hypotension, declining renal function. For patients intolerant of ACE inhibitors, angiotensin receptor blocker (ARB) therapy may be considered (Bolooki HM et al., 2010).

4.4.7 Angiotensin Receptor Blockers

The remarkable success of ACEIs in the treatment of cardiovascular diseases has prompted the search for better alternative drugs to block the RAAS. Hence, Ang II receptor antagonists have been developed (Timmermans PB et al., 1993).

During the past 20 years, experimental and clinic studies have documented that Angiotensin Receptor Blockers (ARBs), either alone or in combination with drugs of other classes, reduce blood pressure (BP), rates of myocardial infarction (MI), stroke, and progression of renal impairment in hypertensive animals and humans. Relevantly ARBs positively impact other markers of cardiovascular (CV) events such as left ventricular hypertrophy (LVH) and urinary protein excretion independent of their effect on BP (Taylor AA et al., 2011).

Sartans are specific blockers of AT1 receptor and their activity results in the elevation of circulating Ang II and thus an overstimulation of AT2 receptor (Spinale FG et al., 1997), suggesting that the effect of ARBs could be partly AT2 receptor mediated.

While it is exciting to speculate about the existence of such actions, it has so far been difficult to design a clinical trial that would unequivocally identify an ARB pharmacologic effect in patients with CV disease that is independent of AT1 receptor blockade and its consequences.

It was demonstrated in mice that deletion of AT2 receptor gene caused deterioration of heart failure and increased mortality during 14 days after MI (Oishi Y et al., 2003), suggesting that AT2 receptor has protective role against the acute phase post-infarction LV remodeling.

The use of sartans, in particularly valsartan, in ischemic mice was effective in inhibition of cardiomyocyte hypertrophy and LV dilatation also improving survival rate (Oishi Y et al., 2006).

Taken together, this evidence strongly supports a role for AngII in the development of myocardial fibrosis.

Commonly, ARBs are used in patients sensitive to ACEi therapy, for treatment of diabetic nephropathy and congestive heart failure. Evidence from controlled clinical trials suggests that the sartans are very well tolerated and generally have a side-effect profile similar to placebo. The most frequently reported side effect is dizziness, not unexpected for a blood pressure–lowering drug and is more likely to occur in patients who are volume-depleted (Cheung BM, 2002).

Moreover, some clinical trials have demonstrated significant benefit in the prevention of cardiovascular events.

VALIANT (Valsartan in Acute Myocardial Infarction) trials, have demonstrated that long-term administration of valsartan plays a critical role in post-infarction LV remodeling and promote greater reduction in LV mass decreasing cardiovascular mortality and morbidity, effectively in patients with heart failure after MI (Dickstein K et al, 2002; Pfeffer MA et al., 2003; Flather MD et al., 2000), and

that valsartan was as effective as ACEi (Captopril) in reducing mortality in post-MI patients, but the combination of valsartan and captopril increased the rate of adverse events without improving survival. From the current information that is available, it would appear that ARBs are able to attenuate ventricular dilatation; however, their effects are modest in comparison to the established anti-remodeling effects of ACE-Is. Combination therapy with an ACE-I and ARB appears to be more beneficial than either agent alone, and supports the concept that more complete RAAS blockade at both the enzyme and receptor level should further attenuate remodeling (Nagesh S and Solomon DS, 2005).

4.5 Surgical Procedure

Percutaneous coronary intervention (PCI) can be performed within 90 minutes of arrival at the hospital in patients with STEMI or MI (Antman EM et al., 2008). PCI is a diagnostic angiography combined with angioplasty and, usually, stenting leading to a restoration of coronary artery blood flow. This procedure is more effective than fibrinolytic therapy, but needs obviously to be performed in by experienced operators in a timely fashion (Grines CL et al., 1993).

However, the short-term mortality advantage is not durable, and PCI and fibrinolysis appear to yield similar survival rates over the long term (Grines CL et al., 1999).

Coronary artery bypass grafting (CABG) is a surgical revascularization indicated in the setting of mechanical complications of MI, such as ventricular septal defect, free wall rupture, or acute mitral regurgitation. Restoration of coronary blood flow with emergency CABG can limit myocardial injury and cell death if performed within 2 or 3 hours of symptom onset. Emergency CABG carries a higher risk of perioperative morbidity (bleeding and MI extension) and mortality than elective CABG. Elective CABG improves survival in post-MI patients who have left main artery disease, three-vessel disease, or two-vessel disease not amenable to PCI.

5 CARDIAC IMAGING

Established imaging modalities for clinical management and research include: echocardiography, cardiovascular magnetic resonance (CMR), cardiac computed tomography (CT), positron emission tomography (PET), single photon emission computed tomography (SPECT) and coronary angiography. They have been used to assess myocardial perfusion left ventricular function, and coronary anatomy. Nuclear cardiology is the a collective term for the modalities requiring the use of radionuclides (Cerqueira MD et al., 2002).

Even if all these techniques produce images of myocardium and ventricle cavity, the orientation of the heart, the angle selection for cardiac planes, the number and nomenclature of segments, the slice display and thickness and the assignment of segments to coronary arterial territories have evolved independently within each imaging field (Cerqueira MD et al., 2002). To optimize and facilitate communication between cardiac imaging modalities a special report from the American Heart Association, American College of Cardiology, and Society of Nuclear Medicine (AHA, ACC, ASNM, 1992) defined standards for plane selection and displayed orientation for serial myocardial slices generated by cardiac 2-dimensional (2D) or tomographic imaging.

In normal human anatomy the heart is positioned in the middle of the thorax with the largest part slightly offset to the left and the apex prominent frontally, so the cardiac planes generated by using the long axis of the body do not cleanly transect the ventricles and atria.

SPECT and 2D echocardiography, the two most widely used cardiac imaging modalities, have defined the long axis of the left ventricle transecting the apex and the center of the mitral valve plane, and short axis are oriented at 90° angles relative to the long axis (ASNC, 1999; Schiller NB et al., 1989; Feigenbaum H, 1994).

Accordingly all cardiac imaging modalities orient, and display the heart sections following this standard convention. Standard names for the orthogonal cardiac planes used in all imaging modalities are short axis, vertical long axis, and horizontal long axis. These correspond to the short axis, apical 2-chamber, and apical 4-chamber planes, traditionally used in 2D echocardiography (Cerqueira MD et al., 2002).

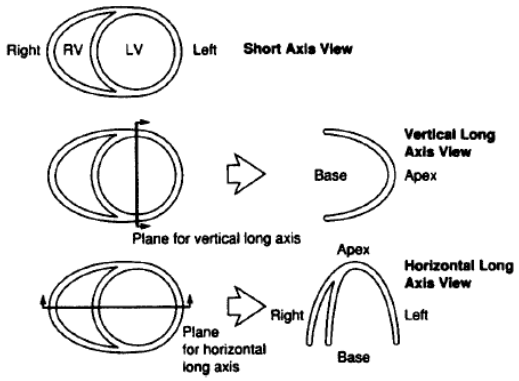

Figure 7. Cardiac planes definition. Short axis view, vertical and horizontal long axis view (Cerqueira D et al., 2002).

Cardiac imaging techniques could be divided into structural: CT, CMR and high-resolution echocardiography providing mainly high-resolution images with anatomical information, and functional SPECT and PET but with coarser resolution. Multimodal imaging fusing different types of images is addressed to deal with the insufficiency of the information provided by a single modality.

5.1 Computed Tomography (CT)

X-ray CT is an imaging procedure that uses X-rays to produce tomographic images of specific part of body. From a series of two-dimensional X-ray images, obtained around a single axis of rotation, with a computer processing, a three-dimensional image of a part of body is generated.

CT offers high contrast between bone and other tissues such as liver, heart, lungs and gut.

Although historically the images generated were in the axial or transverse plane, perpendicular to the long axis of the body, modern scanners allow reformatting the 2D images as volumetric (3D) representations of structures (Ford NL et al., 2003).

Figure 8. Example of computed tomography, short axis (SA) view of heart (RV= right ventricle, LV= left ventricle, PA= pulmonary artery, LA= left atrium, white arrowhead points Aorta).

5.2 Positron Emission Tomography (PET)

PET is a highly specialized imaging technique that allows producing a three-dimensional images of functional processes in the body.

The patient receives a short half-lived radiopharmaceutical (produced by a facility that makes the tracers –cyclotron- that has to be close) such as fluorodeoxyglucose, a glucose analogue which is combined with a radioisotope, to show where glucose is being used, for example in the brain, heart muscle, or a growing tumor.

The system detects pairs of gamma photons emitted indirectly by the tracer and the 3D images of its concentration within the body are then constructed by computer analysis.

Because the radioisotope used in a PET scan is short-lived, the patient receives amount of radiation about twice chest X-rays.

Molecular imaging with PET allows evaluating, in a non-invasive and longitudinal manner, biological processes at a cellular and subcellular level in early steps of heart diseases, to perform quantitative analysis, to study apoptosis, angiogenesis, hypoxia, inflammation, receptor density, and gene expression. In spite of the great specificity and sensitivity of PET, molecular imaging approach can take advantage from simultaneous acquisition of morphological information for localization and quantification. Therefore, hybrid imaging with PET/CT systems is becoming the most used approach in cardiovascular imaging (Gargiulo S et al., 2012).

PET has been used primarily in cardiology, neurology, and oncology.

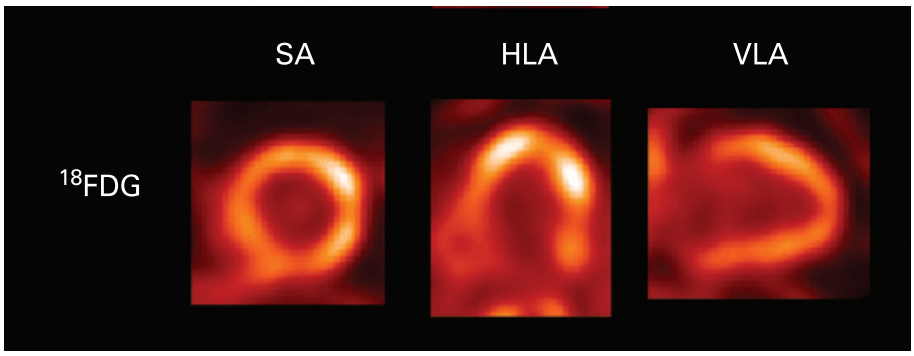

Figure 9. Example of positron emission tomography. Images of [18F] fluorodeoxyglucose (FDG) of short axis (SA), horizontal long axis (HLA) and vertical long axis (VLA). Images regions with normal or even enhanced uptake of FDG as a marker of myocardial viability (Knuuti J et al., 2008).

5.3 Single-Photon Emission Computed Tomography (SPECT)

SPECT is a nuclear medicine tomographic imaging technique using, as PET, gamma rays to obtain 3D information presented as cross-sectional slices of the body.

SPECT is similar to PET in its use of radioactive tracer material and detection of gamma rays. In contrast with PET, that traces simultaneously two gamma photons, the tracer used in SPECT emitted one single photon; this difference is at the basis of a poorer image sensitivity of SPECT and hither potentiality of PET to locate radiopharmaceuticals.

Compared to PET, SPECT is more competitive because radioactive materials used have longer lifetime and don't need to be located near a cyclotron.

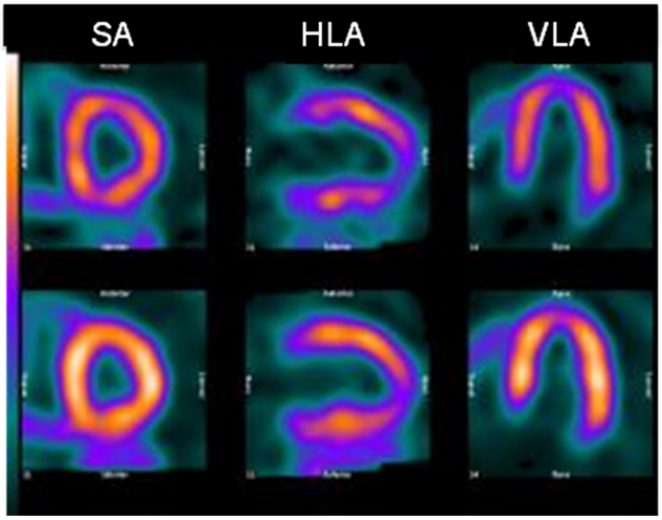

Figure 10. Example of single-photon emission computed tomography. Image shows heart ischemia. Short axis (SA), horizontal long axis (HLA) and vertical long axis (VLA).

5.4 Cardiovascular Magnetic Resonance (CMR)

CMR is a rapidly evolving technology that is increasingly being used for the noninvasive imaging of the expanding heart failure population (Karamitsos TD et al., 2009).

In clinic CMR has been generally performed at a magnetic field strength of 1.5 T (which is around 30000 times stronger than the earth's magnetic field) but recently 3.0 T magnets are becoming more and more widespread. The magnetic field is used to align the nuclear magnetization of hydrogen atoms, which are abundant in the human body. The hydrogen nuclei (proton) are excited by pulses of radiofrequency waves, and the signal emitted from the body in return is detected with receiver coils. Signal from tissues (heart muscle, fat, for example) is determined by proton density, and by 2 distinct MR relaxation parameters, longitudinal relaxation time (T1) and transverse relaxation time (T2). These three parameters can be substantially different for tissues, and these differences are used to generate contrast in MR images by modulating the way the radiofrequency pulses are played out (the MR sequence). For example, in so-called T1-weighted images, myocardial tissue is dark, whereas fat is bright. On the other hand, T2-weighted images highlight unbound water in the myocardium and

are used to show myocardial edema caused by inflammation or acute ischemia (Abdel-Aty H et al., 2007).

CMR sequence consists of a series of radiofrequency pulses, magnetic gradient field switches, and timed data acquisitions, all applied in a precise order to generate the CMR image. Spin echo sequences are mainly used for anatomic imaging and tissue characterization. Gradient echo sequences show fat and blood as white and can be used to acquire cine images. The most recent standard cardiac MR sequences are steady-state free precession, which provide the best contrast between chamber blood (white) and myocardium (dark), and these are now routinely used for imaging of cardiac function (Karamitsos TD et al., 2009).

To prevent artifacts from cardiac motion, most CMR images are generated with fast sequences gated to the R-wave of the electrocardiogram. Respiratory motion, another source of artifacts, is usually eliminated by acquiring CMR images in end-expiratory breath-hold (Karamitsos TD et al., 2009).

Contrast agent, such as gadolinium, can be used to detect infarct and cardiac fibrosis.

The physiological basis of late gadolinium enhancement (LGE) is an increase in its volume of distribution within areas of scarring or fibrosis and an abnormally prolonged washout related to decreased functional capillary density in the irreversibly injured myocardium (Schaefer S et al., 1988; Rehwald WG et al., 2002; Mahrholdt H et al., 2005; Kim RJ et al., 1996). The increase of extracellular gadolinium volume in cardiac damage tissue produces T1 shortening, which manifests as hyper enhancement (high signal) in areas of myocardial injury that appears extremely bright comparing to the black normal myocardium. Recently the use of contrast agent as gadolinium has been linked with acute or chronic severe renal insufficiency or dysfunction and, for this, gadolinium-based contrast agents are not approved by the U.S. Food and Drug Administration for use in cardiac studies in the U.S. (Karamitsos TD et al., 2009).

Compared to other imaging modalities, CMR does not need ionizing radiation or radioactive, and is flexible enough to produce high quality both anatomical and functional images, however for cellular and molecular level still lags behind other modalities (Heijman E, 2008). CMR is also expensive and not compatible with with implanted electronic devices, such as pacemakers or defibrillators (Shellock FG et al., 2004), although this may change in the future with further technical development (MR-compatible pacemakers). Some neurological devices such as cerebrovascular clips are still problematic. Nevertheless, most medical metallic implants are safe in a CMR environment, including nearly all prosthetic cardiac valves, coronary and vascular stents, and orthopedic implants.

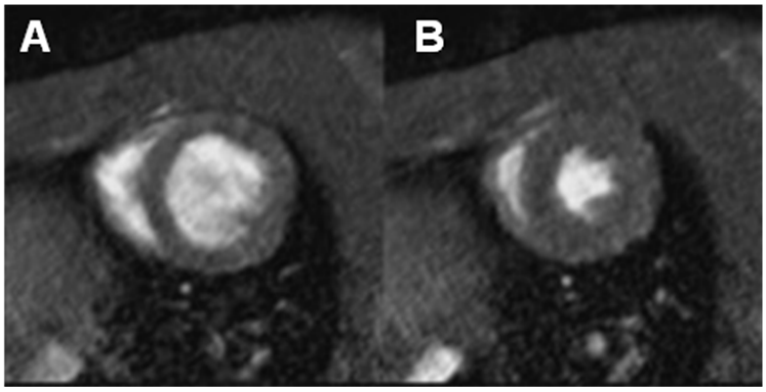

Figure 11. Example of of cardiac magnetic resonance. Short axis (SA): end diastolic frame (A) and end-systolic frame (B).

5.5 Ultrasound Echocardiography

Ultrasound is a mechanical radiation that can be directed in a beam, conforms to the laws of reflection and refraction, and is reflected by small object (Feigenbaum H, 1994). Ultrasound requires a medium for propagation and travels poorly through air and highly dense substances, such as lung and bone, respectively. When ultrasound traveling in one medium reaches a medium with different acoustic impedance (density), a small percent of ultrasound energy is reflected. The intensity of the reflected energy is directly related to the differences in acoustic impedances of the two media and is used by the scan converter on the ultrasonograph to form an image. Reflection is also related to the thickness of the target and the angle of incidence between the target and the ultrasound beam. An important physical characteristic of ultrasound is that it is attenuated as it travels through a medium, and this loss of acoustic energy is directly related to the frequency of ultrasound (Hoit BD, 2006).

For echocardiographic examination the vertical long axis view is usually acquired first because this view allows a general assessment of overall LV size and function (Collins KA et al., 2003).

From this transducer position, a clockwise 90° rotation at the papillary muscle level permit to obtain the short-axis view. From this view, M-mode-derived measures of LV area or dimensions can be obtained.

M-Mode imaging is a 1D projection traced along time allowing to record very high temporal resolution of tissue motion to study the movement of the myocardium, valves or vessel walls and quantify cavity dimensions.

On left ventricle short axis M-mode traces end diastolic and systolic diameter (LVEDd and LVESd), anterior and posterior wall thickness (AWTh and PWTh), were measured.

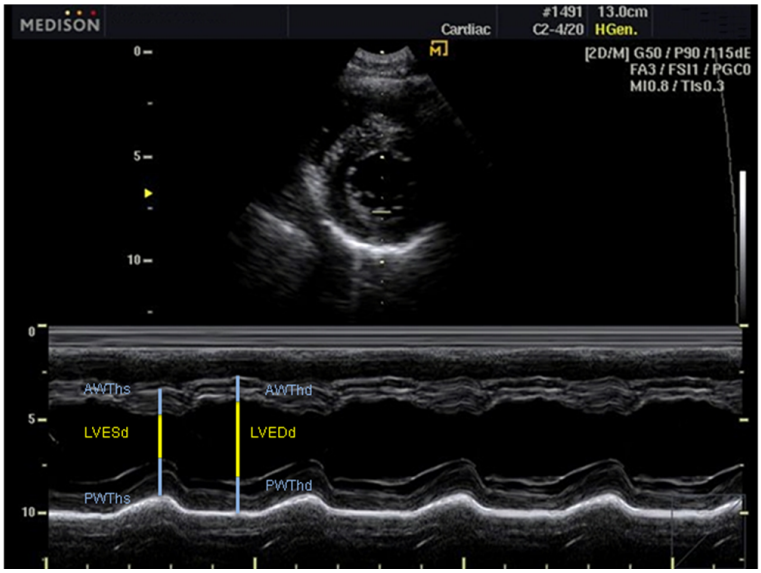

Figure 12. Example of echocardiographic image: a typical M mode image. Standard measures of anterior and posterior wall thickness (AWTh and PWTh), and left ventricle end-diastolic and end-systolic diameter (LVEDd LVESd).

Echography exploits Doppler effect to trace the velocity profile of blood in a sample volume (usually inside a vessel) allowing a very accurate evaluation. Likewise echo color Doppler shows blood velocities encoded as color (red towards the transducer, blue in the opposite direction) and brightness that represents velocity.

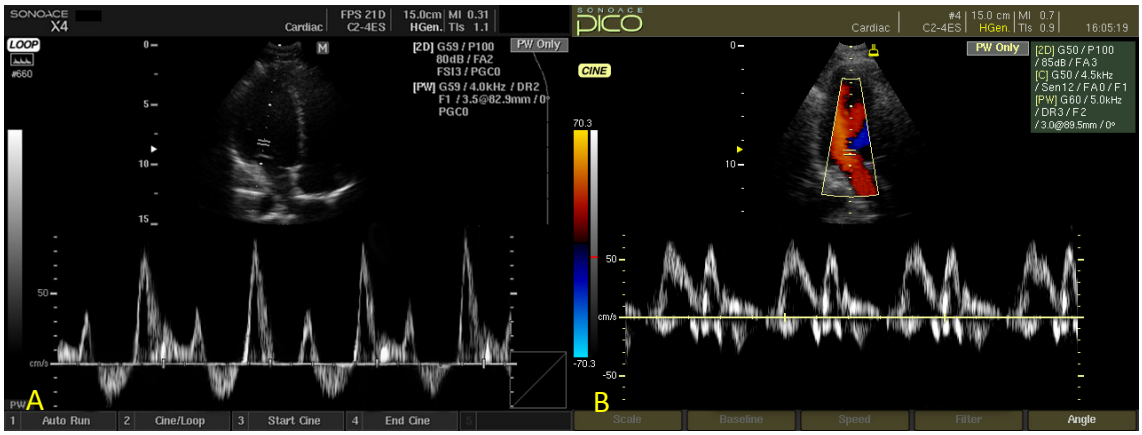

Figure 13. PW Doppler (A) and Color Doppler (B) of mitral valve.

5.6 Regional Analysis

For regional analysis of left ventricular function or myocardial perfusion, the left ventricle is divided into equal thirds perpendicular to the long axis of the heart, and anatomic landmarks are used to select slices: basal (tips of the mitral valve leaflet), mid-cavity (papillary muscles) and apical (beyond papillary muscles but before cavity ends) (Cerqueira MD et al., 2002).

Short axis are divided in segments corresponding to specific areas irrorated by particular coronary arteries, or branch: the basal and mid-cavity slices are divided in 6 segments (anterior, anteroseptal, inferoseptal, inferior, inferolateral, and anterolateral), while apical slice is divided in 4 segments (anterior, septal, inferior and lateral). Segments are in total 16 plus apex that can be considered as a segment itself; their names identify their circumferential location on the ventricular wall (Figure 14). The slice thickness is decided on the basis of specific resolution and clinical relevance (Cerqueira MD et al., 2002).

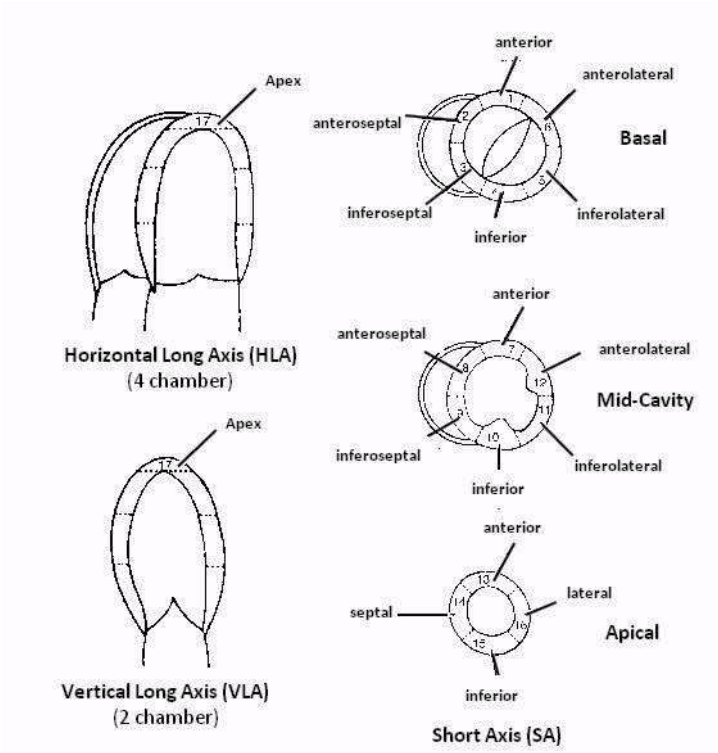

Figure 14. A schematic representation of horizontal long-axis (HLA, approximating the 4-chamber view), vertical long-axis (VLA, approximating the 2-chamber view), and short-axis (SA) planes showing the name, location, and anatomic landmarks for selection of the basal (tips of the mitral valve leaflets), mid-cavity (papillary muscles), and apical (beyond papillary muscles but before cavity ends) short axis slices for the recommended 17-segment system (Cerqueira MD et al., 2002).

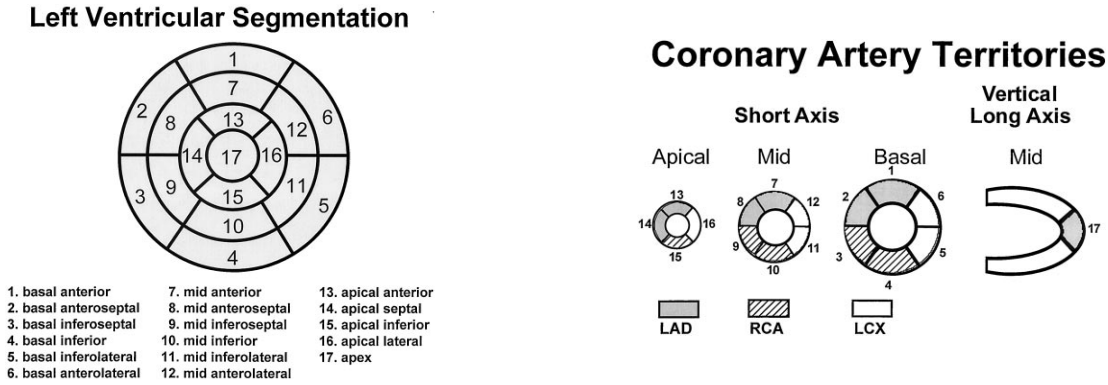

Figure 15. Circumferential polar plot of the 17-myocardial segments, and the recommended nomenclature for tomographic imaging of the heart.
Assignment of the 17-myocardial segments to the territories of the left anterior descending (LAD), right coronary artery (RCA), and the left circumflex coronary artery (LCX) (Cerqueira MD et al., 2002).

During cardiac cycle, left ventricle wall rotates, translates, and deforms in three different directions with two possible orientations:

- radial movement is described as a contraction towards the center of the LV during systole and as an expansion from the center during diastole;
- horizontal rotation which represent the clockwise and counter clockwise movement of the cardiac wall
- vertical rotation which represent the movement towards the base (upwards) during systole and towards the apex during diastole (downwards) (de Sá Rebelo M et al., 2008).

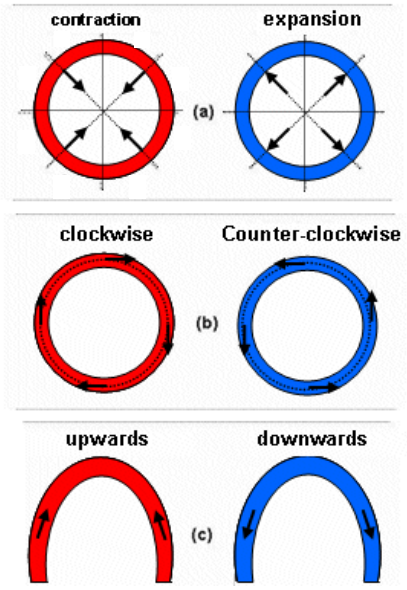

Figure 16. Panel (a) is a representation of radial movement; (b) of horizontal rotation; (c) of vertical rotation. The two orientations for each direction are colored by a defined coding scheme (de Sá Rebelo M et al., 2008).

In normal condition the myocardium moves in the three directions described before, but in pathological conditions there are changes in the expected normal left ventricle wall movements (Remme EW et al., 2004).

Even if global indices as EDV, ESV and EF give us information on ventricular functionality and contractility the analysis of regional cardiac movement can be considered a predictor of cardiovascular events.

Actually, it is demonstrated that subclinical regional myocardial dysfunction (RMD) in asymptomatic adults is independently associated with subsequent development of heart failure and adverse cardiovascular events (Yan RT et al., 2011).

Specifically, the presence of RMD doubles risk for heart failure and increased risk for combined adverse atherosclerotic events over a mean follow-up of 4.6 years among asymptomatic adults of four different ethnic groups, independent of indexes of global LV assessment (Yan RT et al., 2011).

So the evaluation and quantification of LV regional function is a fundamental goal of many cardiac imaging modalities (de Sá Rebelo M et al., 2008).

In the last years echocardiographic and CMR imaging technique were upgraded for myocardial strain analysis (Cottrell C et al., 2010).

Myocardial strain represents the fractional or percentage change from the original dimension, and by definition, negative strain means shortening and positive strain means elongation (Urheim S et al., 2000).

Echocardiographic strain analysis is based on capture of segmental tissue motion on multiple planes and axes (serially over the cardiac cycle) and then track the intramyocardial point ("speckle") displacements integrating detailed information regarding both regional and global LV function, with much greater sensitivity and specificity than conventional measures, including fractional shortening (FS) or ejection fraction (EF) (Cottrell C et al., 2010).

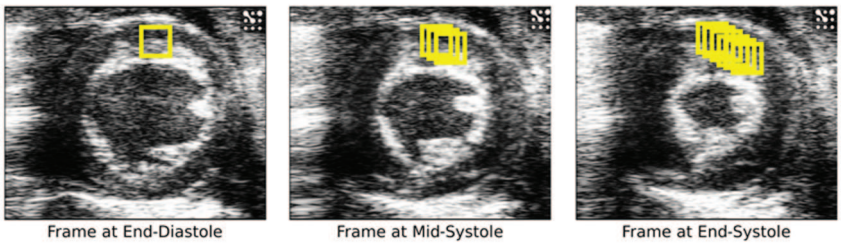

Figure 17. Timed tracking of myocardial deformation allows for the direct measurement of myocardial strain in the longitudinal, circumferential, and radial axes (Bauer M et al., 2011).

Regional ventricular function can be expressed as regional ejection fraction (REF): left ventricular endocardial contours were traced semiautomatically frame-by-frame and manually corrected when

necessary to optimize the boundary position. After segmentation (Hozumi T et al., 1996; Shiota T et al., 1998), regional volumes were calculated throughout the cardiac cycle in order to obtain regional end-diastolic and end-systolic volumes (REDV, RESV). REF was then computed as the difference between REDV and RESV in percentage of REDV (Jaochim Nesser H et al., 2007).

To better visualize regional ventricular function and wall movement, a bull's eye projection is used. It's a 2D map of a 3D left ventricle, whose display is a polar projection with apex in the center, mid-cavity in the middle, and the base in the periphery the ventricular function; in particular the three LV short axis sections were divided into 17 segments according to American Heart Association (AHA) guidelines (Kuhl HP et al., 2004).

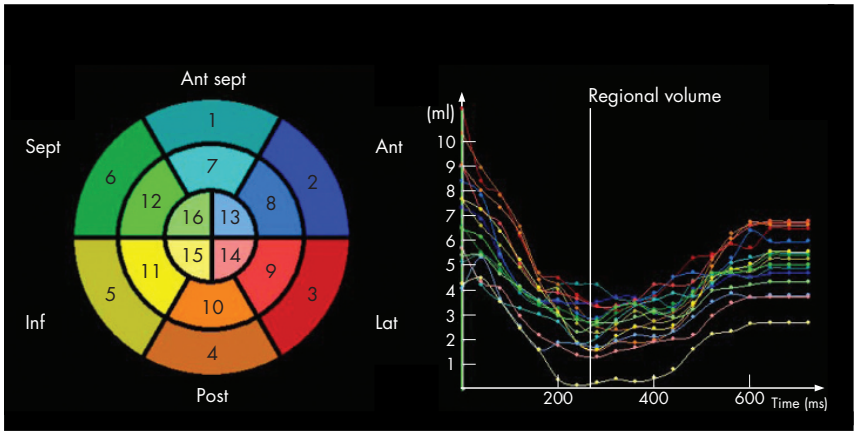

Figure 18. Schematic ''bull's eye'' representation of the three-dimensional segmentation, with the colour notation used for the different segments and the regional left ventricular volume-time curves. Ant: anterior; Ant sept: antero- septal; Inf: inferior; Lat: lateral; Post: posterior; Sept: septal (Jaochim Nesser H et al., 2007).

5.7 Assessments Of Left Atrium Size

The assessment of left atrium (LA) size has important clinical implications and it's necessary a comprehensive view about it (Abhayaratna WP et al., 2006).

As body size is a major determinant of LA size, to allow meaningful comparison the LA size should be indexed to a measure of body size, body surface area is the most commonly used one (Pritchett AM et al., 2003; Vasan RS et al., 1997).

LA size is also gender dependent, and in fact men have been shown to have larger LA size in comparison with women (Pritchett AM et al., 2003). However, these differences are nearly completely accounted for by variation in body size (Spencer KT et al., 2001; Pritchett AM et al., 2003; Knutsen KM et al., 1989).

In table 1 are reported left atrial dimension: range values for adult man.

LEFT ATRIAL DIMENSION	RANGE NORMAL ADULT VALUES
ANTERO-POSTERIOR DIAMETER (mm)	28-40
MEDIAL-LATERAL DIAMETER (mm)	28-43
SUPERO-INFERIOR DIAMETER (mm)	41-61
AREA (cm^2)	‹ 20
VOLUME (ML)	22-58

(Data from Calkins H et al., 2007)

In figure 19 echocardiographic images of parasternal long axis view and apical 4-chamber view.

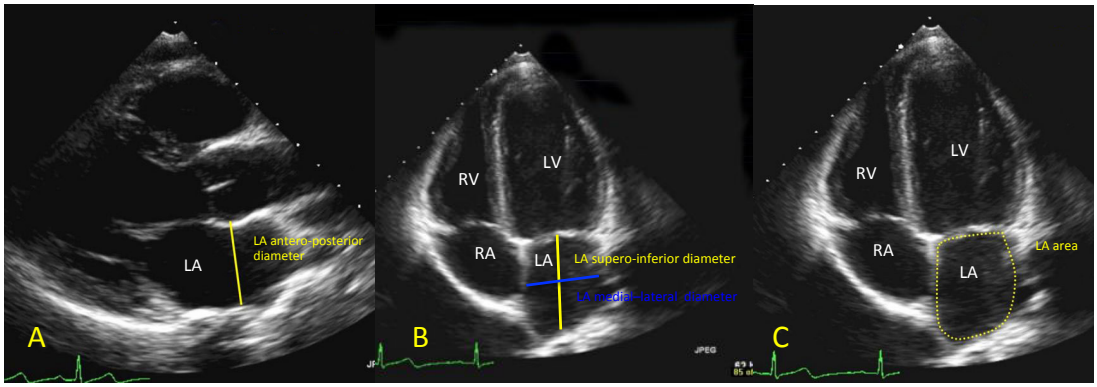

Figure 19. Parasternal long axis view. LA- left atrium and LA antero-posterior diameter (A). Apical four chamber view. Medial–lateral and Supero-inferior diameters (B). Apical four chamber view. LA area (C).

In figure 20, a schematic representation of heart view showing on diameter used to assess LA dimension.

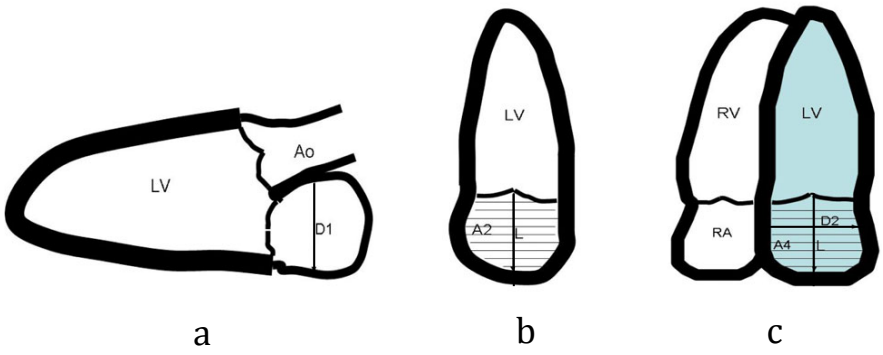

Figure 20. Schematic representation of: parasternal long axis view (a), apical two-chamber view (b) and apical four-chamber view (c).
LV - left ventricle, RV – right ventricle, RA – right atrium, Ao – aortha, D1 – antero-posterior diameter, D2 - medial–lateral diameter, L - supero-inferior diameter, A2 – maximal atrial area in apical 2 chamber view, A4 - maximal atrial area in apical 4 chamber view (Adapted from Khoo CW et al., 2011).

LA size is usually measured by echocardiography at end-systole, when the chamber is at its greatest dimension, different methods of size assessment have been reported:

1) M-Mode antero-posterior diameter is measured from the leading edge of the posterior aortic wall to the leading edge of the posterior LA wall at the parasternal long axis view (D1 in Figure 20a)(Khoo CW et al., 2011).

Although this measurement has been used extensively in clinical and research work, it is now recognized as an inaccurate representation of the true LA size (Lester SJ et al., 1999).

In fact, LA is a ellipsoid structure which presents three different diameters: longitudinal diameter (supero-inferior from the mid point of the mitral annulus to the superior wall), transverse diameter (medial-lateral, from the interatrial septum to the LA lateral wall) and antero-posterior diameter; enlargement of the LA is often asymmetrical and may occur in the medial-lateral as well as in the supero-inferior axes, because enlargement in the antero-posterior direction may be limited by the thoracic cavity.

For this evidence LA antero-posterior dimension is not an accurate reflector of LA volume, moreover the discrepancy between left atrial antero-posterior dimensions and volumes becomes increasingly important as the left atrium dilates (Lester SJ et al., 1999).

It is not surprising that the agreement between LA dimension and LA volume was only fair and that the relationship between LA size and cardiovascular disease burden and outcome is stronger for LA volume than for LA dimension (Pritchett AM et al., 2003; Tsang TS et al., 2006).

2) Ellipsoid method that assumes LA as an ellipse, and LA volume, obtained on the apical four-chamber view can thus be approximated by the equation:

$$\text{Volume} = \pi / 6 * (L * D1 * D2)\,\pi$$

where L is supero-inferior and D2 is the medial–lateral diameter in apical four-chamber view (Figure 20 c); D1 is the antero-posterior diameter in parasternal long-axis view (Figure 20 a).

3) Biplane area-length method that proposed to overcome the limitations of single plane measurements. This biplane area-length method is based on the following equation:

$$\text{Volume} = 8 * (A2) * (A4) / 3\,\pi * (L)$$

where A2 and A4 are the maximal LA area from the apical four-chamber and two-chamber views,

respectively (Figure 20 a and b).
L is measured in both four-chamber and two-chamber views, and the shorter of these is used in the formula.

4) Biplane Simpson's method states that the volume of a geometrical figure can be calculated from the sum of the volumes of the smaller figures of similar shape (Lang RM et al., 2005). This measurement assumes that the LA is oval in shape and the total volume as a series of stacked oval discs can be derived with the formula:

$$\text{Volume} = \pi /4 * (h) * \sum(D1) * (D2)$$

h is height of the discs.

The biplane measurement makes fewer geometric assumptions and therefore is more accurate.
The systematic difference in LA volume between the ellipsoid compared with the area-length and Simpson's method may be related to the dependence on the antero-posterior dimension in the former. Disproportionate increase in the medial–lateral and supero–inferior compared with the constrained antero-posterior dimension will result in greater increase in LA volumes derived by the area-length and Simpson's method, both of which are not dependent on measurement in the antero-posterior dimension. Hence, despite good reproducibility, measurement of LA volume by either area-length or Simpson's method is recommended (Lang RM et al., 2005).
Recently, it has been shown that LA volume by two-dimensional (2D) or 3D echocardiography provides a more accurate and reproducible estimate measure of LA size.

6 IMAGING IN ANIMALS

Noninvasive *in vivo* imaging has acquired a critical role in mouse cardiovascular research; however, the very small size of mouse heart (diameter is approximately 5 mm and left ventricle wall is thinner than 1 mm) and its rapid rate (600 beats/min) pose significant challenges for cardiac imaging, requiring expensive and specific equipment and established expertise.

Imaging systems used clinically have shown unable to provide sufficient spatial resolution to image the equivalent anatomy of a mouse (Ford NL et al., 2003).

In fact some researchers tried to use a human magnetic resonance scanner to study the mouse heart (as Franco and colleagues, who used a 1.5T Philips Gyroscan NT whole body MR scanner, Franco F et al., 1999), but it soon became clear that dedicated hardware was necessary and high spatial and temporal resolution is mandatory (Gargiulo S et al., 2012).

As a result, specialized imaging systems from several modalities are being developed for small animal imaging applications.

In Table 2 (Gargiulo S et al., 2012) are reported the different imaging techniques (and their characteristic) that are currently used for morphological and functional phenotyping of mouse cardiovascular system.

All these techniques are non invasive and allow to study longitudinally the biological, physiological and pathological cardiac processes (Ford NL et al., 2003).

Imaging technique	Physical principle	Spatial resolution	Advantages	Disadvantages
UBM	High frequency sound waves	50 μm	Real-time cardiovascular morphofunctional assessment	Strongly operator dependent, difficult assessing of right ventricle
CT	X-rays	100 μm	Left ventricle morphology	Radiation dose
MRI	High intensity magnetic field	200 μm	High tissue contrast and functional parameters	Most expensive and availability
SPECT	Gamma emitters	Max 0.62 mm FWHM	Molecular imaging, myocardial metabolism and perfusion, 10^{-10}-10^{-11} M sensitivity	Low spatial resolution, radiation dose
PET	Positron emitters	Max 1 mm FWHM	Molecular imaging, myocardial metabolism and perfusion, 10^{-11}-10^{-12} M sensitivity	Low spatial resolution, radiation dose

UBM: ultrasound biomicroscopy; CT: computed tomography; MRI: magnetic resonance imaging; SPECT: single-photon emission computed tomography; PET: positron emission tomography; FWHM: full width at half maximum.

Table 2.

Specialized imaging systems are needed due to the small size and the high heart rates, and both cardiac magnetic resonance imaging (CMR) and echocardiography are currently potential tools. While conventional ultrasound imaging uses probes with centre frequencies up to 15MHz, high-frequency transducers (30–60 MHz) have recently become available, and high-frequency

echocardiography (hf-echo) has been shown to give accurate and reproducible measurements (Bose aK et al., 2007; Okajima K et al., 2007).

Echocardiography has the benefits of being rapid and flexible, and the cost is relatively low. However, image artefacts and or restricted imaging windows are frequent challenges, and the observer dependency is substantial (Amundsen BH et al., 2011). Modern high magnetic field MR with specialized RF coils and gradient systems (Slawson SE et al., 1998; Ruff J et al., 1998; Wiesmann et al., 1998) can, on the other hand, give high-quality images of the beating heart in almost any orientation, but is more time-consuming and has a higher cost. Murine CMR underwent great development since the first results reported in 1997 by Siri and his group (Siri FM et al., 1997). At that time scientists were not very optimistic about using MRI as a tool for imaging the mouse heart. James (James JF et al., 1998) commented that this technique would not be widely used for murine studies in the near future due to the hardware and software requirements. These have been fulfilled in recent MR instruments and the study of mouse heart function is now routinary. Most mouse cardiac studies since 1997 were aimed to measure the global heart functional parameters for two main applications: compare heart function of phenotyping genetically modified mice with wild type controls (Franco F et al., 1999; Brede M et al., 2001; Wilding JR et al., 2005) and haracterize the diseased heart (Yang Z et al., 2004; Zhou R et al., 2003; Ross AJ et al., 2002; Wiesmann F et al., 2002; Hu TC et al., 2004), such as infarcted or hypertrophic heart.

As in human CMR, ECG triggering is necessary to acquire dynamic images, and ECG pads or needles can be used. ECG triggering causes long-time acquisition and so to overcome this problems, a sequence which allows retrospective self-gating for dynamic cine imaging has been designed (Wang Y et al., 1996; Heijman E et al., 2007).

For retrospective self-gating, the gating signals are MR signal themselves (without spatial encoding) and are acquired simultaneously with the image data, and by using time-dependent changes in the gating signal, a trace representative of cardiac motion can be reconstructed; if necessary also respiratory motion can be accounted for in a similar manner (Wang Y et al., 1996; Heijman E et al., 2007).

In recent years, the success of PET-CT imaging in the clinical field has triggered substantial interest in noninvasive molecular and anatomical imaging of small laboratory animals. The low spatial resolution and high specificity of imaging probes allow only acquiring limited morphologic information from micro PET or micro SPECT images, making molecular investigations difficult to interpret (Minino A et al., 2001).

Today, X-ray micro computed tomography (micro-CT) can provide images with high-resolution isotropic voxels (volume elements) and low noise in relatively short acquisition times (Ford NL et al., 2003) and this can be used for small animals.

Then, the introduction of micro-PET/CT hybrid systems for imaging of small animals has greatly enhanced the performance and the accuracy of nuclear imaging, allowing a fine spatial localization of the radiotracer biodistribution and will facilitate the translation of molecular-based imaging to humans (Gargiulo S et al., 2012).

AIM

Cardiovascular disease is a leading cause of mortality, thus the development of new technologies for diagnosis, the release of new landmarks and the research of novel therapeutic agents are fundamental for clinicians and researcher.

The use of animal models, in particular transgenic mice, has contributed to increase our knowledge, providing new approaches focused to improve the diagnostic and the treatments of these pathologies.

In mouse cardiovascular research the use of *in vivo* imaging, for its characteristic on non-invasivity and for the possibility to perform longitudinal analysis in the same animals, has acquired a fundamental role.

However, the very small size of mouse heart (diameter is approximately 5 mm and left ventricle wall is thinner than 1 mm) and its rapid rate (600 beats/min) pose significant challenges for cardiac imaging, requiring expensive and specific equipment and established expertise.

At the light of these remarks the objectives of the experimental activity were:

- set up an animal model of myocardial infarction (MI) induced by permanent coronary artery ligation;
- set up of cardiac imaging of left ventricle, left atrium and appendage in healthy mice;
- evaluation, by imaging techniques, of the anatomical, morphological and functional changes occurring at cardiac level in animals undergoing MI compared to healthy mice.

The second part of the project aimed to validate the effect of pharmacological treatments. In particular we evaluate the effect of valsartan, a drug known to exert a beneficial effect on cardiovascular system, investigating its effects on left ventricular and atrial remodeling after MI.

In particular we aimed to explore the complex interaction between atrium-appendage and ventricular remodeling.

Moreover a relation between the results of imaging techniques and the data obtained with gene expression analysis were investigated.

In order to reach these aims we used two different cardiac imaging techniques: cardiac magnetic resonance (CMR) imaging and high frame rate echocardiography.

CMR imaging is used to investigate global and regional ventricular loss of function and the remodeling occurs after MI. High frame rate echocardiography, because of its higher spatial and temporal resolution, allow to visualize left atrium and its appendage and to assess reference values of anatomy, morphology and function of these structures, and then the remodeling secondary to ventricular dysfunction.

The *in vivo* imaging results were supported by morphological and histological analysis.

MATERIAL and METHODS

1 ANIMAL MODELS

The procedures involving animals and their care respected our institutional guidelines, which comply with national and international law and policies (4D.L. N.116, G.U., supplement 40, 18-2-1992; EEC Council Directive 86/609, OJ L 358,1,12-12-1987; National Institutes of Health's Guide for the Care and Use of Laboratory Animals and US National Research Council 1996), and every effort was made to minimize the number of animals used and their suffering.

For our studies we used male and female C57Bl/6N mice (Charles River Laboratories, Calco, Italy) fed *ad libitum* with standard chow and water.
At the end of experimental protocol the mice were sacrificed under anesthesia (intraperitoneal 75 mg/kg ketamine hydrochloride and 1 mg/kg medetomidine hydrochloride).

1.1 Myocardial Infarction

Myocardial infarction was induced by permanent ligation of the left anterior descending (LAD) coronary artery. Anesthetized mice (intraperitoneal 75 mg/kg ketamine cloridrate and 1 mg/kg medetomidine) were intubated endotracheally in a supine position with a steel tube and ventilated with positive airway pressure (a tidal volume of 140 ml at 150 breaths/min) (Tarnavski O et al., 2004).
Tidal volume and ventilation rate were calculated as:

$Vt = 0.0062 \cdot M^{1.01}$

Ventilation rate (breaths/minutes) $= 53.5 \cdot M^{-0.26}$

Vt is tidal volume and M is animal mass in Kg (Tarnavski O et al., 2004).

The chest cavity was then opened (with dissection at the fourth intercostal space) taking caution not to damage the lung. The heart, partially covered by the lung, was then visible and the pericardium removed so that the antero-lateral heart surface was exposed. The LAD coronary artery should then be visible as a pulsating bright red thin, running in the midst of the heart wall from underneath the left atrium toward the apex. If the LAD artery couldn't be visualized, the left atrial appendage was lifted to locate the origin of the LAD artery from the aorta. The position of the ligation depends on the volume of infarction desired (Tarnavski O et al., 2004). Once the site of ligation had been determined, myocardial infarction was then induced by proximal ligation (1-2 mm below the tip of left auricle) of the LAD coronary artery with a 7.0 silk suture. Occlusion was confirmed by the change of color (becoming pale) of the anterior wall of the left ventricle (LV). The chest cavity was closed by bringing together the 4th and the 5th ribs with one or two 5–0 silk suture (while applying pressure to

the chest wall in order to reduce the volume of free air), then muscles and skin were closed layer by layer with 5–0 silk suture. During surgery, which lasted about 30 min, body temperature was maintained constant at 37.5 °C by means of a heating carpet.

As control of surgery procedure, sham operated mice underwent the same procedure but for tying the suture that was nevertheless passed behind the LAD artery.

After surgery atipamezolo (0.05 mg/kg) was administered to encourage animal awakening, then the animal was extubated and monitored.

2 EXPERIMENTAL PROTOCOLS

2.1 Cardiac Magnetic Resonance Setup And Validation

Thirty C57Bl/6N female mice 8-10 weeks old were divided into two different experimental groups: Myocardial Infarction (MI) n=20 and sham-operated (SHAM) n=10.

Before and nine days after surgery the mice were visualized with cardiac magnetic resonance (CMR). At the end of last CMR examination the animals were sacrificed and the hearts were treated for histological analysis.

2.2 Characterization Of Left Atrium In Normal Mice

Thirty 10-weeks-old C57BL/6N mice (15/15 Male/Female) underwent echocardiography.

To estimate measurement reproducibility, echocardiography was repeated, by the same operator, after one week in 10 mice.

Then mice were sacrificed and heart treated for macroscopic inspection and histological analysis.

2.3 Echocardiographic Study Of Left Atrium In Infracted Mice

Thirty 8-10 weeks-old C57BL/6N female mice were divided in two experimental groups: Myocardial Infarction (MI) n=20 and sham operated (SHAM) n=10.

Mice underwent echocardiography and CMR at different time point: before and 48 hours, 1, 4, 8 and 12 weeks after surgery.

2.4 Effects Of Pharmacological Treatment

Seventy C57Bl/6N female mice were divided into two different experimental groups: Myocardial Infarction (MI, n=55) and sham-operated (SHAM, n=15) mice.

Twenty-four hours after surgery mice were subjected to CMR and echocardiography and the EF% calculated. On the basis of previous analysis, we included into the study MI mice with CMR EF% in range 35%-45%.

The MI mice survived and included were divided into two experimental groups: MI-Vehicle (n=15) and MI-Valsartan (n=15), treated daily with Valsartan 1 mg/Kg/die in drinking water.

All the animals underwent CMR at different time point 1, and 4 weeks after surgery; echocardiographic examination was performed the day after CMR acquisition

After the last echocardiographic examination mice were sacrificed and the hearts treated for histological and genomic analysis.

3 CARDIAC IMAGING

3.1 Cardiac Magnetic Resonance (CMR) Imaging

The Department of Pharmacological and Biomolecular Sciences of University of Milan is equipped with a 4.7 T vertical-bore MR magnet (Bruker Avance II 200) for small animals, a system of anesthesia, two different birdcage coil (3.8 cm diameter for mice and 6.4 cm diameter for rats) and a software (Intragate) for retrospective self-gating dynamic cine imaging.

3.1.1 CMR Imaging Acquisition

For cardiac magnetic resonance (CMR) imaging acquisition, mice were anesthetized with inhaled isofluorane (1.5–2 vol% in oxygen), fixed on a holder and placed into the 3.8 cm coil. During image acquisition isofluorane administration was maintained and the mice temperature was monitored rectally (Franzosi M et al., 2011).

The cine images were recorded using a gradient echo sequence with: TE=1.9 ms, TR=10 ms, FoV=4x4 cm with a slice thickness of 1mm and an in-plane resolution of 312 mm^2.

A series of scout images were first acquired to define landmark points for the acquisition of the long-axis 4 chamber view and then, orthogonally to it, the short-axis sections.

Magnetic resonance volume data (to evaluate left ventricular function) was acquired in multiple contiguous short-axis slices (from apex to base, every 1 mm covering all the left ventricle) using 12 frames for each cardiac cycle. Long and short axis cine acquisition was based on a gradient echo sequence (Intragate, Bruker) with a non-spatially encoded free induction decay (FID) navigator for every acquired echo (Heijman E et al., 2007) used for retrospective gating as follows: the module and phase of the FID signal, together with their derivatives, were combined to obtain a time-dependent signal that provides information on heartbeat and respiration cycle that was used to “sort” pieces of

information that give rise to the images to the right cardiac frame. This retrospective reconstruction allows for high quality cardiac cine images even in the presence of considerable variations in respiratory and/or cardiac rates during the acquisition time (Franzosi M et al., 2011).

3.1.2 *CMR Image Analysis*

3.1.2.1 Global ventricular function

The magnetic resonance images were analyzed using custom software implemented in Matlab (The Mathworks Inc., Natick, MA). Our software measures left ventricle area for each short axis section.
First, the images are cropped manually selecting a region of interest (ROI) surrounding the LV on the end-diastolic frame .
In each images the endocardial border is semi-automatically detected using a local thresholding technique (Caiani EG et al., 2006). Then the area of the LV cavity is computed (Franzosi M et al., 2011).

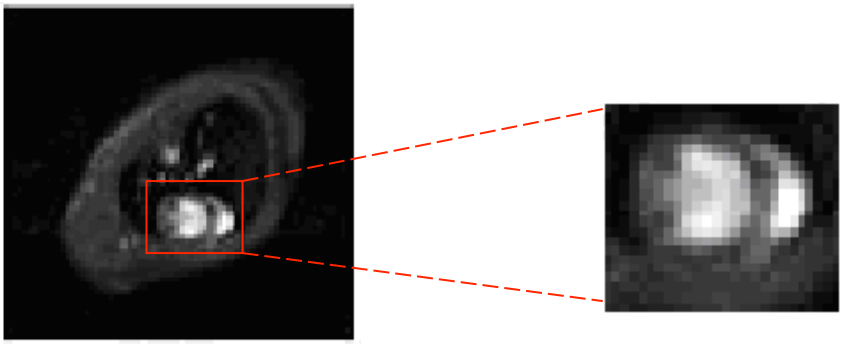

Figure 21A. Selection of region of interest (ROI) included left and right ventricles.

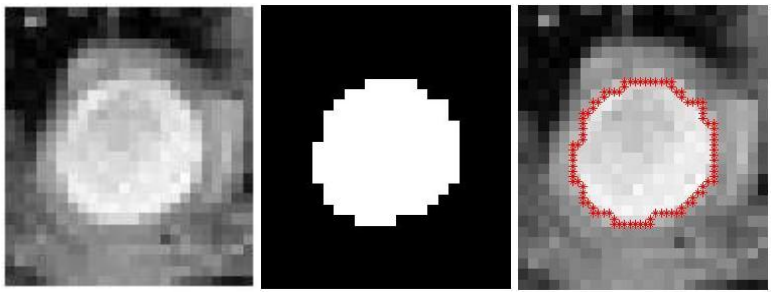

Figure 21B. Detection of left ventricle endocardial border.

For each short axis slice an Area max (A max) and Area min (A min) are computed.
End diastolic and end systolic volumes (EDV and ESV) are then computed as sum of A max and A min for each short-axis slices multiplied by the slice thickness.

Stroke volume (SV, i.e. the blood volume ejected for each beat) and ejection fraction (EF%, percentage of blood volume ejected for each beat) are derived as:

- SV = EDV- ESV.
- EF% = SV / EDV*100

3.1.2.2 Regional ventricular function

For a quantitative analysis of regional endocardial wall motion and regional ejection fraction, the LV cavity of each short axis slice are divided into six 60° sectors (anterior, antero-septal, septal, lateral, posterior and inferior). The sectors are univocally determined by the centroid of the cavity and an operator provided point at the junction between the right ventricular free wall and the interventricular septum.

For each sector the software produces the regional fractional area change (RFAC) as:

(Regional end diastolic area – regional end systolic area) / regional end diastolic area * 100.

This procedure is repeated for each slice.

RFAC is graphically displayed in a ''bull's eye'' format in which the inner circle represents LV apex, and the outer rings the consecutive slices from the apex to the base; RFAC is color coded: red tones represent lower and the green tones higher values.

In order to compute group averages our software could interpolate different number of slices according to the length of each ventricle.

In order to classify RFAC values in "normal" and "reduced" to validate bull's eye with histology a ROC analysis was performed (Franzosi M et al., 2011).

3.1.2.3 Left ventricle diameter and wall thickness

On mid-papillary slice, in end-diastolic frame we measured (Photoshop) left ventricle internal diameter anterior and posterior wall thickness

3.2 High Frame Rate Echocardiography (Echo)

The Department of Pharmacological and Biomolecular Sciences of University of Milan is equipped with high resolution echocardiography for small animals (Vevo 2100, VisualSonics, Toronto, Canada). Animals were anesthetized (1% isoflurane in 100% oxygen) and laid supine on a heated support to maintain physiological body temperature. Their legs were gently taped to conductive pads to provide ECG and respiration monitoring and recording. Animals were stabilized until HR ≥ 420 bpm, then the examination lasted about 30 min.

All images were acquired using a 30-MHz linear array transducer providing axial and lateral resolution of respectively 50 μm and110 μm. Respiration and ECG tracings were synchronised with imaging.

For image analisys Vevo software (VisualSonics, Toronto, Canada) was used for left ventricle (LV) M-mode, 2D measurements, and pulsed Doppler velocities; Medimatic software (Medimatic, Genova, Italy) was used for the left atrium (LA) 2D measurements. Recordings were analysed off-line blindly.

Based on a previous pilot study, mice were imaged in four views:

1) the left parasternal long axis view (2D LV long axis);

2) the parasternal short axis view (M-mode and 2D LV dimensions and systolic function);

3) the standard apical 4-chamber view optimized for the LA cavity [2D LA dimensions and function; mitral valve (MV) annulus dimensions and mitral pulsed Doppler flow velocity](Figure 22).

4) an apical 4-chamber view modified with a counter-clockwise rotation around the tip of the transducer to visualize left atrium appendage (LAA) (2D dimensions and pulsed Doppler flow velocity), the LA-LAA duct, and a right pulmonary vein (PV) (Figure. 23A). Then, from this view, clock- and counter-clockwise rotations around the transducer axis allowed to image additional PVs (Figures. 23 B-C). Pulsed Doppler PV flow sampling was limited to the former vein, the only providing reproducible data.

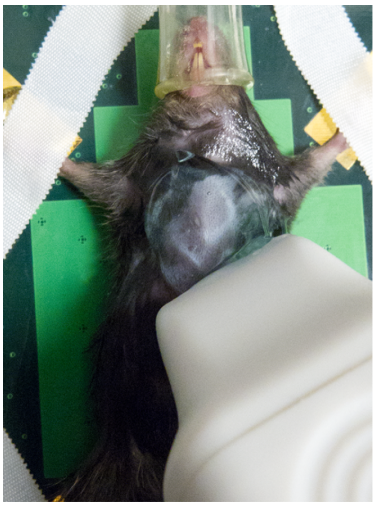

Figure 22. Standard apical 4-chamber to visualize Left Atrium.

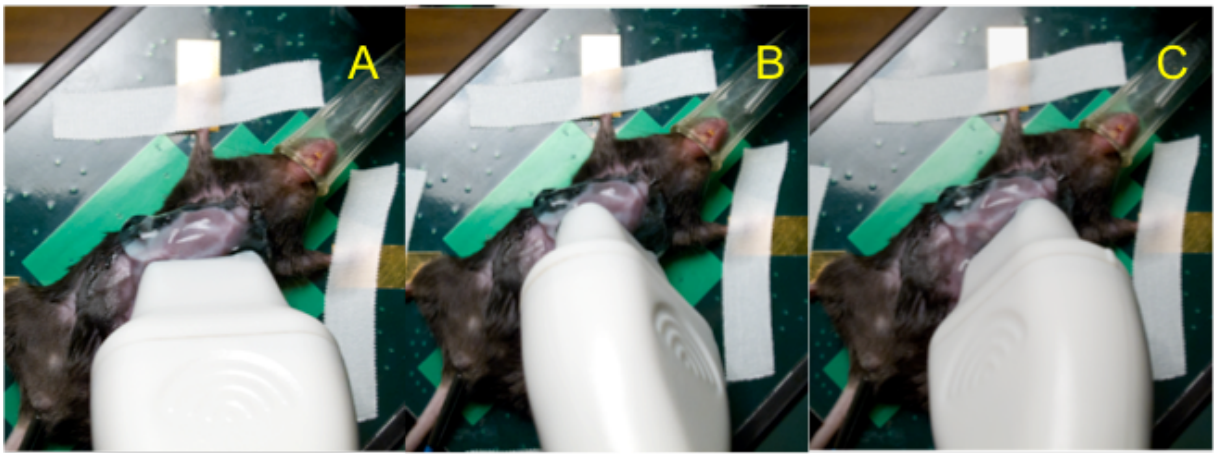

Figure 23. Modified apical 4-chamber view to visualize left atrial appendage, duct and the right superior PV (A); Transducer rotated clockwise to visualize left PV (B) and Transducer rotated counter-clockwise to visualize right inferior PV(C).

3.3 Measurements

ECG: The R-R and P-R (from the end of the P wave to the beginning of the QRS) intervals were measured, and the Q wave used as a time reference for pulsed Doppler blood flow velocities.

3.3.1 Left Ventricle

To calculate LV end-diastolic (EDV) and end-systolic volume (ESV), stroke volume (SV), ejection fraction% (EF%) and cardiac output (CO) we used Visualsonic's Simpson protocol, based on end diastolic and end systolic areas of 3 characteristic short axis slice (apical, mid-papillary and base) and long axis dimension (on end diastolic and end systolic frame) from apex to plane of the mitral valve

leaflet. From the same views, long axis systolic shortening and long/short axis ratio were also calculated.

On M-mode LV short axis view we measured all, end diastolic and end systolic, posterior and anterior, LV wall thickness and LV diameter. From these fractional shortening was computed and LV mass estimated.

Isovolumic contraction (IVCT), relaxation (IVRT) and LV ejection times were measured on pulsed Doppler recordings of simultaneous LV outflow and transmitral flow and used to calculate the myocardial performance index (MPI) as [(IVCT + IVRT) / LV ejection time].

3.3.2 Left Atrium

The area of each frame of three consecutive cardiac cycles was measured by planimetry and plotted as LA function curve. Three frames attracted attention: the minimum and maximum area and a frame (named "notch") during LA filling when a pause in LA dimension increase was observable. In these frames longitudinal (supero-inferior, from the mid point of the mitral annulus to the superior wall) and transverse diameters (septal-lateral, from the interatrial septum to the LA lateral wall, using the upper border of the LA-LAA duct as a marker) were also measured in order to calculate LA volumes using Simpson's formula. Accordingly absolute and fractional volume changes were computed during: early (from min to notch), late (from notch to max) and total LA reservoir filling.

The longitudinal/transverse LA axis ratio at minimum and maximum were also computed.

3.3.3 Left Atrial Appendage

The LAA maximum long axis was measured as the mid-line curve between the LAA apex and duct. The maximum and minimum diameters were measured deriving duct diameter fractional, and the minimum, maximum and mean duct areas were calculated (assuming a circular orifice).

The trans-ductal LAA flow pattern in the pilot study showed two positive early and late filling waves, and a negative diastolic outflow wave. Duration, peak velocity and the velocity-time integral of each were measured by calculating: total reservoir inflow integral (early + late filling); early/late inflow integral ratio; total inflow/outflow integral ratio; reservoir inflow (integral × mean duct area) and emptying outflow volumes (integral × maximum duct area).

Left appendage volume reservoir was calculated as the average of Doppler total inflow and outflow reservoir.

3.3.4 Atrial reservoir and conduit flow

Total left venous reservoir volume was estimated as sum of 2D left atrium reservoir filling and left appendage volume reservoir. Total conduit flow was calculated as: LV SV – total left venous reservoir volume.

3.3.5 Pulmonary Vein

The maximum diameter of the right superior PV was measured proximally to the LA orifice on colour Doppler images, 2D imaging alone being of insufficient quality, and PV area was calculated (circular geometry). The flow pattern in the pilot study showed two forward early and late LA filling waves, a single forward diastolic wave and no reverse flow. The duration, peak velocity and velocity-time integral of each wave were measured, diastolic flow volumes (velocity integral × PV area) were calculated.

3.3.6 Mitral Valve

The annulus diameter was measured as the distance between the leaflet hinge points at valve opening. The mid-point systolic displacement (LV base descent) was also measured. Peak velocity, total velocity-time integral, and duration of flow were measured on color Doppler images.

4 TISSUE ANALYSIS

4.1 Mouse hearts preparation

4.1.1 Histology

The abdominal aorta was cannulated, the heart was arrested in diastole with a solution of CdCl2 (0.1M) and KCl (1M), retrogradely perfused for 10 min with 0.01M phosphate saline buffer (PBS) and then with 4% (vol/vol) phosphate-buffered formalin for 10 min, postfixed in 4% phosphate-buffered formalin for 24 hours, embedded in Paraplast (Sigma-Aldrich).

4.1.2 Macroscopic Inspection

Vascular cast were prepared: 10 hearts (5/5 M/F) were retrogradelly perfused with a silicone elastomer (1 ml/min) through the cannulated abdominal aorta to build vascular and heart cast;

4.1.3 Genomic Studies

The abdominal aorta was cannulated and the heart (n=6 for each group) was retrogradely perfused for 10 mins only with PBS. A portion of posterior wall was collected in RNA later and stored for 2 weeks at 4°C, then they were removed from RNA later and freeze at -80°C.

4.2 Histological Analysis

4.2.1 Section Preparation

Coronal or axial (from base to apex) consecutive eight micrometers sections were prepared. An axial section corresponding to each CMR slice was selected for *hematoxilin - eosin s*taining.

4.2.2 Hematoxilin – Eosin And Sirius Red Staining

After deparaffination (6 + 6 mins in xilene) and rehydratation (3 mins each in absolute, 96%,70%,50% ethylic alcool and H2O bidist) the sections were stained, then washed, disidratated (1 min each in 70%, 96% and absolute ethylic alcool and 10 mins in xilene) and mounted with DPX mountant for microscopy (BDH) and acquired with a high-resolution digital camera using 1:1 macro-lens.
For hematoxilin-eosin staining the sections were incubated for 4 mins in each solution; for Sirius red staining the sections were incubated with 0.1% Sirius Red Solution (Direct Red 80, Sigma Alcrich) in picric acid for 30 mins.

4.2.3 Immunohistochemistry

Deparaffinized and rehydrated heart sections were incubated in 10% normal goat serum (Dako) in 0.01M PBS, 0.1% Triton X-100 for 45 min. Primary and secondary antibodies were prepared in PBS and 0.1% Triton X-100.
Appropriate secondary antibodies were applied for 2 h at room temperature.
For nuclear staining, the sections were washed with Hoechst 33258 (2.5 g/ml; Invitrogen) in PBS for 15 min, and analysed by using an inverted fluorescence microscope (200 M; Zeiss) with a CCD camera (AxioCam HRm; Zeiss) connected to a PC loaded with Axiovision software (Zeiss). The staining was semi-quantitatively assessed by two blinded reviewers, and the average of the two analyses was reported.
To detect, respectively, cardiomyocytes, smooth muscle cells and cardiac fibroblasts, the sections were incubated overnight at 4°C with a dilution of mouse monoclonal antibody anti α-sarcomeric actin (1:800), α-smooth muscle actin (1:600), or anti-vimentin (1:1500) (all Sigma-Aldrich). To detect

endothelial cells, endogenous peroxidase activity was blocked in 3% H2O2 in methyl alcohol/PBS 50/50 for 20 min, and the sections were incubated overnight at 4°C with isolectin B4 peroxidase (1:100; Sigma-Aldrich). Appropriate secondary antibodies (Alexa 555 goat anti-mouse IgG [1:600, Invitrogen], Alexa 546 goat anti-mouse IgM [1:600, Invitrogen], and fluorescein-conjugated goat anti-horseradish peroxidase [1:100 Jackson ImmunoResearch]) were applied for 2 h at room temperature. The staining was semi-quantitatively assessed by two blinded reviewers, and the average of the two analyses was reported.

4.2.4 Infarct Size

On Sirius red staining (one section for each mm) for 5 hearts/group, the infarct size (in percent) was calculated as infarct length divided by the total LV circumference.

4.3 CMR Bull's Eyes Validation With Histology

On images of hematoxylin-eosin staining (one section for each mm), left ventricular cavity was manually divided into six 60° sectors (anterior, antero-septal, septal, lateral, posterior and inferior) based on the position of the junction between the right ventricular free wall and the interventricular septum.

The bull's eye sector of 7 mice for each experimental groups were compared to respective histological one.

On the basis of scar tissue and fiber organization/disorganization each segment was classified as abnormal (ischemic) if the percentage of scar tissue contained in each sector was more than 50% of the relevant myocardium. Otherwise, it was classified as normal.

The number of the sector concordant (true positive and negative), as well as discordant (false positive and negative) were counted.

Segment counts were used to calculate the sensitivity, specificity and accuracy

4.4 Gene Expression Analysis

From non-infarcted posterior wall of 6 hearts/group, total RNA from was extracted using Tripure isolation buffer (Roche, Italy) and RNeasy Mini kit (Qiagen, CA, USA).

RNA integrity and quantity was assessed by capillary electrophoresis using RNA 6000 Pico Chips on a 2100 Bioanalyzer (Agilent Technologies).

Microarray data pre-processing and quality assessment and missing data imputation were performed using the GenomeStudio version 2011.1 software (Illumina). The software package BRB-ArrayTools

version 4.3.0 Beta_1, developed by Dr. Richard Simon and BRB-ArrayTools Development Team at the National Cancer Institute (NCI), NIH, was used for data adjustment, gene filtering, and statistical analysis. The package includes R version 2.15.1, a software environment for statistical computing and graphics, and tools from Bioconductor version 2.10 for the analysis and annotation of Illumina chips.

Whole-genome gene expression profiling will be performed, following the manufacturer's instructions, using Mouse Illumina Expression BeadChip microarrays, which provide genomewide transcriptional coverage of all annotated genes, gene candidates, and splice variants.

Identification of genes differentially expressed between MI-vehicle and MI-valsartan, RNA pools was performed by ANOVA on log intensities in combination with the random variance model (Wright GW et al., 2003), setting the threshold p-value to < 0.001. In order to control for the false discovery rate (FDR), a q-value was estimated for each gene (Storey JD et al., 2003). The q-value was used as an FDR-based measure of significance and the threshold α was set to < 0.01. Finally, a fold change cut-off of±1.2 was applied to focus on meaningful differentially expressed genes.

Gene functional classification was performed using the online Database for Annotation, Visualization and Integrated Discovery (DAVID) v. 6.7 Bioinformatics Resources at the National Institute of Allergy and Infectious Diseases (NIAID), NIH (http://david.abcc.ncifcrf.gov). DAVID functional annotation chart tool was used to test Gene Ontology (GO) terms for *biological process* and *molecular functions* and Swiss-Prot (SP) and Protein Information Resource (PIR) keywords for functional categories, in order to identify significantly over-represented biological themes in the differentially expressed gene set. GO gene set enrichment analysis was performed using the EASE algorithm, which compares the representation of functional classes for genes within differentially regulated subset to the entirety represented on the array. EASE performs a conservative adjustment of the Fisher's exact test to calculate the probability that the composition of the differentially expressed set occurs by chance. The DAVID tool was run with the following settings: a function/process was considered modulated by treatment if it contains at least 3 genes differentially expressed (count threshold per term) and the significance level (modified Fisher Exact *p*-value, EASE score) was less than 0.05.

5 STATISTICAL ANALYSIS

5.1 Cardiac Magnetic Resonance Setup And Validation

To evaluate the changes occurring to LV parameters the two experimental groups were compared using unpaired t test.

In order to test the reliability of MR with retrospective gating in providing information useful for automated regional wall motion interpretation, we proceeded as follows: for each sector (anterior,

antero-septal, septal, lateral, posterior and inferior), ROC analysis was computed by comparing the histological interpretation obtained in the sub-group of 7 mice with the RFAC results obtained from the corresponding MR images by counting the segments where concordant (true positive and negative) as well as discordant (false positive and negative) readings were made.

To allow the averaging of RFAC in mice with a different number of slices covering the LV, the values from different slices in each mouse were resampled using cubic spline interpolation to obtain 10 values for each of the six sectors. These values were then averaged on a point-by-point basis to obtain mean RFAC±1SD and mean every 10% of LV length from the base to the apex. This process was used for all the mice of both the Sham and MI groups, and allowed testing for differences in each 10% of LV length (unpaired t-test)

All of the echocardiographic data are the average of three measurements at end-expiration.

5.2 Characterization Of Left Atrium In Normal Mice

Gender differences were compared using unpaired t test, while paired t test was used for within-group comparisons of the echocardiographic variables in the different phases of the cardiac cycle. Selected variables were correlated with Pearson's coefficient. Multiple forward stepwise regression analysis was used to find the independent determinants of LV SV, based on the results of univariate analysis.

Inter- and intra-observer repeatability in 10 randomly selected mice, and intra-animal reproducibility (checked by the same observer making repeated acquisitions after one week), were assessed as the absolute difference in percent of the mean of the repeated measurements for the following variables: 2D LA maximum and "notch" areas, the LAA diastolic wave integral, and the LAA and PV early systolic integrals. These statistical analyses were performed using SPSS v.15 (SPSS Inc.).

5.3 CMR – Echocardiograpy Left Ventricle Parameters Comparison

Bland-Altman analysis was performed to compare CMR with Echocardiographic left ventricle functional parameters.

5.4 Echocardiographic Study Of Left Atrium In Infracted Mice

In this protocol the focus was to get temporal overview of the post MI remodelling, so the two groups were compared, at each time, using unpaired t test.

5.5 Effects Of Pharmacological Treatment

To study the chronic effect of the pharmacological treatment the response variables were considered longitudinally at 1 and 4 weeks after MI. The value of response variables at 24h, acquired just before treatment, were included as covariates to model the surgical variability (only when comparing MI vs. VALSA groups, i.e. the infarcted). As echographic measurements are subject to the quality of acoustic window the dataset presents missing values and consequently the experiment is unbalanced, moreover the sphericity of variance is violated. To avoid the inflation of degrees of freedom due to the pseudo-replication of the longitudinal measurements (violation of independence of within-group errors) the linear mixed effect (LME) model was chosen. This model can discriminate between fixed effects that influence only the mean and random effects that influence only the variance, i.e. in the particular case of longitudinal studies random effects explain variations of the responses in each single individual (mouse) that could be caused by unobserved variables. To assess the real need for random effects, a model with no random effect, a model with only random intercept and a model with random intercept and slope were compared using the maximum likelihood principle. If differences were nonsignificant, according to the Occam Razor (or principle of parsimony), the simplest model was choosen. Then fixed effects were assessed with Anova and, when non significant, removed one at a time starting with least significant and a simpler model re-fitted and accepted if maximum likelihood difference test was nonsignificant. LME analysis was performed using the lme function of non linear mixed effect (nlme) package of the R software.
In all analysis $p < 0.05$ was considered significant. The data are presented as mean±1 SD.

5.6 Microarray *Data Processing And Analysis*

The pipeline included the following steps:

- Signal variance was stabilized by applying Variance Stabilization Transformation (VST), implemented in the *lumi* R package.
- Data were normalized and chips were scaled using Robust Spline Normalization (RSN), implemented in the *lumi* R package.
- To focus on the most informative probes, we used two combined filtering criteria: a gene was excluded whether (*a*) the *p*-value of its log-variation was greater than 0.01 and (*b*) the 33th percentile of probe intensities was less than 110 (*i.e.*, a gene was not expressed by at least all the mice in one of the three treatment groups). The signal intensity threshold of 110 was chosen based on the detection *p*-value assigned to every probe by the GenomeStudio pre-processing step: 110 is the minimum intensity value above which every positive probe has a detection *p*-

value less than 0.01, *i.e.* the probe has a signal that is significantly above the background and the negative controls.

- The genes/probes that passed filtering criteria were further analyzed.
- A univariate ANOVA (F-test) on VST/RSN adjusted intensities, followed by estimation of all pairwise class contrasts controlling for multiple comparisons, was used to identify genes/probes differentially expressed between sham-, vehicle-, and Valsartan-treated mice. The F-test was used in combination with the random variance model (RVM), which is helpful when the number of experiments is small. The RVM assumes that the variance of the residuals in ANOVA for each gene is a random variable from a common gamma distribution with unknown parameters; by sharing the variance estimate across multiple genes, a better estimate for the true residual variance of a given gene can be formed, effectively boosting the residual degrees of freedom. The nominal significance level of each univariate test was set to less than 0.001 (parametric *p*-value). To control for multiple testing and to estimate the false discovery rate (FDR), permutation *p*-values for significant genes were computed based on 10000 random permutations: the significance level were set to $p < 0.005$ and FDR < 0.06 (6%), respectively.
- Unsupervised hierarchical clustering of samples and differentially expressed genes was performed on mean centered values. Genes and samples were clustered by uncentered Pearson's correlation, as distance metrics, and average linkage.
- We then performed a pairwise comparison between classes using a threshold for significantly different gene expression at alpha = 0.01.
- Finally, to focus on the most meaningful differences, we kept only those genes that exhibited a fold change (FC) ≥ ±1.2 in any of the two valid comparisons (*i.e.*, Vehicle *vs.* Sham and Valsartan *vs.* Vehicle).

RESULTS

1 CARDIAC MAGNETIC RESONANCE SETUP AND VALIDATION

1.1 Cardiac Surgery

After cardiac surgery the survival of MI animals was 70% (17% of mortality within 24 hours and 13% within 1 week after surgery) while the survival of sham-operated animals was 97% (Figure 24A).

The intrinsic surgical variability in the occlusion point along the variable branching of the LAD coronary artery lead to three distinct time evolution patterns that could be classified according to the EF measured at 24 h. If EF(24h) was higher than 45% (that is more or less a reduction of 15% respect the normal condition) the damage didn't evolve anymore and EF remained almost unchanged (compared to 24h) while, if EF(24h) was lesser than 35% we observed a rapid reduction of EF leading to death in 5-7 days.

Consequently in all the following studies were chosen only the mice with an EF(24h) between 35% and 45%, that showed a progressive decrease of EF (Figure 24B).

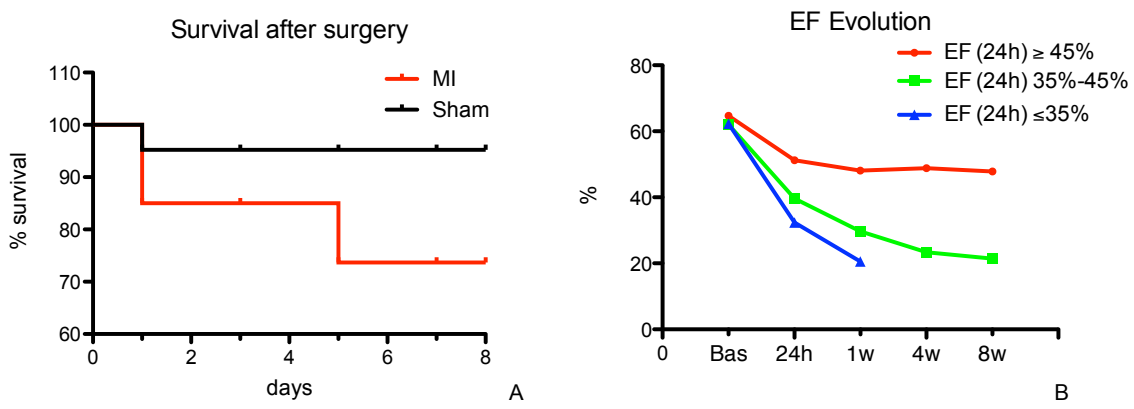

Figure 24. Graphs of animal's survival (A) and of EF evolution (B) after surgery.

1.2 Cardiac Magnetic Resonance Imaging

Two series of T2*-weighted scout images allowed us to find the anatomic landmarks needed to acquire standardized 4 chamber long-axis and 2 chamber short-axis images.
Intragate sequence, with its retrospective gating, allowed the acquisition of cine images in 2–3 min per slice, a very short time when compared to 10 min per slice (or more) necessary for ECG and respiration triggered normal gradient echo cine sequence.

Of the 30 infarcted mice that underwent LAD coronary artery ligation (MI group), 7 died for complications arose during (or shortly after) surgery, and 2 died during the CMR acquisition (70% survival rate). All, except one, sham-operated mice survived the surgery.
Nine days after surgery, we observed a significant increase in left ventricular volumes (end-diastolic and end-systolic) in MI group compared to sham-operated and a significant reduction of EF; the stroke volume was unchanged.

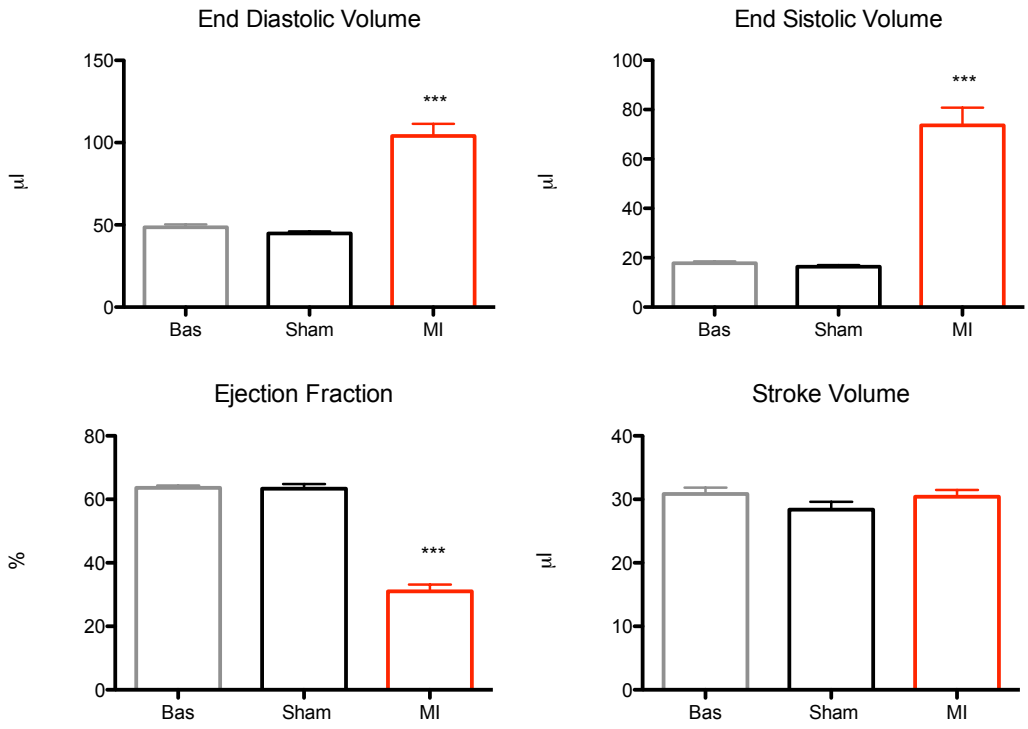

Figure 25. Graphs of EDV, ESV EF and SV Baseline and in Sham and MI groups 9 days after surgery. *** $p<0.0001$ vs. Sham and Baseline.

Left ventricular end-diastolic diameter as index of cavity enlargement was measured and was significantly higher in MI than in Sham mice as showed in Figure 26.

Also the length of the heart increased in MI, actually while Sham hearts needed an average of 5 slices to cover the entire left ventricle, LAD hearts needed 6-7.

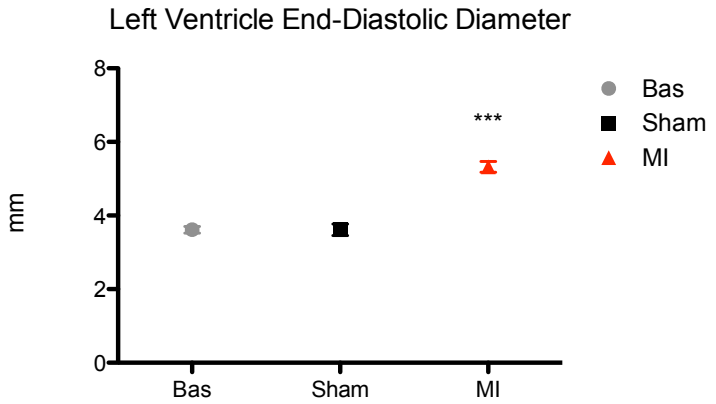

Figure 26. Graphs of Left Ventricle Internal Diastolic Diameter for Baseline, Sham and MI groups, 9 days after surgery. *** p<0.0001 MI vs. Sham and Baseline.

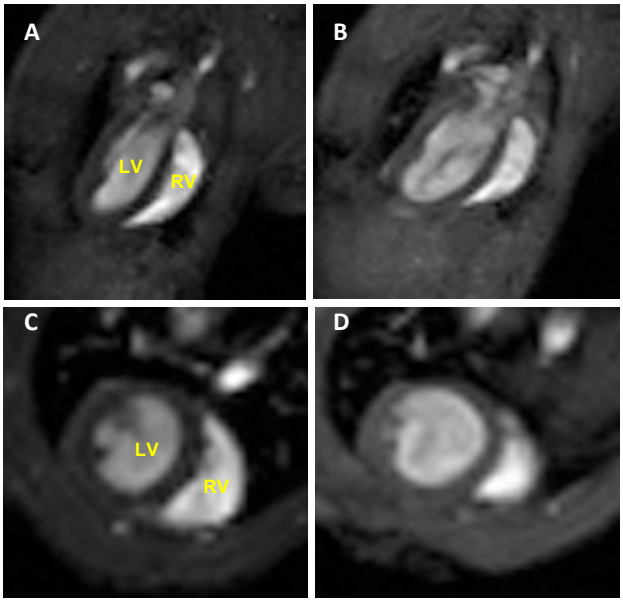

Figure 27. A representative 4-chamber long-axis and short axis of Sham (A and C) or MI mouse (B and D). The enlargement of left ventricular cavity can be observed. LV: Left Ventricle, RV: Right Ventricle.

The LV anterior and posterior wall thickness also varied with a reduction in anterior thickness in MI mice and compensatory increase in posterior wall thickness.

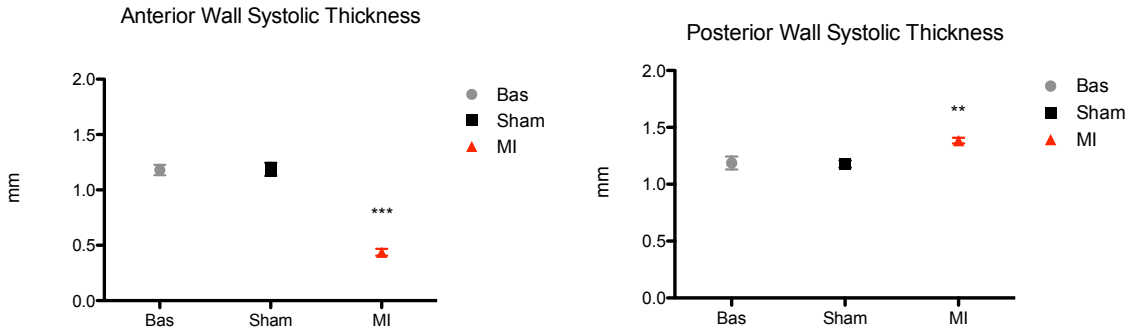

Figure 28. Graphs of Left Ventricle Anterior and Posterior wall thickness for Baseline, Sham and MI groups, 9 days after surgery. ** p< 0.05; *** p<0.0001 MI vs. Sham and Baseline.

1.3 Regional Ventricular Function

The evaluation of RFAC and its representation with bull's eyes for infarcted and sham operated mice confirmed the occlusion of LAD coronary artery and the reduced functionality of anterior and lateral segments from apical to mid-cavity slices.

In sham operated mice bull's eyes showed an increase in RFAC from the base to the apex with a minimum in the basal septal segment (55%) and a maximum in the mid-lateral segment (90%).

On the contrary, in MI mice bull's eyes showed a decrease in RFAC and this reduction is significant in the antero-septal, septal and inferior sectors only at the mid- and apical-level. The anterior sector resulted to be the most extensively damaged, as expected being the myocardial region directly irrorated by the LAD. The sectors adjacent to the anterior one (i.e., lateral and antero-septal) showed a reduced RFAC, with mean values below the corresponding regional normality threshold.

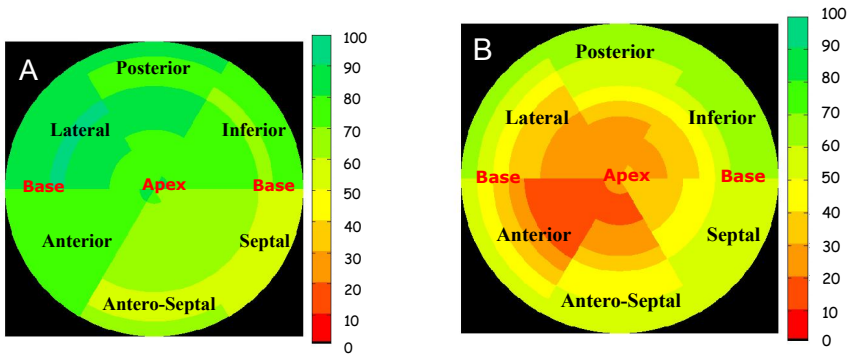

Figure 29. Bull's eye representations of mean regional fractional area change in the Sham operated (A) and infracted mice (B). The slices from the LV Apex to Base are shown from the inner to the outer circle. The red and the green tones indicate lower and higher values respectively: the corresponding scales are shown as color bars beside the panels.

1.4 Bull's Eyes Validation

Nine days after MI, left ventricle size increased so that, in 4 mice 6 short axis slices were needed to cover the entire ventricle length, in the remaining 3 mice 7 slices were needed. A total of 270 histological and CMR segments (45 short axis per 6 segments each) were analyzed. Segments were classified in normal and ischemic: for histology on the basis of cardiomyocytes organization while for RFAC a ROC analysis was performed.

MR images showed normal RFAC in 145/270 segments (54%) while normal histology in 164/270 segments (71%) and abnormally reduced RFAC in the remaining 125/270 segments (46%) while ischemic histology in 106/270 segments (39%).

So bull's eyes interpretation disagreed with the ''gold standard'' in 37/270 segments (14%), of which 17 were false positive, and 20 were false negative.

Sensibility (88%), specificity (71%) and accuracy (79%) were computed.

When this analysis is applied to the Sham group, the regional thresholds resulted in 6/306 false positives (2%), thus evidencing an optimal accuracy (98%) in correctly interpreting segments with normal wall motion.

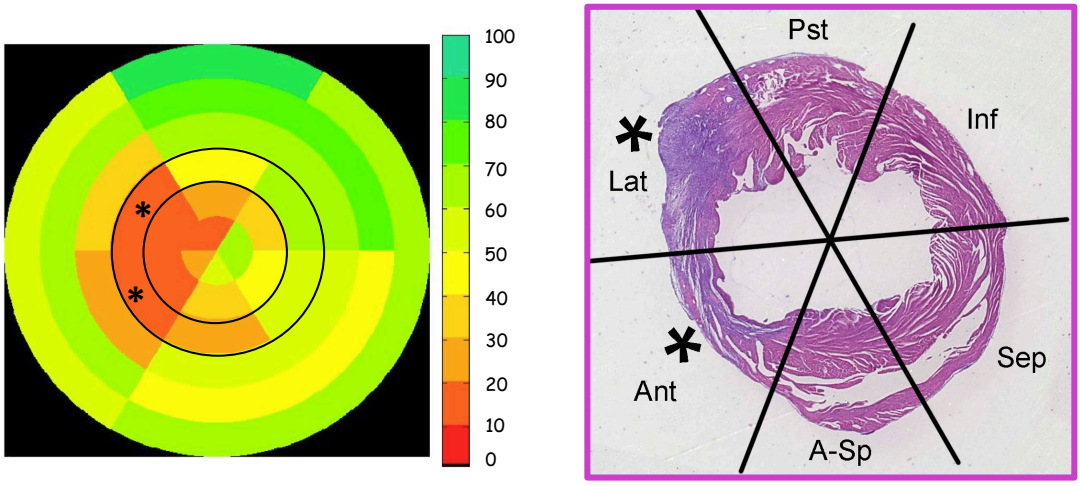

Figure 30. Representative bull's eyes and example of histological section at mid-apical level with superimposed the 6-sectors (Sep: septal, A-Sp: antero-septal, Ant: anterior, Lat: lateral, Pst: posterior, Inf: inferior). Black contour superimposed on bull's eyes indicate the level of selected histological section.
* Indicate sectors classified as abnormal.

2 CHARACTERIZATION OF LEFT ATRIUM IN NORMAL MICE

2.1 Left Atrium And Appendage Histology

Mouse heart histology showed a very little left atrium (compared to left ventricle) connected through a duct (DU) to a trabeculate appendage (LAA) comparable in size to atrium (Figure 31 A).

Immunofluorescence staining of LA and LAA showed that these structures had a similar cells composition consist of two layers of cardiomyocytes (α-sarcomeric actin positive, 58±10% vs. 44±5.8%) crossing each other and cardiac fibroblasts (vimentin positive, respectively 16±6.9% vs. 28±7.4%). Both structures showed a dense capillary network (isolectin-B4 positive, 19±8.9% vs. 25±6%) and few well-organized α-smooth muscle actin-positive cells (5.7±4% vs. 3.5±1 %) (Figure 31B-E); LAA and LA cells composition percentage were in graphs (panel F).

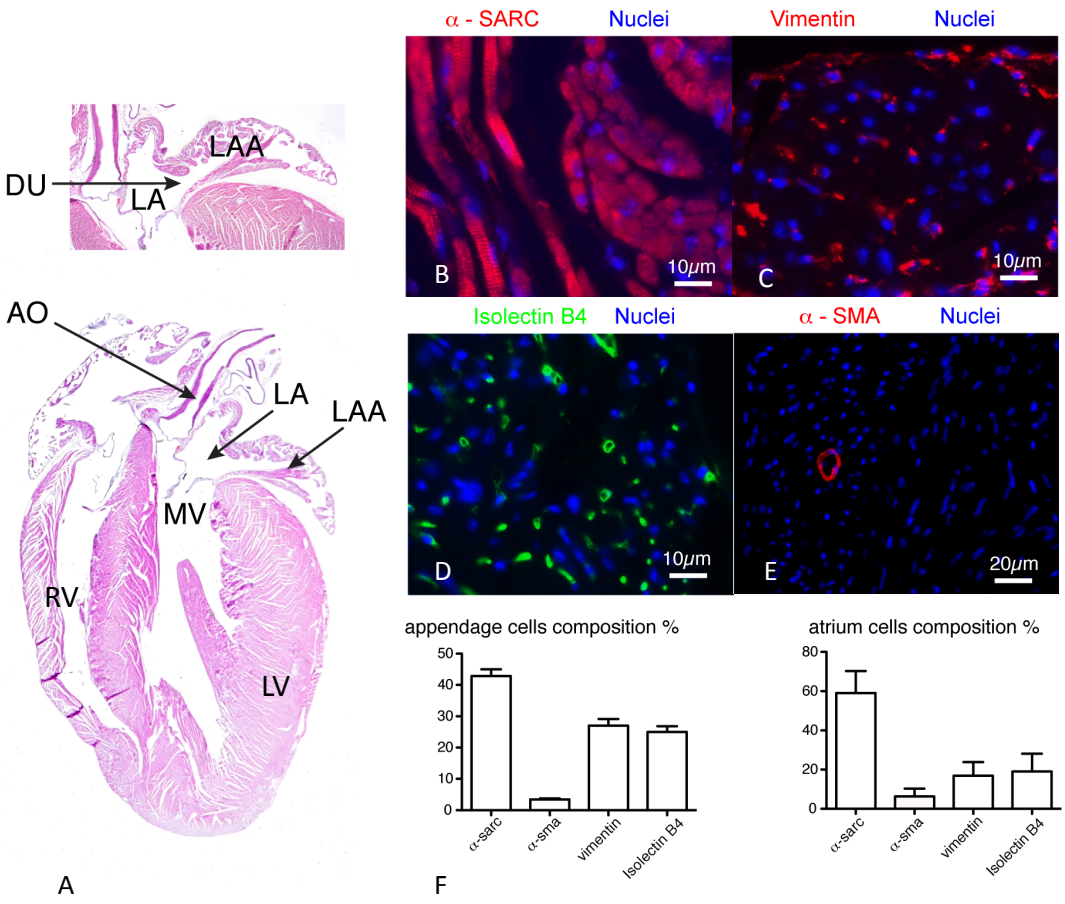

Figure 31. Representative murine coronal section and zoom of LAA-LA structures. The LA and LAA bodies consisted of two thin layers of cardiomyocytes (A) crossing each other, and cardiac fibroblasts (C). Both structures exhibited a dense capillary network (D) and few α-smooth muscle actin positive cells (E). LA and LAA cells composition percentage are in graphs (F).

a-sarc: alpha-sarcomeric actin; a-sma: alpha-smooth muscle actin; AO: aorta; DU: LA-LAA duct; LA: left atrium; LAA: LA appendage; MV: mitral valve; left ventricle (LV)and right ventricle (RV).

2.2 Macroscopic Anatomy Of Heart And Circulatory System

The resin cast of the whole heart showed frontally, in antero-lateral position to LV base, the trabeculated LAA that hide other structures of the venous reservoir (Figure 32A). After remove the pulmonary artery (PA), Figure 32B showed all the venous reservoir components: LA, LAA and PVs. A magnification of left atrium showed its round shape and its connections: laterally with LAA through a duct, inferiorly with LV through the mitral valve, and superiorly with three different pulmonary veins (PVs) entering separately into LA and identified as right inferior PV, right superior PV and left PV (Figures 32C and D).

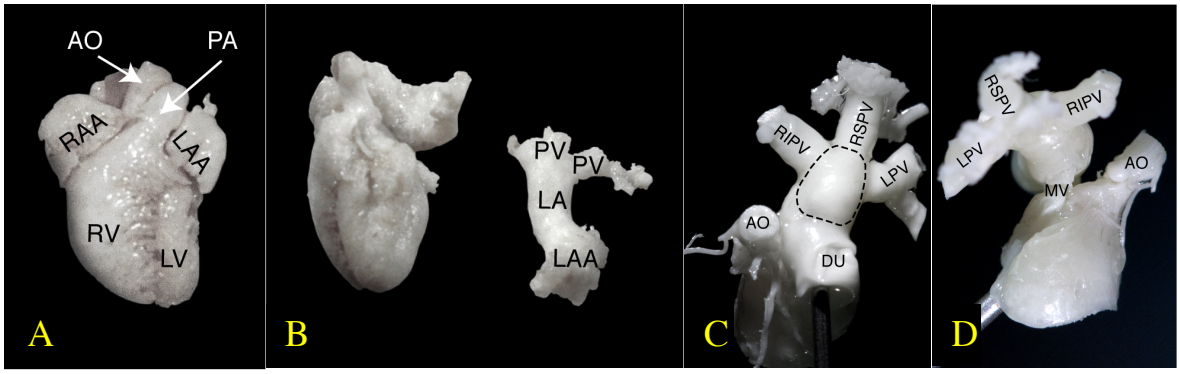

Figure 32. Resin cast of whole mouse heart (A) and after removing left venous reservoir(B). Views of isolated left venous reservoir and its connections: LA (delimited by the dotted line) (C) aorta (AO) with coronary arteries, the duct (DU), mitral valve (MV) and three PVs (right inferior PV, right superior PV and left PV) (D).

2.3 Echocardiography Studies

Male mice weighed more than females (25±1 *vs* 19±1.5 g, p<0.001), and for this echocardiographic parameters were normalized on body weight.

During echocardiographic examination mice heart rate was 484±45 bpm, an P-R interval is 35±5 ms, without significant gender difference.

Mean frame duration was 3.8 ms, and mean frames per cardiac cycle were 35.1±7.4

2.3.1 Left ventricle

Among all ventricle parameters only diastolic anterior wall thickness and mass were gender related, greater in male mice; the differences disappears after normalization by body weight.

Ejection fraction is 74±10%; end diastolic and end systolic volumes were 53±11µl and 14±4µl respectively; stroke volume was 40±9µl and cardiac output 20±7ml/min.

All the other parameters are reported in Table 3.

Table 3. Left ventricle: anatomy and function.

		All n= 30	Male n= 15	Female n= 15
End-diastolic diameter	mm	2.1±0.4		
End-systolic diameter	mm	3.7±0.7		
Anterior wall thicness, diastole	mm	0.85±0.2	0.96±0.3	0.77±0.1*
Posterior wall thicness, diastole	mm	0.73±0.1		
Anterior wall thicness, systole	mm	1.4±0.3		
Posterior wall thicness, systole	mm	1.2±0.2		
Mass	mg	101±20	112±21	93±14†
Fractional shortening	%	43±7		
Long axis, diastole	mm	7.2±0.7		
Long axis shortening	%	22±0.9		
Long/short axis, diastole		1.9±0.2		
Long/short axis, systole		2.7±0.6		
Isovolumic contraction time	ms	9.2±5.1		
Ejection time	ms	51±6		
Isovolumic relaxation time	ms	16.5±6		
Myocardial performance index		0.51±0.16		

P values *vs.* male: *p<0.05; †p <0.01.

2.3.2 Left Atrium and Left Appendage

Left atrium appeared as a small circular structure, in which longitudinal and transversal axes were: minimum 1.5 and 1.4 mm, maximum 2.1 and 2 respectively.

The sphericity was confirmed by minimum and maximum longitudinal/transversal ratio, which were 0.98±0.16 and 1.1±0.1 respectively.

LA planimetry were traced frame by frame in the 4-chamber view and, for each mice, plotted in a function curve in which three important frame were identifiable: minimum and maximum which were divided by an intermediate frame named “notch” where the area increase paused for a few frames (Figure 33).

Notch frame divided atrial reservoir phase into early and late that were different in time duration and in percentage of volume increase.

Actually the duration and the increase in volume during early reservoir is almost double than in late reservoir (Table 4).

During total reservoir phase the increase in LA volume was greater in males in which it more than doubled, but absolute differences disappeared after normalization by weight.

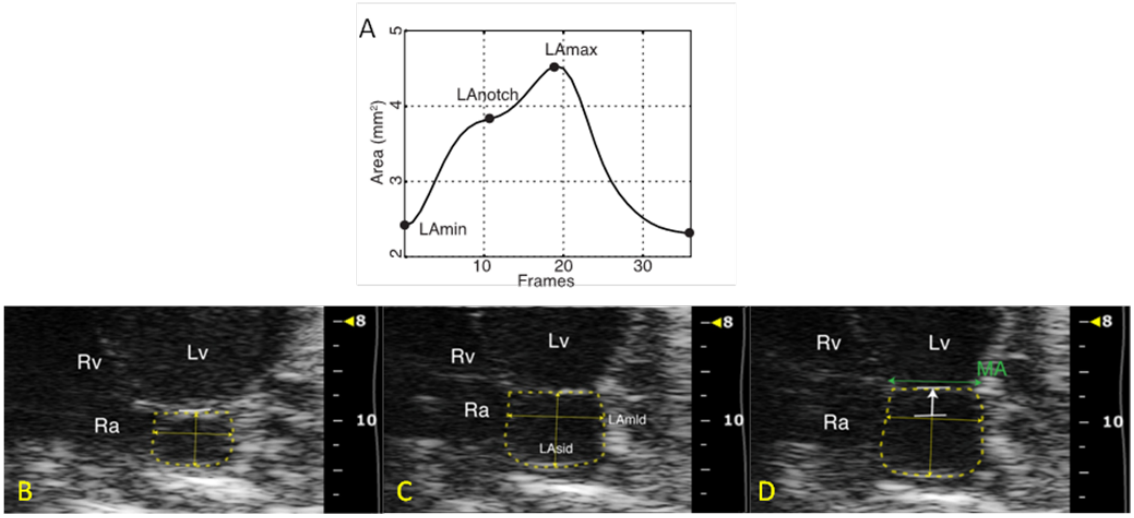

Figure 33. Representative smooth atrial function curve (A), images of minimum (B), notch (C) and maximum area (D). MA: mitral annulus.

The left atrium maximum volume (mean 5.4±1.7 μl, male 6.3±1.7 μl and female 4.7±1.3 μl) is about 10% of LV maximum volume (53±11 μl), the minimum and notch were 2.1±0.7 and 4.3±1.4μl.

Left atrium communicated laterally, through a short contractile duct (maximum and minimum diameters 1.3±0.2 mm and 0.7±0.2 mm respectively and duct diameter fractional 48±2%), with a large appendage (LAA) which length (LAAla) was 3.8±0.5 mm (male 4.3±0.3 mm and female 3.4±0.2 mm) (Figure 34); duct area values are reported in Table 5.

The LAA long axis was 2 times longer than the LA diameters and correlated with maximum LA volume (r=0.63, p=0.009), LA total reservoir filling (r =0.62, p=0.01), and LV base descent (r=0.64, p=0.007).

Two filling, and a single emptying waves (corresponding to blood flowing from and to left atrium) were detected by color Doppler.

The modified 4-chamber view showed increasing and a decreasing in LAA volume and in long axis and duct diameter during filling and emptying phase respectively confirming the contractile activity of LAA. Calculated LAA systolic filling and diastolic emptying flow volumes were equivalent (Tables 5), and the former was 3 times the LA 2D total reservoir volume increase (Table 4). The LAA diastolic integral correlated negatively with, LV base descent (r= -0.45, p=0.04), and LV SV (r= - 0.47, p=0.039).

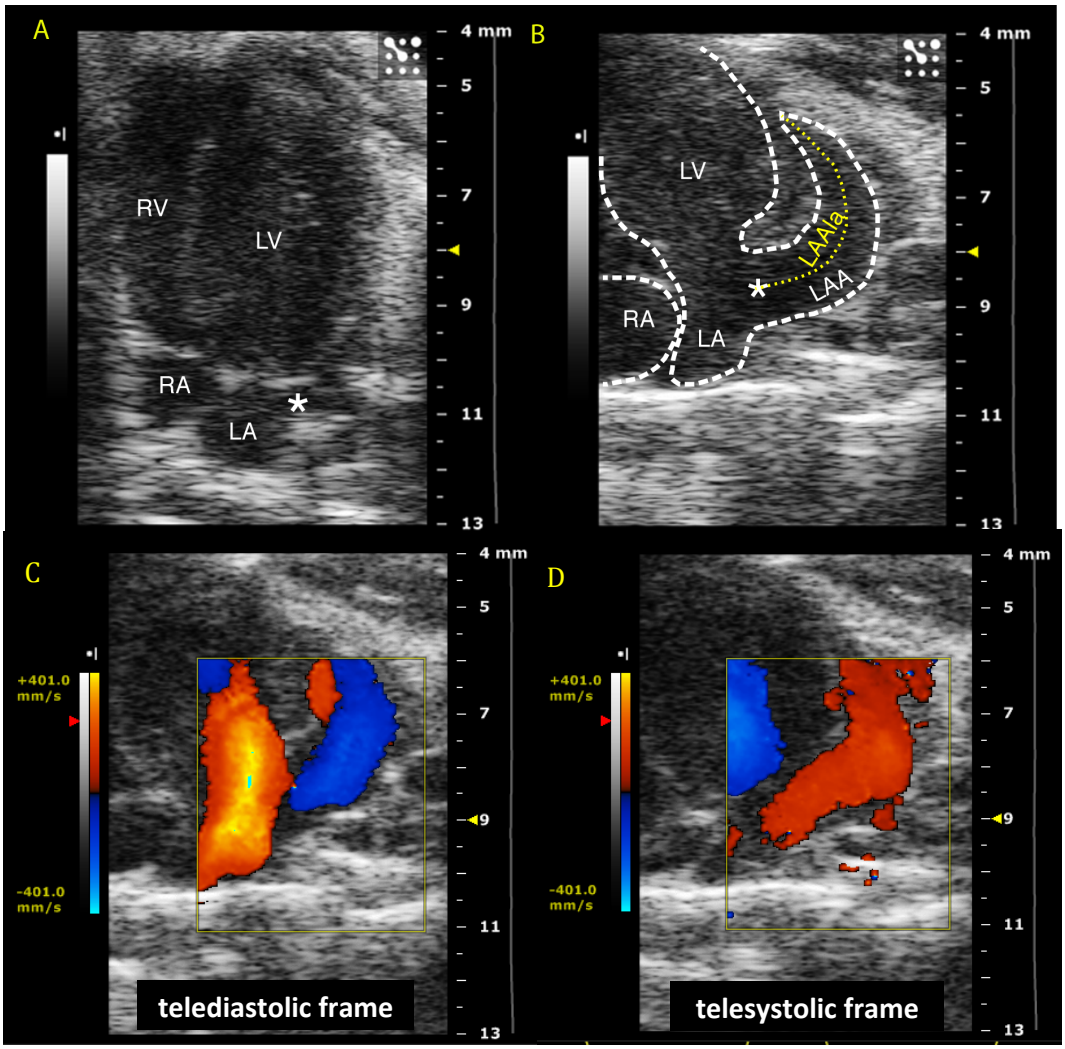

Figure 34. Apical 4-chamber view (A) to visualize LA, LV, RA and RV (A); modified apical 4-chamber view to visualize the LAA and duct (*) and duct diameter (Dd); the dotted line shows the LAA long axis with (LAAla) (B). LAA color Doppler flow velocities in diastolic (C) and systolic frame (D).

*: LA-LAA duct; Dd: diameter duct; LA: left atrium; LAA: left atrial appendage; LAAla: LAA long axis; LV: left ventricle; RA: right atrium; LV: left ventricle; RV: right ventricle.

Table 4. Left atrium: timings, volumes, anatomy and function.

		All n= 30	Male n= 15	Female n= 15
ER filling time	ms (%)	46±7 (37)		
LR filling time	ms (%)	24±5 (19)		
TR filling time	ms (%)	70±9 (55)		
ER volume increase	μL	2.2±1.1	2.7±1.1	1.8±0.9*
ER volume increase	%	110±54		
LR volume increase	μL	1.1±0.7	1.4±0.7	0.9±0.5*
LR volume increase	%	27±16		
TR volume increase	μL	3.3±1.3	4.1±1.2	2.6±1.9†
TR volume increase	%	164±62	191±59	141±56*

ER: Early reservoir; LR: late reservoir; TR: total reservoir..P values *vs* male: *p<0.05; †p≤0.01.

Table 5. LA appendage anatomy and pulsed Doppler flow profile.

		All n=30	Male n= 15	Female n= 15
Early filling wave, duration	ms	44±6		
Early filling wave, integral	mm	9.2±2.8		
Late filling wave, duration	ms	34±5		
Late filling wave, integral	mm	6.1±1.6		
Early/late filling integral ratio		1.5±0.4		
Total filling integral	mm	15±4		
Emptying wave, duration	ms	44±6		
Emptying wave, integral	mm	7.4±2.7		
Total filling/emptying integral ratio		2.3±1.3		
		n= 16	n= 8	n= 8
LAA / LA long axis, maximum		1.8±0.3	1.9±0.2	1.7±0.3
Duct area, minimum	mm^2	0.36±0.15		
Duct area, maximum	mm^2	1.4±0.33		
Duct area, mean	mm^2	0.79±0.2		
Early filling flow volume	μL	6.4±2.1		
Late filling flow volume	μL	4.4±1.6		
Total filling flow volume	μL	10.8±3.4		
Emptying flow volume	μL	10.4±3.4		

LAA: left atrial appendage. P values *vs* male: *p <0.01; †p≤0.001

2.3.3 *Pulmonary Vein Anatomy and Flow Profile.*

As in resin cast also with echocardiography three different pulmonary veins (PVs) entering the LA cavity at different angles were observed:

- a right superior PV (next to the LA septum and opposite to the LAA duct) (Figure 35A);
- a right inferior PV (Figure 35B);
- a left PV (Figure 35C).

Right superior PV diameter (measured in 16/30 mice) did not change during the cardiac cycle, diameter: 0.6±0.09mm and area 0.29±0.08mm^2.

The single diastolic wave was predominant over both early and late systolic waves and this was confirmed by their integral, significantly different $p<0.001$ (early systolic wave integral: 6.6±3.6 mm, late systolic wave integral: 5.1±2.1 mm, diastolic wave integral: 17.1±5.2 mm and total PV wave integral 27±2,8 mm).

Both the total and PV diastolic integrals correlated with LV SV ($r=0.63$, $p=0.001$ and $r=0.8$, $p<0.001$).

Wave duration, peak velocity and flow volume data are reported in Table 6

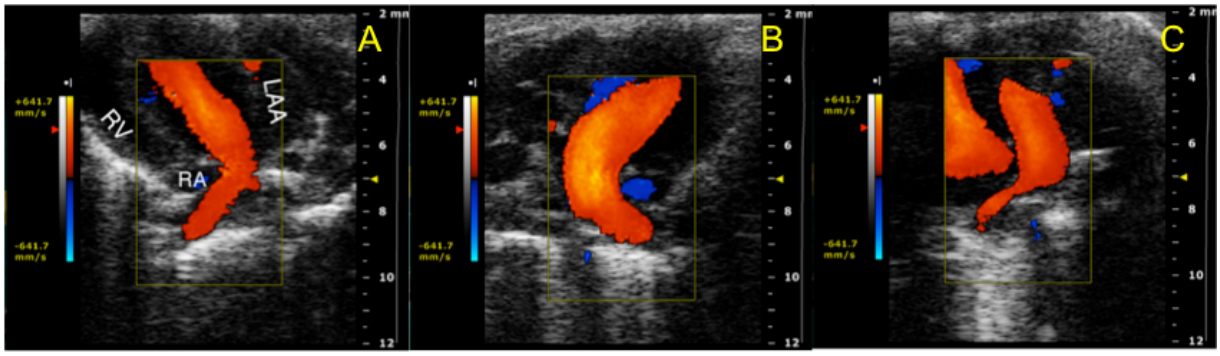

Figure 35. Color Doppler LA inflow from the right superior PV (A); from the left PV (B) and from right inferior PV (C).LAA: left atrial appendage; RA: right atrium; RV: right ventricle.

Table 6. Right superior pulmonary vein diameter and pulsed Doppler flow profile.

		n= 30
Early systolic wave, duration	ms	32±4
Early systolic wave, peak velocity	mm/s	210±68
Late systolic wave, duration	Ms	37±8
Late systolic wave, peak velocity	mm/s	156±47
Diastolic wave, duration	Ms	42±5
Diastolic wave, peak velocity	mm/s	541±141

		n= 16
Early systolic flow volume	μL	1.9±1.2
Late systolic flow volume	μL	1.7±1.1
Total systolic flow volume	μL	3.3±1.5
Diastolic flow volume	μL	4.9±2.2
Total flow volume	μL	8.1±3.7

2.3.4 Mitral Annulus and Valve Flow Profile

Annulus size was 1.8±0.3 mm, gender independent.

A single pulsed Doppler wave (labelled as A+E wave in Figure 36) was detected in 27/30 mice secondary to a combination of a high heart rate and a relatively long P-R interval (compared with the 49±7 ms duration of diastolic flow). The remaining 3 mice were excluded.

Mitral wave followed the ECG P wave and peak wave=815±153 cm/s; total velocity-time integral=22±5 mm were gender-independent.

The LV base descent (0.64±0.14 mm) was greater in males (0.7±0.1 mm vs. 0.59±0.15, $p< 0.05$), but differences disappeared after normalization by weight. It correlated positively with cardiac output ($r=0.4$, $p=0.03$) and LA maximum and total reservoir filling volumes ($r=0.55$, $p=0.001$ and $r=0.55$, $p=0.003$).

2.3.5 Cardiac Cycle Timing

The timing of atrial functional curve was related to MV, LAA and PV (right superior) flow pattern. As expected the early and late atrial reservoir phase were synchronous with the two distinct PV systolic filling (early and late respectively) and to two LAA inflow Doppler peaks.

When atrial pressure exceeds the ventricular and the mitral valve opens, a monophasic flow is observed at Doppler mitral flow, corresponding to LAA emptying flow and pulmonary vein predominant flow. Mitral valve flow occurred after the ECG P wave (Figure 36).

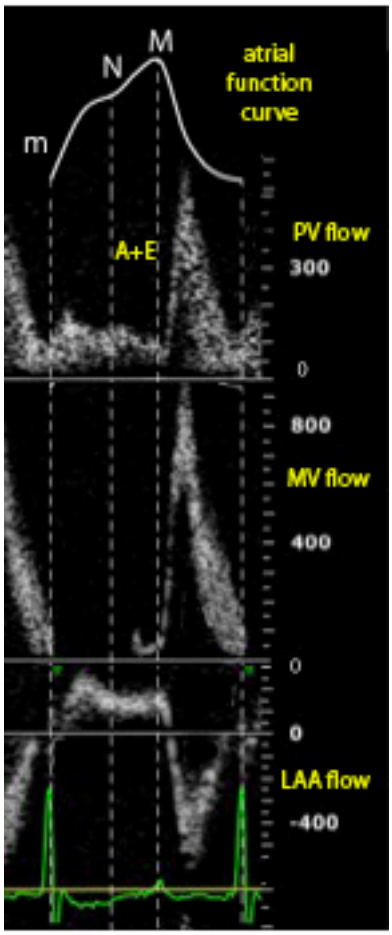

Figure 36. Left atrial function curve timing related to pulsed Doppler pulmonary vein flows (PV flow), mitral valve (A+E) flow (MV flow) and appendage flow (LAA flow).

2.3.6 Variability of Echocardiographic Measurements

The intra- and inter-operator for the selected variables were respectively: 2D LA maximum area 8%, 10%; 2D LA notch area 11%, 14%; the LAA diastolic wave integral: 9%, 23%; the PV early systolic wave integral: 11%,19% and the LAA early systolic wave integral: 12%, 27%. Intra-animal reproducibility was: 2D LA maximum area 13%; 2D LA notch area 15%; the LAA diastolic wave integral: 27%; the PV early systolic wave integral: 24% and the LAA early systolic wave integral: 29%.

3 ECHOCARDIOGRAPHIC STUDY OF LEFT ATRIUM IN INFARCTED MICE

3.1 CMR – Echocardiograpy Left Ventricle Parameters Comparison

EDV, ESV and EF, evaluated with both CMR and echocardiography in normal and ischemic mice, were compared with Bland-Altman analysis. A good correlation was found between CMR and Echocardiographic measures.

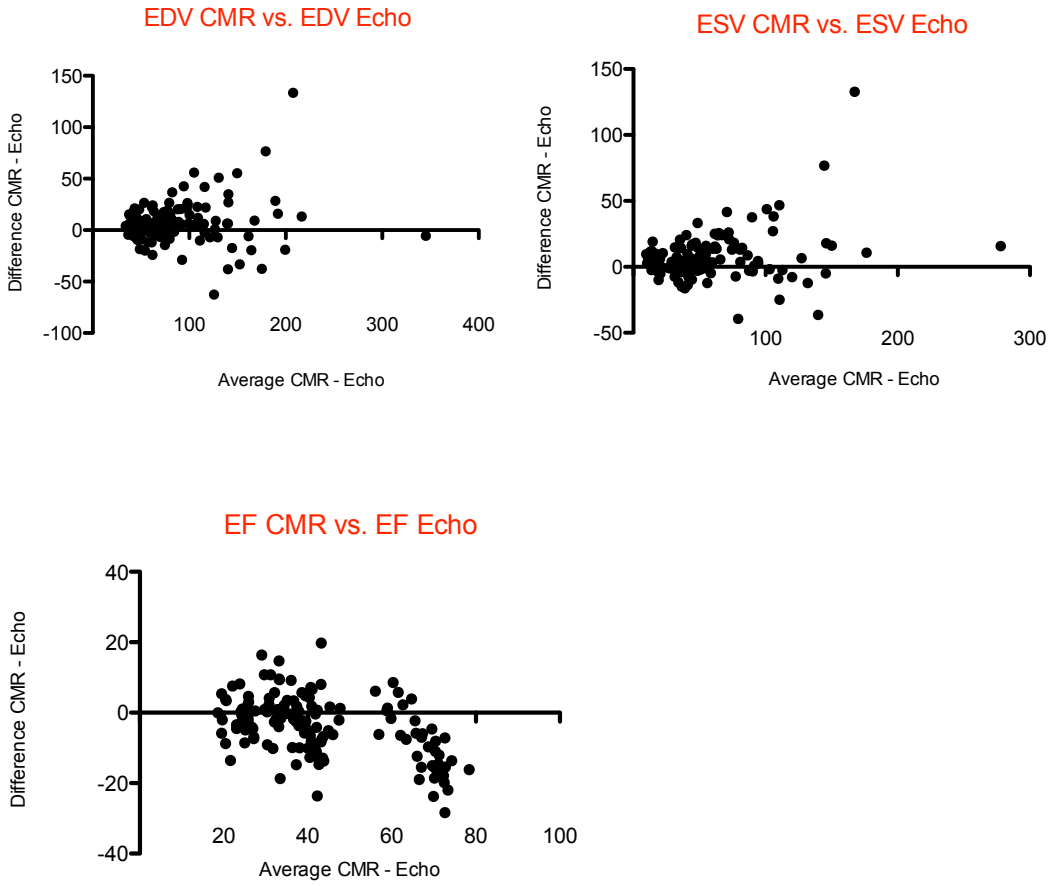

Figure 37. In graphs Bland-Altman comparison between CMR and Echoacrdiographic LV measurements: EDV, ESV and EF.

3.2 Body Weight And Heart Rate

All the parameters we evaluated were similar at baseline within the two groups and during the follow up period remained unchanged for sham-operated mice.

No sham operated mice died and only 1 infarcted mouse died 4 weeks after surgery; 1 week after MI this mouse presents EDV and ESV outlier values.

Body weight in two groups increased in similar way along the follow up period and there were no difference between the two groups, so it was no necessary to normalize the variables for body weight. No significant differences were found in heart rate between the two groups

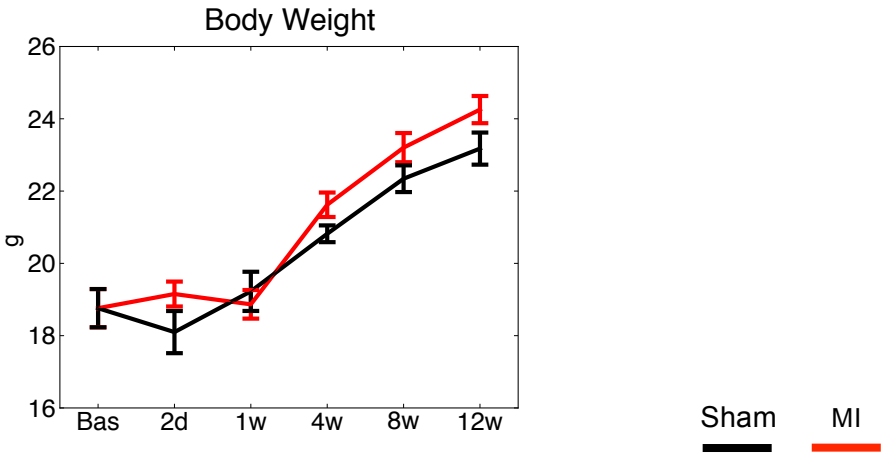

Figure 38. In graph body weight in sham and MI groups for a follow up period of 12 weeks. * p<0.05; ** p<0.01

3.3 Time Course Of Regional Function

A time course of bull's eyes visualization showed a progressive expansion of damaged myocardium not only in apical and anterior sectors, but also in lateral and posterior mid-basal levels indicating a progressive loss of contractility in remote non-infarcted tissue as showed in Figure 39.

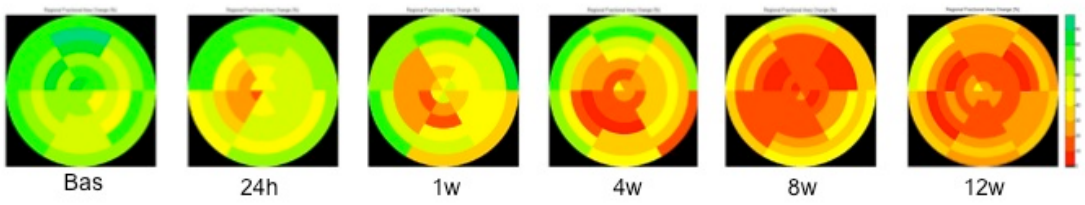

Figure 39. Time course of bull's eye visualization.

3.4 Echocardiograpy Measurements

3.4.1 Left Ventricle

Cardiac magnetic resonance and echocardiography agreed in showing a dramatic reduction of EF in infracted mice compared to sham starting from two days after MI (EF(2d) 35.2±6.7µl vs 66.6±9.1µl; EF(12w) 27.6±7µl vs. 68.25±5µl), the reduction was associated to an infarct size (12 weeks after MI) bigger than 50% of total left ventricular length.

The left ventricle end-diastolic and end-systolic volumes (EDV and ESV) immediately increased in MI mice with an initial stronger and predominant increase of ESV (2-fold after two days) over EDV (1.3 fold after two days) leading to an initial reduction of SV (SV(2d) 22.3±3µl vs. 29.1±4.2µl; MI vs. sham) that then recovers between 1 and 4 weeks after MI (Figure 40).

In response to MI we also observed an increase in isovolumic contraction (IVCT) and relaxation (IVRT) times and consequently in MPI (MPI (12w) 1.4±0.5 vs. 0.7±0.2; MI vs. sham), an index of systolic and diastolic performance, which is higher in response to a reduction of ventricular contractility.

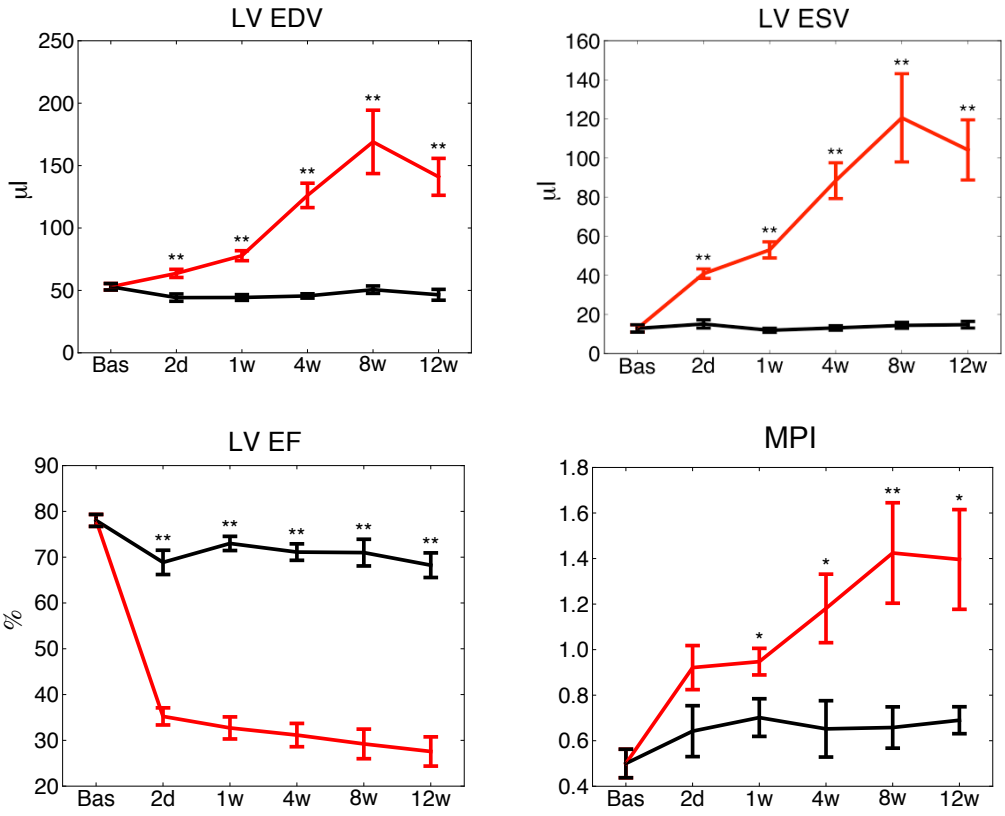

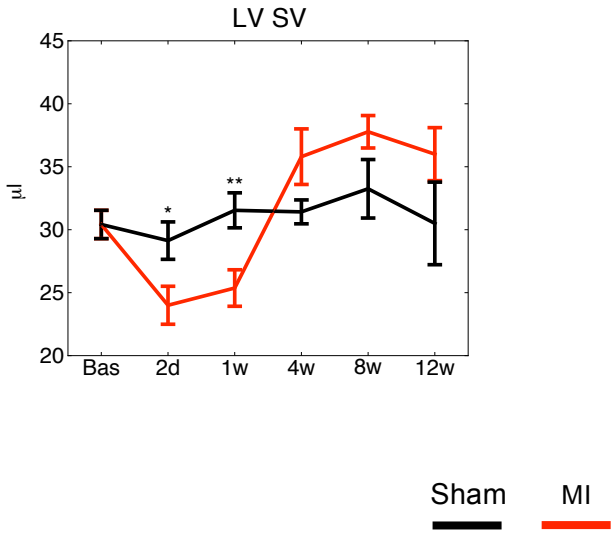

Figure 40. In graphs Left Ventricle (LV) end-diastolic volume (EDV), end-systolic volume (ESV), ejection fraction (EF) and myocardial performance index (MPI) and stroke volume (SV) in sham and MI groups for a follow up period of 12 weeks. * p<0.05; ** p<0.01.

Long axis 2D images showed cavity enlargement (Figure 41) and anatomical measurements assessed anterior wall thinning (1.27±0.22mm vs. 0.4±0.1mm p<0.001), reduction of long axis shortening (16±3.4% vs. 9.2±3.0% p<0.05) and reduction in diastolic and systolic long/short axis ratio (1.7±0.2 vs. 1.3±0.2 p<0.01 and 2.3±0.28 vs. 1.4±0.1 p<0.001), indicating a progressive sphericity of left ventricle.

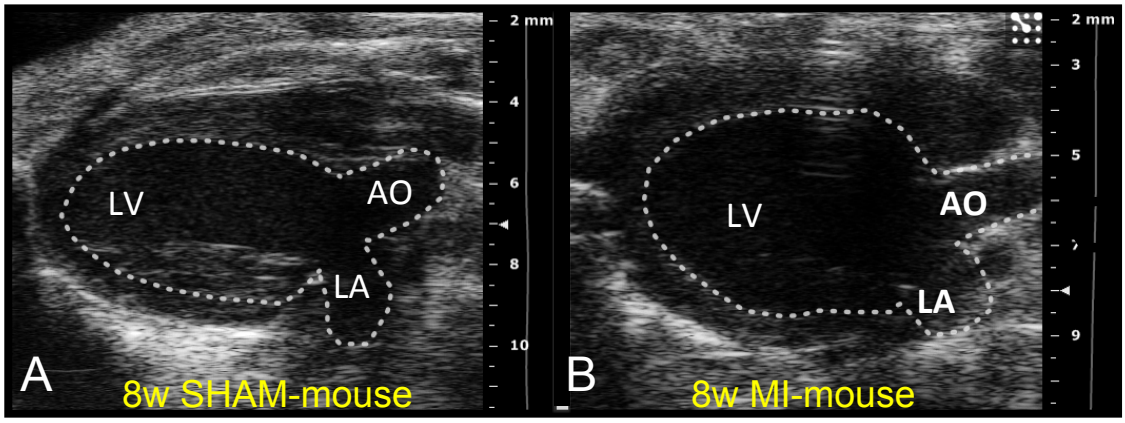

Figure 41. Left ventricle visualized in 2D long axis. Representative images of left atrium in sham (A) and MI (B) mice 8 weeks after surgery. LV: Left Ventricle; AO: Aorta; LA: Left Atrium.

3.4.2 Left Atrium And Appendage

Left ventricular remodeling doesn't take place on its own but is accompanied by left atrial (LA) remodeling.

Starting from two days after MI both maximum and minimum atrial volumes gradually increased with the progression of ventricular dysfunction and stabilized after 4 weeks; maximum ratio minimum

volume remained almost unchanged as well as volume fractional reservoir (total LA reservoir filling). In particular LAmin(12w): 4.69±1.55µl vs. 2.81±0.95µl and LAmax (12w): 8.52±2.4µl vs. 5.56±1.06µl MI vs. sham, all p‹0.01.

The enlargement of left atrial cavity 8 weeks after MI compared to sham operated mice can be observed in Figure 42.

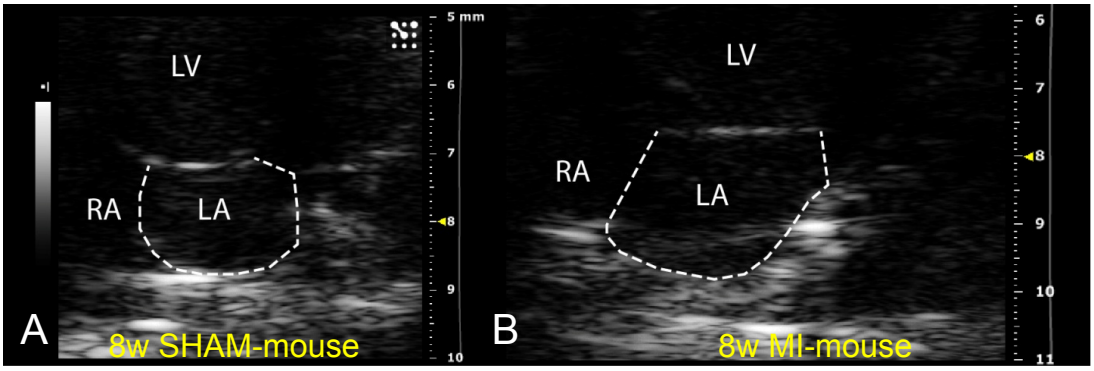

Figure 42. Left atrium visualized in four chamber view. Representative images of left atrium in sham (A) and MI (B) mice 8 weeks after surgery. LV: Left Ventricle; LA: Left Atrium; RA: Right Atrium.

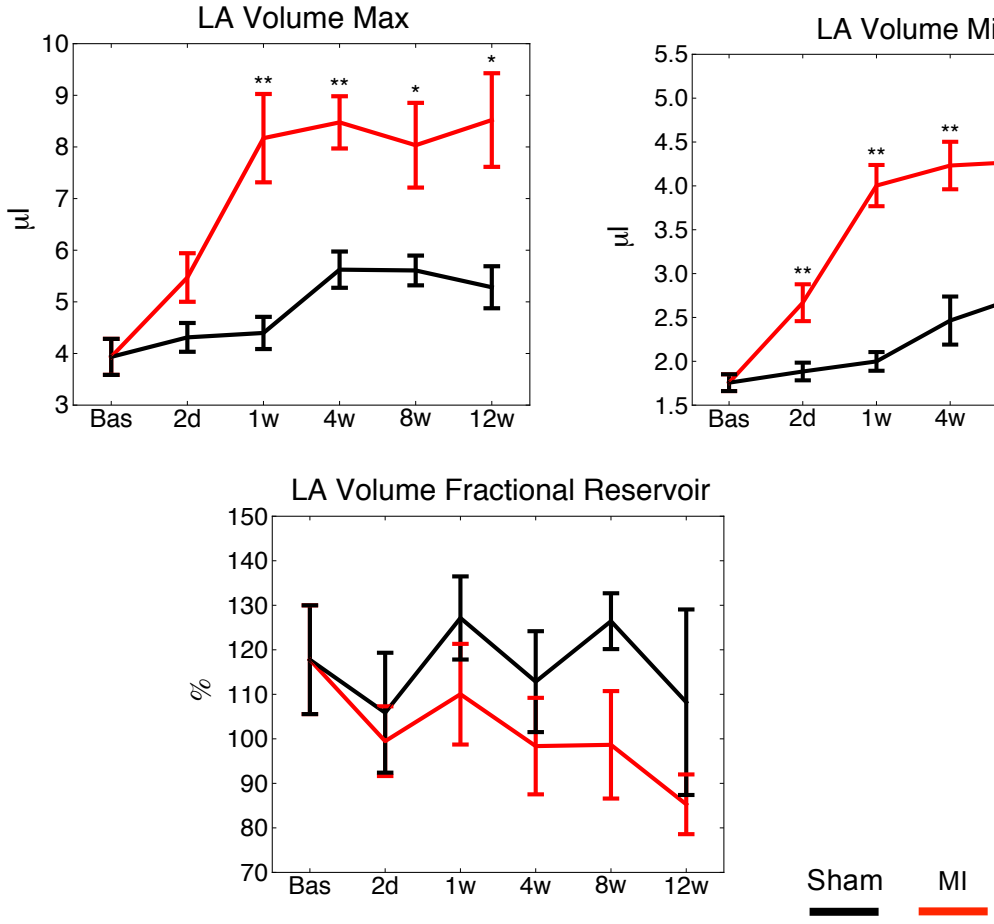

Figure 43. In graphs Left Atrial (LA) volume maximum (Max), minimum (Min) and Fractional Reservoir in sham and MI groups for a follow up period of 12 weeks. * p<0.05; ** p<0.01.

Also left atrial appendage increased in dimension, following the left atrial enlargement, in particular in long axis length and in duct dimension with a significant reduction in fractional duct diameter an index of duct contractility.In particular LAAla(12w): 4.6±0.6μl vs. 3.55±0.33μl and LAA duct fractional diameter(12w): 18.8±6.2% vs. 52.8.±5% MI vs. sham, all p‹0.01.

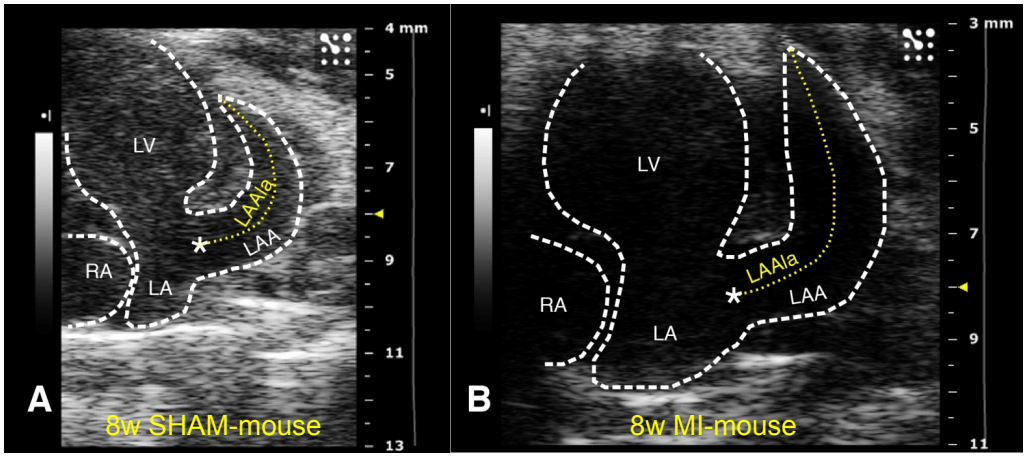

Figure 44. Left appendage visualized in modified apical four chamber view. Representative images of left appendage in sham (A) and MI (B) mice 8 weeks after surgery. LV: Left Ventricle; LA: Left Atrium; RA: Right Atrium; LAA:; LAAla: Left Atrial Appendage long axis.

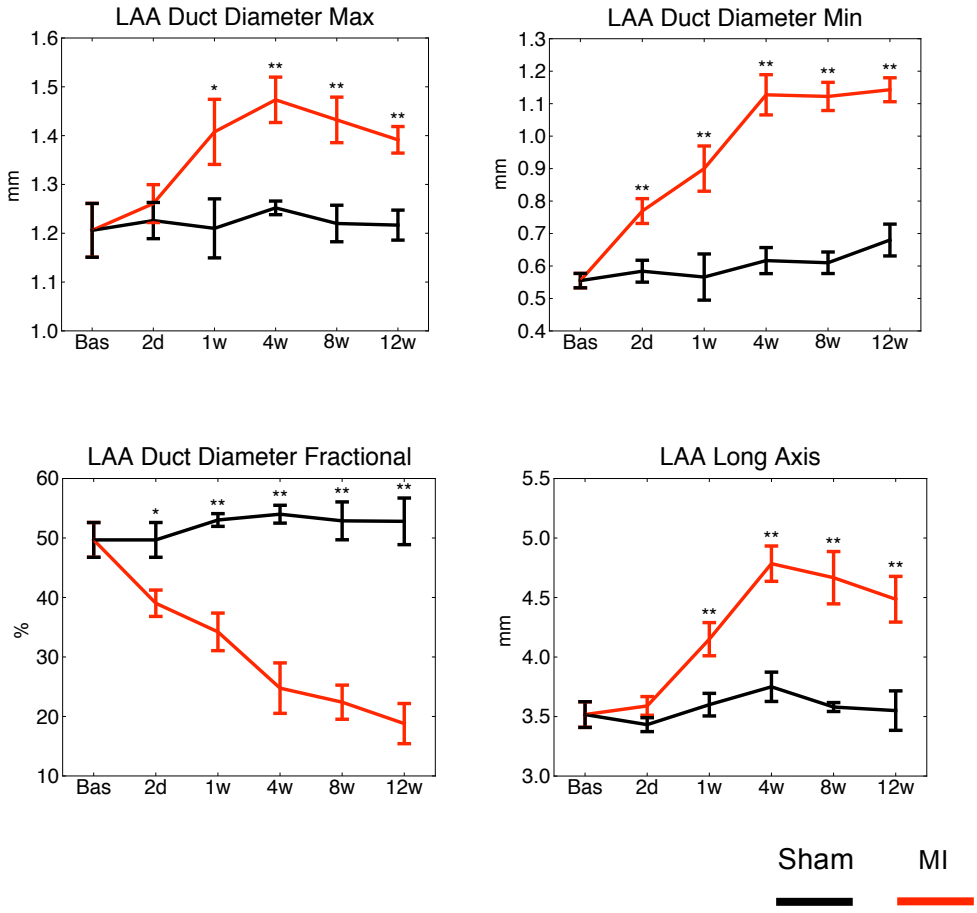

Figure 45. In graphs Left Atrial Appendage (LAA) duct diameter maximum (Max), minimum (Min) and fractional, and LAA long axis length in sham and MI groups for a follow up period of 12 weeks. * p<0.05; ** p<0.01

LA 2D volume reservoir showed a significant increase starting from 1 week while LAA volume reservoir (Doppler) showed a significant reduction two days after injury and then recovered. As a combination of LA 2D volume reservoir and LAA volume reservoir (Doppler) total volume reservoir showed an initial dramatic decrease, when LAA flow volume can not be compensated by LA reservoir increase, followed by a recovery in chronic that, after 1 week restored the baseline conditions; the same happened to atrial conduit volume with a recover from 4 weeks.

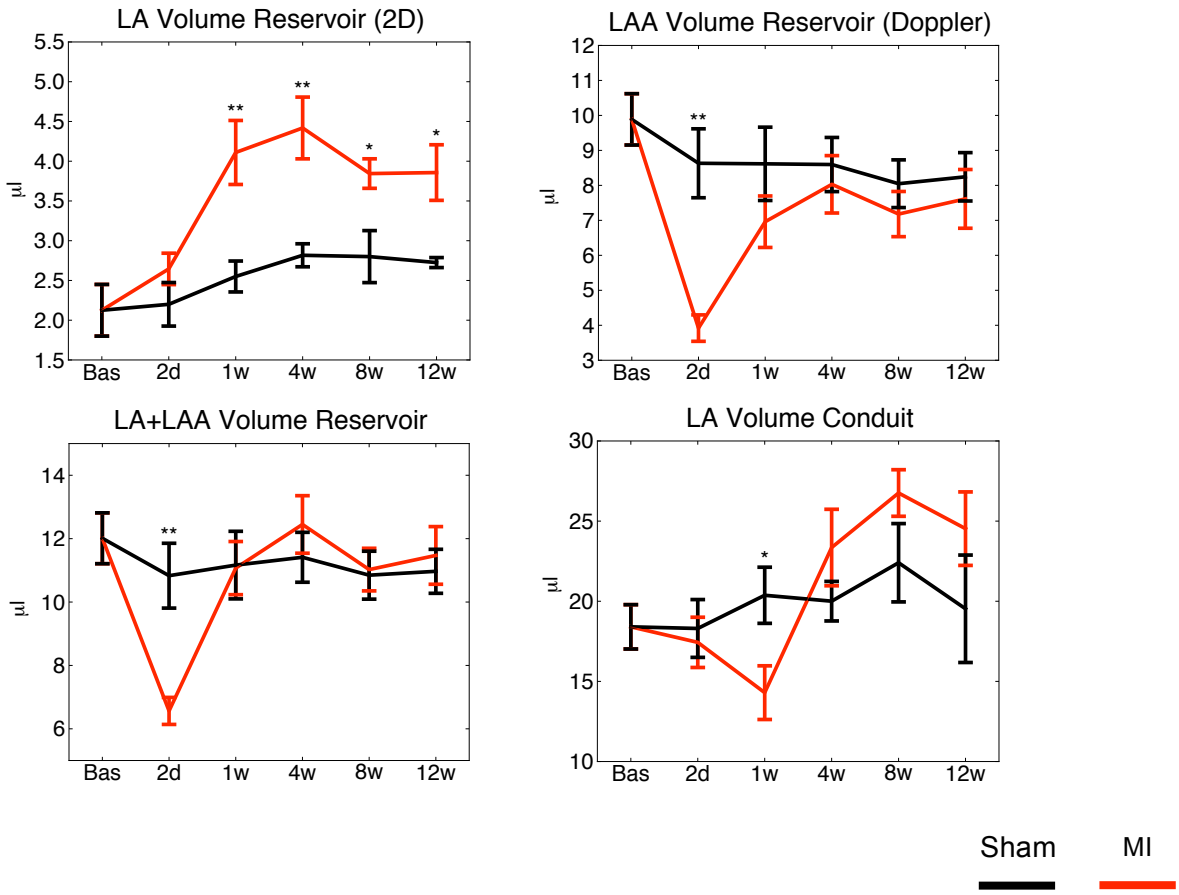

Figure 46. In graphs LA volume reservoir, LAA volume reservoir, total (LA+LAA) volume reservoir and LA volume conduit in sham and MI groups for a follow up period of 12 weeks. * $p<0.05$; ** $p<0.01$.

3.5 Effects Of Pharmacological Treatment

As described previously all the parameters we evaluated were similar at baseline within the three experimental groups and during the protocol remained unchanged for sham-operated mice.

In the follow up period body weight increased without difference between groups, as a consequence no weight normalization was needed. Mice survival was in line with our previous studies.

3.5.1 Assessment Of Global LV Function

Global left ventricular parameters evaluated with CMR agreed with the same parameters evaluated by echocardiography.

As previously described, after surgery left ventricle EF immediately decreased in MI-vehicle and MI-valsartan compared to sham group; the pharmacological treatment didn't affect EF decreasing trend.

The increase of ESV, related to the initial and predominant effect of surgery, was not affected by pharmacological treatment, while a significant effect was observed in LV EDV (an index of LV chronic remodeling): a moderate increase was observed in MI-valsartan group compared to dramatic increase in MI-vehicle.

Stroke volume (LV SV), after initial decrease in MI-vehicle and MI-valsartan, without differences between the two MI groups, recovers in chronic.

LV internal diastolic diameter (LViDd) moderately increased in MI-valsartan group compared to MI-vehicle group, reflecting the LV EDV evolution. LV internal systolic diameter LViSd was not affected as for LV ESV (Figure 47).

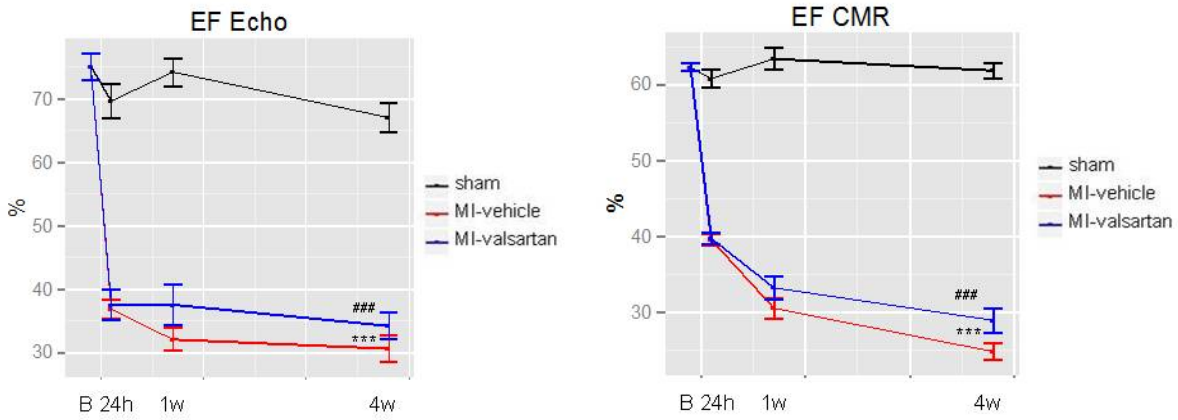

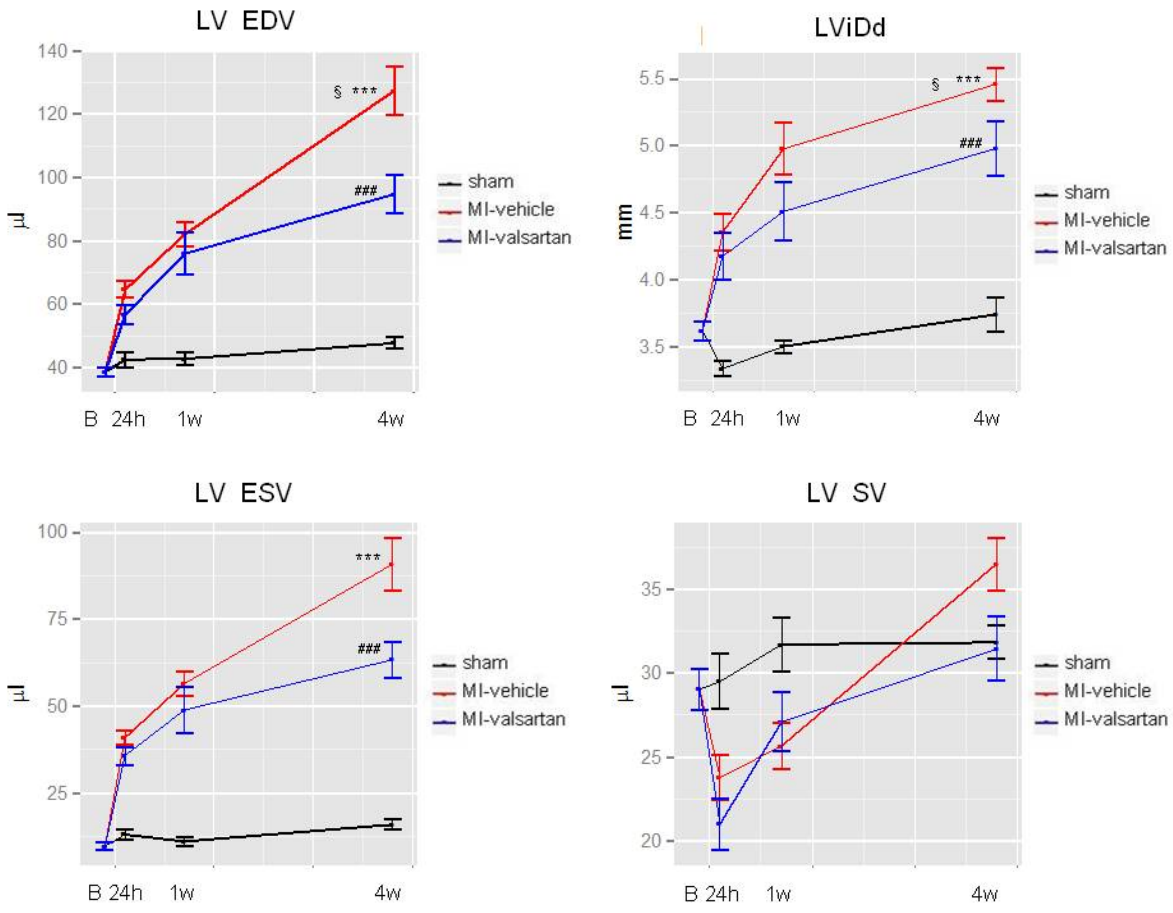

Figure 47. In graphs follow-up evolution of Left Ventricle ejection fraction (EF) evaluated with Echo and CMR, Left Ventricle end diastolic, end systolic volumes and stroke volume (LV EDV, LV ESV and LV SV), and Left Ventricle internal diastolic diameter (LViDd) in sham, MI-vehicle and MI-valsartan groups. *** p<0.001 MI-vehicle vs. Sham; ### p<0.001 MI-valsartan vs. Sham; § p<0.05 MI-valsartan vs. MI-vehicle.

At 4 weeks, anterior wall thickness was severely depressed in both MI-valsartan and MI-vehicle groups compared to sham (0.4±0.05 mm vs. 0.8±0.12 mm).

The posterior wall systolic thickness (PWTkS) and left ventricle mass (LV mass) both increased starting from twenty-four hours after myocardial infarction and in chronic remained unchanged and similar to sham in MI-valsartan while a progressive increase was observed in MI-vehicle.

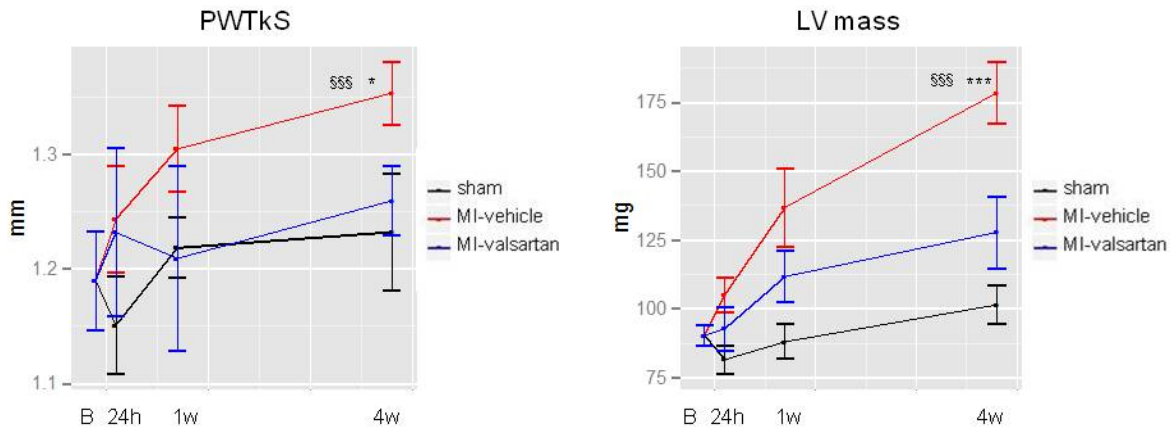

Figure 48. In graphs posterior wall systolic thickness (PWTkS) and left ventricle mass (LV mass) follow-up evolution in sham, MI-vehicle and MI-valsartan groups. * p<0.05 and *** p<0.001 MI-vehicle vs. Sham; §§ p<0.01 and §§§ p<0.001 MI-valsartan vs. MI-vehicle.

In vivo findings are in agreement with those of infarct size measured on histology sections: in the MI-vehicle group infarct size ranged from 45-55% of the whole LV length compared to 38-40% in MI-valsartan group.

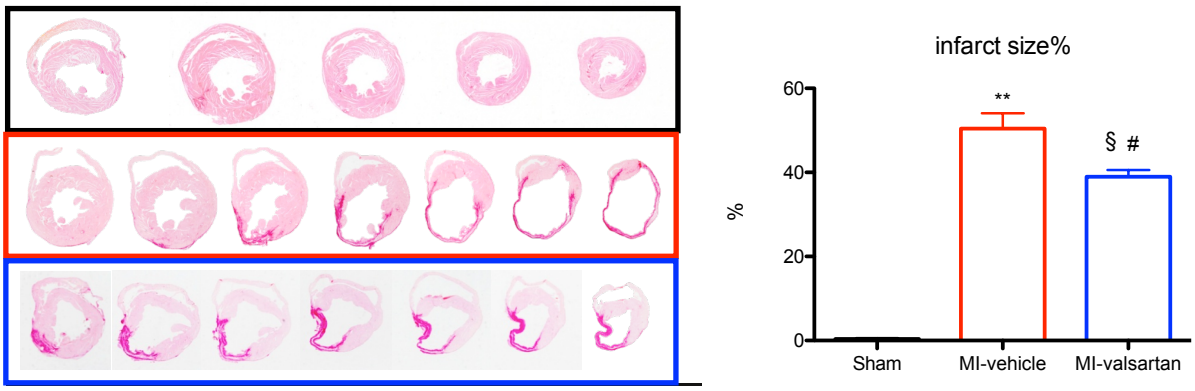

A B

Figure 49. In panel A sirius red staining representative for each experimenatal group (sections from base to apex); in panel B graph of infarct size%. ** p<0.01 MI-vehicle vs. Sham; # p<0.05 MI-valsartan vs. Sham; § p<0.05 MI-valsartan vs. MI-vehicle.

3.5.2 Assessment Of Regional LV Function

Bull's eyes representation of regional LV function showed, 24 hours after MI, a similar condition between MI-vehicle and MI-valsartan group with reduced functionality of apex, anterior and lateral segments of apical slice.

At the end of follow up period (4w), a dramatic reduced function was observed in MI-vehicle also at the basal and posterior segment, while the pharmacological treatment localized and limited the loss of function most in apical, anterior and lateral mid-cavity segments.

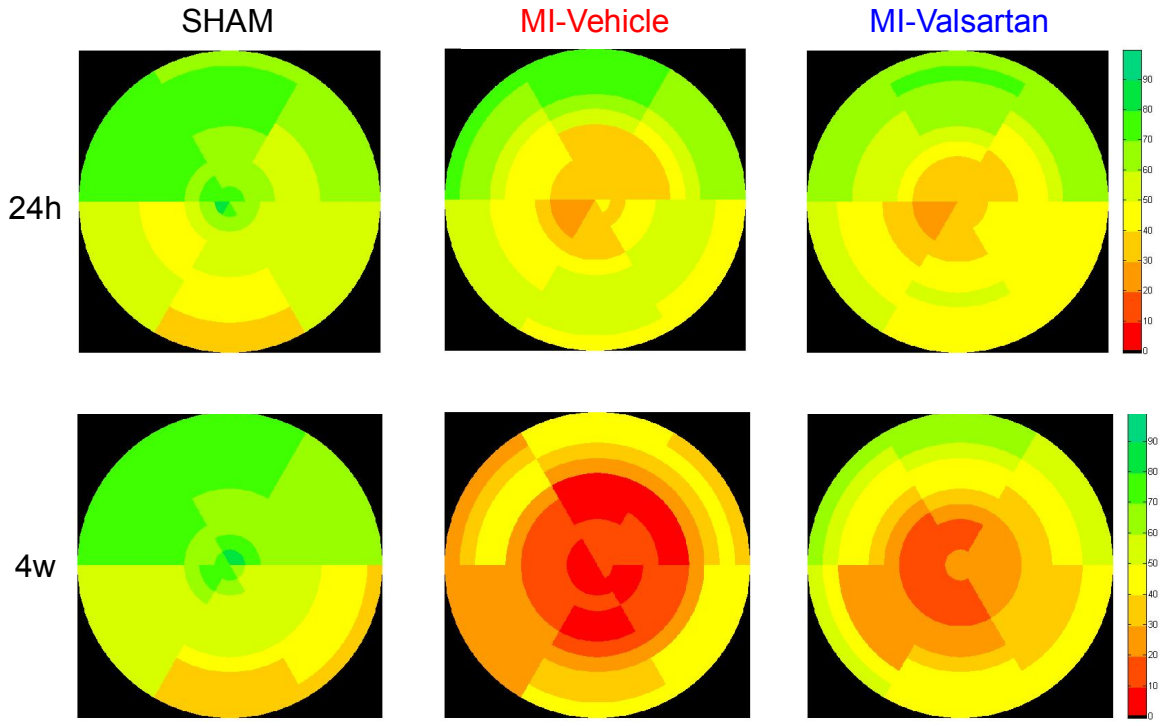

Figure 50. Bull's eye representations of mean regional fractional area change in the Sham, MI-vehicle and MI-valsartan groups 24 hour and 4w after MI.

3.5.3 Gene Expression Of Non-Infarcted Wall

In mouse heart tissue analyzed a total of 12996 cDNA sequences were expressed at detectable levels, 224 of which were significant at 0.001 level of the univariate test. The final list included 138 transcripts (probes), 41 of which were duplicates or triplicates (two or three probes for the same gene): thus, we identified **119** relevant (unique) genes that were differentially expressed between MI-vehicle and sham at 0.01 level.

These were gene involved in regulation of cell adhesion, growth, and apoptosis and involved in ECM deposition and remodeling.

Among these genes, 38 were differentially expressed between MI-vehicle and MI-valsartan.

In particular genes encoded for ECM proteins displayed enhanced expression in MI-vehicle MI-valsartan, for example expression of fibulin-2, procollagen, collagen VIII proteins involved in fibrotic and hypertrophic process, microfibrillar associated protein 5 (Mfap5) and secreted acidic cysteine

rich glycoprotein (Sparc) glycoproteins involved in ECM remodeling, actin Acta1 characteristic of activated fibroblast and metalloproteinase (MMP) was higher expressed in untreated group.

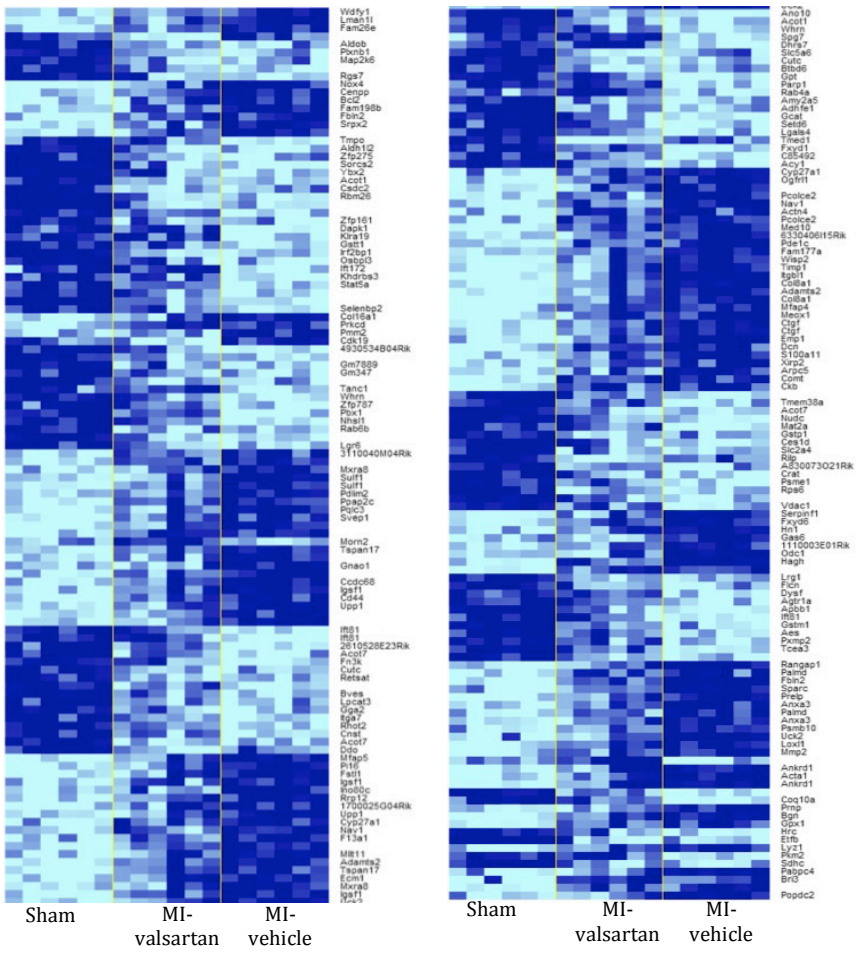

Figure 51. Pattern of gene expression in sham, MI-valsartan and MI-vehicle groups.

3.5.4 Assessment Of LA-LAA Function

In chronic, starting from 1 week after injury, LA volume minimum was preserved in MI-valsartan mice while a progressive increase was observed in MI-vehicle and this difference is significant between the two experimental groups; also LA volume maximum shows a recover in MI-valsartan, but not significantly. LA volume fractional reservoir was preserved in MI-valsartan (no significant difference to sham) while deteriorate in MI-vehicle.

At the end of the follow up period, LAmax and LAmin volumes were in MI-vehicle and MI-valsartan respectively LAmax(4w): 10.71±4.16 µl vs. 4.67±0.89µl and LAmin(4w): 6.65±3.4µl vs. 1.98±0.47 µl MI-valsartan compared to MI-vehicle.

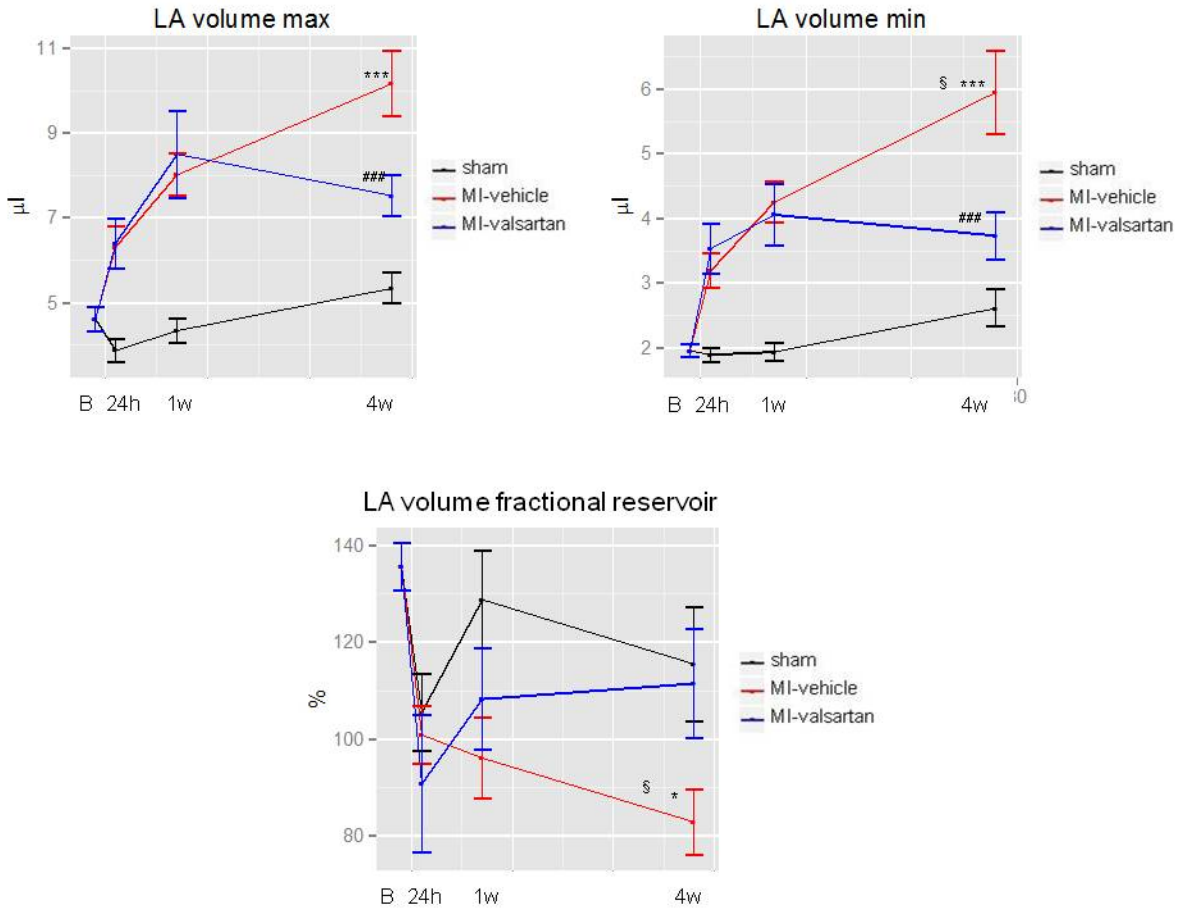

Figure 52. In graphs LAmax and LAmin volumes and Fractional reservoir follow-up evolution in sham, MI-vehicle and MI-valsartan groups. * p<0.05 and *** p<0.001 MI-vehicle vs. Sham; ### p<0.001 MI-valsartan vs. Sham; § p<0.05 and MI-valsartan vs. MI-vehicle.

Appendage long axis length remained almost unchanged two days after surgery in both MI-vehicle and MI-valsartan groups, and, in chronic, LAAla length was maintained in MI-valsartan group in contrast with the dramatic increase occurred in MI-vehicle (3.9±0.59 mm vs. 4.7±0.54 mm, MI-valsartan vs. MI-vehicle).

In MI-valsartan group LAA maintained not only its dimension but also its contractility, in particular maximum and minimum duct dimension were unchanged compared to twenty-four hour measure, and duct fractional diameter was preserved in contrast with MI-vehicle group that showed an increase in both values and a loss of contractility compared to MI-valsartan (duct fractional diameter 41.8±5% vs. 22.3±7%, MI-valsartan vs. MI-vehicle).

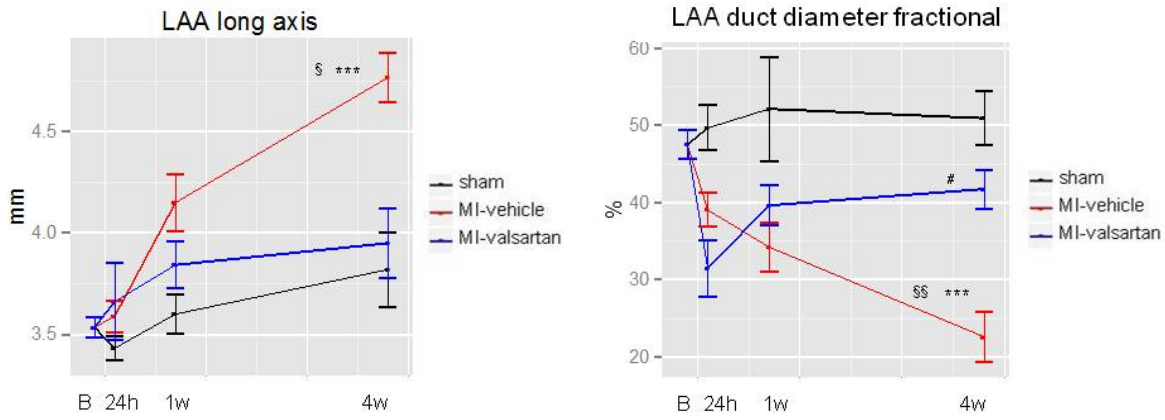

Figure 53. In graphs LAA long axis (LAAla) and duct fractional diameter follow-up evolution in sham, MI-vehicle and MI-valsartan groups. *** p<0.001 MI-vehicle vs. Sham; # p<0.05 MI-valsartan vs. Sham; § p<0.05 and §§ p<0.01 MI-valsartan vs. MI-vehicle.

DISCUSSION

Cardiovascular disease (CVD) defines several pathological conditions occurring to heart and circulatory system and is among the leading causes of death and disability in the world (Kovacic JC et al., 2011).

The most common CVDs are ischemic heart disease (43%) and cerebrovascular disease (33%), while the remaining are peripheral vascular disease, rheumatic and congenital heart disease, aortic aneurysm and dissection, deep venous thrombosis and pulmonary embolism.

Despite progress in diagnosis and treatment led to a significant reduction of the rate of death attributable to CVDs (minus 30.6% from 1998 to 2008), many efforts ought to be done to modify the extent of disease, outcome and to enhance protection.

Therefore, the development of new technologies in support of diagnosis, the release of new landmarks and the research of novel therapeutic agents are important targets for clinicians and researchers.

During the past 40 years, basic and translational researches have used small animal models to explore the pathophysiology of heart failure and to develop novel therapies that might slow down the progression of this widespread and fatal disease. Heart failure models are commonly developed in mouse because of numerous potential advantages such as much lower cost than for large animals for their housing and maintenance and the possibility to obtain transgenic animals facilitating a particularly elegant approach to identify novel therapeutic targets and offering a "proof of principle" approach to explore the mechanisms underlying heart failure and its progression (Pattern RD et al., 2009).

In addition, more recent technological advances in noninvasive *in vivo* imaging techniques for small animals allow a very detailed study of mouse heart anatomy and function.

The imaging approach offers the possibility to perform longitudinal studies, in which each animal is its own control, thus reducing the number of animals used and the interindividual variability according to the principle of *"refinement, reduction, and replacement"* (Gargiulo S et al., 2012), also improving the statistical power.

Moreover, another important feature of *in vivo* imaging, being the same used in clinics, is the translational potential towards human studies.

Among CVDs, myocardial infarction (MI) is the most common; clinical evidence suggests that MI affects both left ventricle (LV), which is directly damaged, and left atrium (LA). The LA modulates left ventricular filling in three LA phases: the reservoir, or expansion, during systole, the conduit during early diastole, and the active contractile phase during late diastole. Tsang and colleagues also reported the ability of LA to respond to a decrease in LV compliance by increasing its size: after MI, LV end-diastolic pressure increases and LA is directly exposed to this increase. To maintain adequate LV filling, LA pressure and wall tension increase consequently (Greenberg BH et al., 1979) resulting in

dilatation and stretching of atrial myocardium (Tsang TS et al., 2002). Therefore LA volume reflects the severity of diastolic dysfunction and the long-term exposure to abnormal LV diastolic function (Tsang TS et al., 2002). Strong evidence also suggests that the LA plays a central role in the early detection of cardiac disease and prognosis (Suh IW et al., 2008) and in particular LA size predicts the risk of ventricular and valvular disease (Matsuda Y et al., 1983; Vaturi M et al., 2001).

However whereas in clinic the role of atrium and its remodeling are well known, in basic sciences only few studies, performed in rats (Milliez P et al., 2005), evaluate only anatomical/morphological LA remodeling occurring after MI finding LA increase in size and collagen deposition.

In this work we focused our attention on a mouse model of myocardial infarction (MI) investigating the effect on left ventricle and, for the first time, its consequence on both left atrium and left atrium appendage (together named as left venous reservoir system). Mouse models of MI, induced by permanent ligation of left anterior descending (LAD) coronary artery, and the availability of imaging techniques for small laboratory animals, such as cardiac magnetic resonance (CMR) and high frame rate echocardiography, offer the great opportunity to investigate early and long term heart remodeling, and the changes in function occurring after MI and pharmacological intervention.

The first step in this study was to set up the surgery procedure and to assess the extent of cardiac damage by CMR imaging considered in clinic as the reference technique. This passage was hampered by many difficulties, when compared to human setting: the small dimension of murine heart, the much higher heart rate, the need of anesthesia and the impossibility to acquire breath-held images limited somewhat the damage extent assessment to LV function only. Our results showed that the time evolution of LV damage is highly influenced by the surgical variability. In particular mice with ejection fraction (EF)(24h)>45% did not develop a significant LV remodeling, whereas mice with EF(24h)<35% developed a large LV remodeling and, worst, seldom lived to 4w after MI. Therefore the use of CMR EF(24h) to select infarcted mice in this restrained range become fundamental in all our following studies. The longitudinal imaging evaluation of selected MI animals vs. sham operated showed a development of LV dysfunction in the similar way as described in Bauer et al., 2011, Protti et al., 2012 and Yang et al., 2002. We observed a significant increase in LV dimension (EDV, ESV and ventricle diameters), anterior wall thickness thinning, a dramatic reduction in EF occurred already 24 hours after injury and consequently, a progressive deterioration in all LV functions occurring during the 12 weeks follow-up period.

Regional fractional area change analysis (RFAC) and its visualization with bull's eyes, applied for the first time in mice, has been useful in confirming that, immediately after MI, the ventricular loss of function occurred in particular in apical and anterior sectors, coinciding with the LAD irrorated myocardium.

A time course of bull's eyes visualization showed a progressive expansion of damaged myocardium not only in apical and anterior sectors, but also in lateral and posterior mid-basal levels indicating a progressive loss of contractility in remote non-infarcted tissue, as a result of LV stiffness and remodeling. RFAC analysis was also able to detect small variations in contractility in the posterior myocardium i.e. regions not directly connected with LAD and had good sensibility, specificity and accuracy versus histology gold standard.

Nevertheless our results showed that CMR, despite being the clinic gold standard, both for lack of spatial and temporal resolution, was unable to refine the post MI assessment to smaller structures such as LA, so we turned towards echocardiography that in very recent time had experienced an impressive evolution for laboratory animal application. Compared to CMR, echocardiography certainly overcomes both spatial and temporal resolution limitations, however it is dependent on the very variable acoustic window that suffers particularly in the early post surgery time. Also, the evaluation of LV volumes in echocardiography is based on extrapolation and geometric assumption on LV shape that changes significantly during MI remodeling. For all these reason, after having been reassured by the strong correlation between CMR and echocardiographic data, we choose to use CMR EF(24h) to select MI animals since at this stage the use of echocardiography is hampered by the surgery suture and then to use longitudinally CMR to evaluate the development of systolic ventricular dysfunction (EF) and echocardiography to assess all the other anatomical and functional parameters.

Following these initial settings, next step was to characterize murine left venous reservoir, to our knowledge never studied before. In order to reach this goal we used a double approach: echocardiography for the function, and resin casts and histology for morphology and tissue characterization.

Echocardiographic data showed that left atrial appendage (LAA) was two times longer than LA; its Doppler estimated volume increase being twice than LA, and its cellular composition was similar to LA, with predominant cardiomyocyte component, making it a contractile chamber together with LA. All these data show incontrovertibly that, studying the mouse, the appendage cannot be neglected as usual in humans, in which LAA can be surgically removed to prevent thrombosis risk.

Another noticeable finding obtained independently by macroscopic anatomy and color Doppler imaging of LAA, both techniques never performed before, is that LA is unequivocally supplied by three pulmonary veins (PVs). In previous literature there are few histological studies describing a single PV entering the LA chamber dorsally (Kruithof BP et al., 2003; Wessels A et al., 2003), that is not surprising because even ours histological results were unable to describe the anatomy and clarify the numbers of PVs. Also a single combined *in vivo* echocardiography and corpse magnetic resonance imaging study had also hypothesized a single PV (Zhou YQ et al., 2004) however their

echocardiographic equipment was less capable than the one that was used in this study with respect to both temporal and spatial resolution, further on the corpse it is likely that some PVs were hidden by their collapse after death.

As LAA assumed a primary role in venous reservoir system we characterized its dimensions, its Doppler flows, and its connection with LA: a contractile large duct that, being open and large almost as much as LA itself during the systolic filling, let LAA enhance the LA reservoir function almost constituting together a single chamber. This is further supported by the synchronicity of filling and emptying Doppler flow pattern of LA and LAA.

In this experiment a full set of normality parameters of both LV and venous reservoir were recorded and used as a reference in the following studies. A multiple linear regression between them suggests that LV SV is influenced by LAA diastolic flow, both total (systolic + diastolic) and diastolic PV flow, and LV base descent.

After characterization of left venous reservoir in normal mouse, we then went to study its acute and chronic response after MI using echocardiography. Our results, according to literature, show a dramatic initial loss of contractility and consequently decline in systolic function resulting in an initial fall in LV SV.

In a short/mid term LA volume and LAA length increase, probably for increase in LV afterload, to reach their maximum at 1-4 weeks after MI when LV SV recovers. Increase in afterload is due to increase of LV rigidity due to several factors: increase in peripheral vascular resistance, increase in force of contractility, and activation of neurohumoral (noradrenergic and angiotensin-aldosterone) systems. During this process the duct between LA and LAA is heavily involved: loosing its contractility it seems to enhances LAA contribution to atrial function not only during systole as observed in normal mice but even during diastole. The echocardiographic longitudinal analysis show also that the total (LA+LAA) venous reservoir compliance, after initial decrease, is completely restored in chronic helping to maintain LV preload thus helping to preserve LV SV. The LV SV recovers only at the expense of increase in length of LAA and LA volume, and reduction of duct contractility, indexes of increased venous volume reservoir.

In order to evaluate the applicability of all the above techniques to pharmacological studies and to better investigate the role of venous reservoir system in MI, we finally choose to block the activation of RAAS, which is involved in after and preload in several cardiovascular diseases. Moreover, some clinical trials have demonstrated that long-term administration of blockers of RAAS, such as ACEi and ARBs, plays a critical role in post-infarction LV remodeling and promote greater reduction in LV mass decreasing cardiovascular mortality and morbidity.

To totally block the RAAS activity, we choose, as pharmacological treatment, to use valsartan, a selective inhibitor of AT1 receptor of Ang II, whose activity is directed to stop Ang II effects. The dose

1mg/kg/die was chosen as known not having effects on systemic pressure (Ohishi Y et al., 2006). Our LV EDV, LV RFAC bull's eyes, posterior wall thickness, LV mass, infarct size assed with histology, and ECM gene expression data, all significant vs. MI-vehicle, confirm the known effect on LV remodeling of valsartan at this dose. In particular, despite not significant difference in global EF (the observed difference was slightly lower than we expected and not significant as our planned experiment had not enough statistical power: to detect it there would have needed many more animals) at the end of follow-up period, bull's eyes showed a protective effect of pharmacological treatment on posterior wall contractility compared to MI-vehicle together with a reduction in posterior wall thickening. These data were also supported by microchip study of the mRNA expression in the posterior non-infarcted myocardium of MI-group treated with valsartan compare to the untreated one. We found that a total of 25 genes were differently expressed compare to untreated mice. In particular, we found an important modulation in ECM gene expression, such as fibulin-2, procollagen, collagen VIII proteins involved in fibrotic and hypertrophic process, microfibrillar associated protein 5 (Mfap5) and secreted acidic cysteine rich glycoprotein (Sparc) glycoproteins involved in ECM remodeling, actin Acta1 characteristic of activated fibroblast and metalloproteinase (MMP).

The techniques we set up for left venous characterization showed even more significant effects of the pharmacologic treatment in LA volume min, LA fractional reservoir, LAA long axis, and duct fractional diameter. Noticeably both LA fractional reservoir and LAA long axis were also not different vs. sham. As for MI-vehicle also in MI-valsartan the LV SV recovers but without LAA and LA increase in dimension.

Conclusions

Our cardiac magnetic resonance and high frame rate echocardiography results show that murine model can be used to study pharmacological treatment of MI at a deeper level than the simple LV function.

Many aspects of novelty appears in this work, in particular: i) for the first time RFAC was applied to evaluate LV function on murine heart and represented it as bull's eye; ii) the first anatomic and physiopathologic investigation of the LAA was performed in order to define new reference value useful in detecting changes after surgical and pharmacological modulations, and iii) an original comprehensive characterization of LA was carried out in mice. All the above new techniques were applied in synergy with other already established such as gene expression analysis to demonstrate their efficacy in the evaluation of damage and recover after MI with or without pharmacologic treatment. Nevertheless this study needs to be supported by histological and *in vivo* hemodynamic studies through pressure/volume catheterism.

We are confident that this comprehensive approach could be used to give new insights in many different heart and valves diseases and/or dysfunctions.

REFERENCES

Abdel-Aty H, Simonetti O, Friedrich MG. T2-weighted cardiovascular magnetic resonance imaging. *J Magn Reson Imaging 2007;26: 452–9.*

Abhayaratna WP, Seward JB, Appleton CP, Douglas PS, Oh JK, Tajik AJ, Tsang TS. Left atrial size: physiologic determinants and clinical applications. *J Am Coll Cardiol. 2006 Jun 20;47(12):2357-63.*

Al-Saady NM, Obel OA, Camm AJ. Left atrial appendage: Structure, function, and role in thromboembolism. *Heart. 1999 Nov;82(5):547-54.*

American Heart Association, American College of Cardiology, and Society of Nuclear Medicine. Standardization of cardiac tomographic imaging. *Circulation. 1992 Jul;86(1):338-9.*

American Society of Nuclear Cardiology. Imaging guidelines for nuclear cardiology procedures, Part 2. *J Nucl Cardiol. 1999 Mar-Apr;6(2):G47-84.*

Amundsen BH, Ericsson M, Seland JG, Pavlin T, Ellingsen Ø, Brekken C. A comparison of retrospectively self-gated magnetic resonance imaging and high-frequency echocardiography for characterization of left ventricular function in mice. *Lab Anim. 2011 Jan;45(1):31-7.*

Anavekar NS, Solomon SD. Angiotensin II receptor blockade and ventricular remodelling. *J Renin Angiotensin Aldosterone Syst. 2005 Mar;6(1):43-8.*

Andreson J, Adams C, Antman E et al. ACC/AHA 2007 guidelines for the management of patients with unstable angina/non-ST elevation myocardial infarction: A report of the American College of Cardiology/American Heart Association Task Force on Practice Guidelines. *J Am Coll Cardiol. 2007 Aug 14;50(7):e1-e157.*

Antman E, Hand M, Armstrong P et al. 2007 focused update of the ACC/AHA 2004 Guidelines for the Management of Patients with ST-Elevation Myocardial Infarction: A report of the American College of Cardiology/American Heart Association Task Force on Practice Guidelines. *J Am Coll Cardiol. 2008, 51: 210-2147.*

Antman EM, Anbe DT, Armstrong PW. ACC/AHA guidelines for the management of patients with ST-elevation myocardial infarction: a report of the American College of Cardiology/American Heart Association Task Force on Practice Guidelines (Committee to Revise the 1999 Guidelines for the Management of Patients with Acute Myocardial Infarction) 2004. *J Am Coll Cardiol 2004;44:671–719; Circulation 2004;110:588– 636.*

Anversa P, Olivetti G, Capasso JM. Cellular basis of ventricular remodeling after myocardial infarction. *Am J Cardiol. 1991 Nov 18;68(14):7D-16D.*

Appleton CP, Hatle LK, Popp RL. Relation of transmitral flow velocity patterns to left ventricular diastolic function: new insights from a combined hemodynamic and Doppler echocardiographic study. *J Am Coll Cardiol. 1988 Aug;12(2):426-40.*

Barbier P, Solomon SB, Schiller NB, Glantz SA. Left atrial relaxation and left ventricular systolic function determine left atrial reservoir function. *Circulation. 1999 Jul 27;100(4):427-36.*

Bauer M, Cheng S, Jain M, Ngoy S, Theodoropoulos C, Trujillo A, Lin FC, Liao R. Echocardiographic Speckle-Tracking Based Strain Imaging for Rapid Cardiovascular Phenotyping in Mice. *Circ Res. 2011 Apr 15;108(8):908-16.*

Billet S, Aguilar F, Baudry C, Clauser E. Role of angiotensin II AT1 receptor activation in cardiovascular diseases. *Kidney Int. 2008 Dec;74(11):1379-84.*

Boixel C, Fontaine V, Rucker-Martin C, Milliez P, Louedec L, Michel JB, Jacob MP, Hatem SN. Fibrosis of the left atria during progression of heart failure is associated with increased matrix metalloproteinases in the rat. *J Am Coll Cardiol. 2003 Jul 16;42(2):336-44.*

Bolooki HM, Askari A. Acute Myocardial Infarction. *August 1, 2010.*

Booz GW, Baker KM. Role of type 1 and type 2 angiotensin receptors in angiotensin II-induced cardiomyocyte hypertrophy. *Hypertension. 1996 Oct;28(4):635-40.*

Bose AK, Mathewson JW, Anderson BE, Andrews AM, Martin Gerdes A, Benjamin Perryman M, Grossfeld PD. Initial experience with high frequency ultrasound for the newborn C57BL mouse. *Echocardiography. 2007 Apr;24(4):412-9.*

Bozkurt E, Arslan S, Acikel M, Erol MK, Gurlertop Y, Yilmaz M, Koca H, Atesal S. Left Atrial Remodeling in Acute Anterior Myocardial Infarction. *Echocardiography. 2007 Mar;24(3):243-51.*

Brasier AR, Recinos A 3rd, Eledrisi MS. Vascular inflammation and the renin-angiotensin system. Arterioscler Thromb *Vasc Biol. 2002 Aug 1;22(8):1257-66.*

Braunwald E, Antman EM, Beasley JW et al. ACC/AHA 2002 guideline update for the management of patients with unstable angina and non-ST-segment elevation myocardial infarction: a report of the American College of Cardiology/American Heart Association Task Force on Practice Guidelines (Committee on the Management of Patients with Unstable Angina) 2002. *J Am Coll Cardiol 2002;40:1366–1374; Circulation 2002;106:1893–1900.*

Braunwald E, Zipes DP, Libby P. Heart Disease (6th ed.). *Philadelphia: Saunders, 2001, p. 1–18, 1114–1219, 1955–1976.*

Brede M, Hadamek K, Meinel L, Wiesmann F, Peters J, Engelhardt S, Simm A, Haase A, Lohse MJ, Hein L. Vascular hypertrophy and increased P70S6 kinase in mice lacking the angiotensin II AT(2) receptor. *Circulation. 2001 Nov 20;104(21):2602-7.*

Brodsky MA, Allen BJ, Capparelli EV, Luckett CR, Morton R, Henry WL. Factors determining maintenance of sinus rhythm after chronic atrial fibrillation with left atrial dilatation. *Am J Cardiol. 1989 May 1;63(15):1065-8.*

Brown B, Hall AS. Renin–angiotensin system modulation: the weight of evidence. *Am J Hypertens 2005; 18:127–133.*

Brown PO, Botstein D. Exploring the new world of the genome with DNA microarrays. *Nat Genet. 1999;21:33–37.*

Cabrera JA, Sánchez-Quintana D, Ho SY, Medina A, Wanguemert F, Gross E, Grillo J, Hernandez E, Anderson RH. Angiographic anatomy of the inferior right atrial isthmus in patients with and without history of common atrial flutter. *Circulation. 1999 Jun 15;99(23):3017-23.*

Caiani EG, Toledo E, MacEneaney P, Bardo D, Cerutti S, Lang RM, Mor-Avi V. Automated interpretation of regional left ventricular wall motion from cardiac magnetic resonance images. J *Cardiovasc Magn Reson. 2006;8(3):427-33*.

Calkins H, Ho SY, Cabrera JA, Della Bella P, Farré J, Kautzner J, Tchou P. Anatomy of the left atrium and pulmonary veins. *August 5, 2007.*

Campbell DJ. Circulating and tissue angiotensin systems. *J Clin Invest. 1987 Jan;79(1):1-6.*

Canadian Cardiovascular Society; American Academy of Family Physicians; American College of Cardiology; American Heart Association, Antman EM, Hand M, Armstrong PW, et al. 2007 focused update of the ACC/AHA 2004 guidelines for the management of patients with ST-elevation myocardial infarction: a report of the American College of Cardiology/American Heart Association Task Force on Practice Guidelines. *J Am Coll Cardiol. 2008 Jan 15;51(2):210-47.*

CAPRIE Steering Committee. A randomised, blinded, trial of clopidogrel versus aspirin in patients at risk of ischaemic events (CAPRIE). *Lancet 1996;348:1329–1339.*

Casaclang-Verzosa G, Gersh BJ, Tsang TS. Structural and Functional Remodeling of the Left Atrium. *J Am Coll Cardiol. 2008 Jan 1;51(1):1-11.*

Cerqueira MD, Weissman NJ, Dilsizian V, acobs AK, Kaul S, Laskey WK, Pennell DJ, Rumberger JA, Ryan T, Verani MS; American Heart Association Writing Group on Myocardial Segmentation and Registration for Cardiac Imaging. Standardized myocardial segmentation and nomenclature for tomographic imaging of the heart: a statement for healthcare professionals from the Cardiac Imaging Committee of the Council on Clinical Cardiology of the American Heart Association. *Circulation. 2002 Jan 29;105(4):539-42.*

Cheung BM. Blockade of the renin-angiotensin system. *Hong Kong Med J. 2002 Jun;8(3):185-91.*

Chu KY, Leung P. Angiotensin II in type 2 diabetes mellitus. *Curr Protein Pept Sci 2009; 10:75–84.*

Circulation. 2003 Nov 18;108(20):2543-9.

Cohn JN, Ferrari R, Sharpe N. Cardiac Remodeling—Concepts and Clinical Implications: A Consensus Paper From an International Forum on Cardiac Remodeling. *J Am Coll Cardiol. 2000 Mar 1;35(3):569-82.*

Collins KA, Korcarz CE, Lang RM. Use of echocardiography for the phenotypic assessment of genetically altered mice. *Physiol Genomics. 2003 May 13;13(3):227-39.*

Colucci WS, Braunwald E. Pathophysiology of heart failure. In: Zipes D, Libby P, Bonow RO, Braunwald E, editors. Braunwald's Heart Disease: A Textbook of Cardiovascular Medicine. 7th edition. Philadelphia, PA: *W.B. Saunders, 2005:509 –38.*

Cottrell C, Kirkpatrick JN. Echocardiographic strain imaging and its use in the clinical setting. *Expert Rev Cardiovasc Ther. 2010 Jan;8(1):93-102.*

de Sá Rebelo M, Meneghetti JC, Gutierrez MA. Functional bull's eye based on three dimensional velocity information to quantify left ventricle motion in gated-SPECT. *Conf Proc IEEE Eng Med Biol Soc. 2008;2008:209-13.*

Dent CL, Bowman AW, Scott M, Allen JS, Lisauskas JB, Janif M, Wickline SA, Kovács SJ. Echocardiographic characterization of fundamental mechanisms of abnormal diastolic filling in diabetic rats with a parameterized diastolic filling formalism. *J Am Soc Echocardiogr 2001;14:1166–1172.*

Dickstein K, Kjekshus J, OPTIMAAL Steering Committee of the OPTIMAAL Study Group. Effects of losartan and captopril on mortality and morbidity in high-risk patients after acute myocardial infarction: the OPTIMAAL randomised trial. Lancet. 2002 Sep 7;360(9335):752-60.

Duggan DJ, Bittner M, Chen Y, Meltzer P, Trent JM. Expression profiling using cDNA microarrays. *Nat Genet. 1999;21:10–14.*

Dzau V, Braunwald E. Resolved and unresolved issues in the prevention and treatment of coronary artery disease: a workshop consensus statement. *Am Heart J. 1991 Apr;121(4 Pt 1):1244-63.*

Dzau VJ, Antman EM, Black HR, Hayes DL, Manson JE, Plutzky J, Popma JJ, Stevenson W. The cardiovascular disease continuum validated: clinical evidence of improved patient outcomes: part I: Pathophysiology and clinical trial evidence (risk factors through stable coronary artery disease). *Circulation. 2006 Dec 19;114(25):2850-70.*

Ekmekci A, Toyoshima H, Kwoczynski JK, Nagaya T, Prinzmetal M. Angina pectoris V. Giant R wave and receding S wave in myocardial ischemia and certain non-ischemic conditions. *Am J Cardiol. 1961 Apr;7:521-32.*

Feigenbaum H. Echocardiography. 5th ed. *Philadelphia, Pa: Lea & Febiger; 1994.*

Fishbein MC, Maclean D, Maroko PR. The histopathologic evolution of myocardial infarction. *Chest. 1978 Jun;73(6):843-9.*

Flather MD, Yusuf S, Køber L, Pfeffer M, Hall A, Murray G, Torp-Pedersen C, Ball S, Pogue J, Moyé L, Braunwald E. Long-term ACE-inhibitor therapy in patients with heart failure or left-ventricular dysfunction: a systematic overview of data from individual patients. ACE-Inhibitor Myocardial Infarction Collaborative Group. *Lancet. 2000 May 6;355(9215):1575-81.*

Ford NL, Thornton MM, Holdsworth DW. Fundamental image quality limits for microcomputed tomography in small animals. *Med Phys. 2003 Nov;30(11):2869-77.*

Franco F, Thomas GD, Giroir B, Bryant D, Bullock MC, Chwialkowski MC, Victor RG, Peshock RM. Magnetic resonance imaging and invasive evaluation of development of heart failure in transgenic mice with myocardial expression of tumor necrosis factor-alpha. *Circulation. 1999 Jan 26;99(3):448-54.*

Frangogiannis NG, Entman ML. Chemokines in Myocardial Ischemia. *Trends Cardiovasc Med. 2005 Jul;15(5):163-9.*

Frangogiannis NG, Smith CW, Entman ML. Review. The inflammatory response in myocardial infarction. *Cardiovasc Res. 2002 Jan;53(1):31-47.*

Franzosi M, Guerrini U, Castiglioni L, Sironi L, Nobili E, Tremoli E, Caiani EG. Feasibility of quantitative analysis of regional left ventricular function in the post-infarct mouse by magnetic resonance imaging with retrospective gating. *Comput Biol Med. 2011 Sep;41(9):829-37.*

Gardin JM, Siri FM, Kitsis RN, Edwards JG, Leinwand LA. Echocardiographic assessment of left ventricular mass and systolic function in mice. *Circ. Res. 1995;76:907-914.*

Gargiulo S, Greco A, Gramanzini M, Petretta MP, Ferro A, Larobina M, Panico M, Brunetti A, Cuocolo A. Review Article. PET/CT Imaging in Mouse Models of Myocardial Ischemia. *J Biomed Biotechnol. 2012;2012:541872.*

GISSI-3. Effects of lisinopril and transdermal glyceryl trinitrate singly and together on 6 week mortality and ventricular function after acute myocardial infarction: Gruppo Italiano per lo Studio della Sopravvivenza nell'infarto Miocardico. *Lancet. 1994;343:1115–1122.*

Greenberg BH, Chatterjee K, Parmley WW, Werner JA, Holly AN. The influence of left ventricular filling pressure on atrial contribution to cardiac output. *Am Heart J. 1979 Dec;98(6):742-51.*

Grines CL, Browne KF, Marco J, Rothbaum D, Stone GW, O'Keefe J, Overlie P, Donohue B, Chelliah N, Timmis GC, et al. A comparison of immediate angioplasty with thrombolytic therapy for acute myocardial infarction. The Primary Angioplasty in Myocardial Infarction Study Group. *N Engl J Med. 1993 Mar 11;328(10):673-9.*

Grines CL, Cox DA, Stone GW, et al. Coronary angioplasty with or without stent implantation for acute myocardial infarction. Stent Primary Angioplasty in Myocardial Infarction Study Group. *N Engl J Med. 1999, 341: 1949-1956.*

Hall C. Interaction and modulation of neurohormones on left ventricular remodelling. In: St. John Sutton MG, ed. Left Ventricular Remodelling After Acute Myocardial Infarction. *London: Science Press Ltd; 1996: 89–99.*

Hamawaki M, Coffman TM, Lashus A, Koide M, Zile MR, Oliverio MI, DeFreyte G, Cooper G 4th, Carabello BA. Pressure overload hypertrophy is unabated in mice devoid of AT1A receptors. *Am J Physiol. 1998 Mar;274(3 Pt 2):H868-73.*

Hara H, Virmani R, Holmes DR Jr, Buchbinder M, Lesser JR, Van Tassel RA, Mooney MR, Schwartz RS. Is the left atrial appendage more than a simple appendage? *Catheter Cardiovasc Interv. 2009 Aug 1;74(2):234-42.*

Harada K, Komuro I, Shiojima I, Hayashi D, Kudoh S, Mizuno T, Kijima K, Matsubara H, Sugaya T, Murakami K, Yazaki Y. Pressure overload induces cardiac hypertrophy in angiotensin II type 1A receptor knockout mice. *Circulation. 1998 May 19;97(19):1952-9.*

Heijman E, de Graaf W, Niessen P, Nauerth A, van Eys G, de Graaf L, Nicolay K, Strijkers GJ. Comparison between prospective and retrospective triggering for mouse cardiac MRI. *NMR Biomed. 2007 Jun;20(4):439-47.*

Heijman E. Mouse Cardiac MRI. Eindhoven. Eindhoven University of Technology, 2008.

Ho SY, Anderson RH, Sánchez-Quintana D. Review. Atrial structure and fibres: morphologic bases of atrial conduction. *Cardiovasc Res. 2002 May;54(2):325-36.*

Ho SY, Sanchez-Quintana D, Cabrera JA, Anderson RH. Anatomy of the left atrium: implications for radiofrequency ablation of atrial fibrillation. *J Cardiovasc Electrophysiol. 1999 Nov;10(11):1525-33.*

Hoit BD, Shao Y, Gabel M. Left atrial systolic and diastolic function accompanying chronic rapid pacing-induced atrial failure. *Am J Physiol. 1998 Jul;275(1 Pt 2):H183-9.*

Hoit BD. Echocardiographic characterization of the cardiovascular phenotype in rodent models. *Toxicol Pathol. 2006;34(1):105-10.*

Holdsworth DW, Thornton MM. Micro-CT in small animal and specimen imaging. *Trends Biotechnol. 20, S34–S39. 2002.*

Holland RP, Brooks H. Precordial and epicardial surface potentials during myocardial ischemia in the pig. A theoretical and experimental analysis of the TQ and ST segments*. Circ Res. 1975 Oct;37(4):471-80.*

Holmes JW, Borg TK, Covell JW. Structure and mechanics of healing myocardial infarcts. *Annu Rev Biomed Eng. 2005;7:223-53.*

Hozumi T, Yoshikawa J, Yoshida K, Akasaka T, Takagi T, Yamamuro A. Three-dimensional echocardiographic measurement of left ventricular volumes and ejection fraction using a multiplane transesophageal probe in patients. *Am J Cardiol. 1996 Nov 1;78(9):1077-80.*

Hu TC, Bao W, Lenhard SC, Schaeffer TR, Yue TL, Willette RN, Jucker BM. Simultaneous assessment of left-ventricular infarction size, function and tissue viability in a murine model of myocardial infarction by cardiac manganese-enhanced magnetic resonance imaging (MEMRI). *NMR Biomed. 2004 Dec;17(8):620-6.*

ISIS-4 (Fourth International Study of Infarct Survival) Collaborative Group. ISIS-4: a randomised factorial trial assessing early oral captopril, oral mononitrate, and intravenous magnesium sulphate in 58,050 patients with suspected acute myocardial infarction. *Lancet. 1995 Mar 18;345(8951):669-85.*

Iwai N, Shimoike H, Kinoshita M. Cardiac renin-angiotensin system in the hypertrophied heart. *Circulation. 1995 Nov 1;92(9):2690-6.*

Jaffe AS, Babuin L, Apple FS. Biomarkers in acute cardiac disease. *J Am Coll Cardiol. 2006 Jul 4;48(1):1-11.*

Jaffe AS, Ravkilde J, Roberts R, Naslund U, Apple FS, Galvani M, Katus H. It's time for a change to a troponin standard. *Circulation. 2000 Sep 12;102(11):1216-20.*

James JF, Hewett TE, Robbins J. Cardiac physiology in transgenic mice. *Circ Res. 1998 Mar 9;82(4):407-15.*

Jaochim Nesser H, Sugeng L, Corsi C, Weinert L, Niel J, Ebner C, Steringer-Mascherbauer R, Schmidt F, Schummers G, Lang RM, Mor-Avi V. Volumetric analysis of regional left ventricular function with real-time three-dimensional echocardiography: validation by magnetic resonance and clinical utility testing. *Heart. 2007 May;93(5):572-8.*

Jin XQ, Fukuda N, Su JZ, Lai YM, Suzuki R, Tahira Y, Takagi H, Ikeda Y, Kanmatsuse K, Miyazaki H. Angiotensin II type 2 receptor gene transfer downregulates angiotensin II type 1a receptor in vascular smooth muscle cells*. Hypertension. 2002 May;39(5):1021-7.*

Joho S, Ishizaka S, Sievers R, Foster E, Simpson PC, Grossman W. Left ventricular pressure-volume relationship in conscious mice. *Am J Physiol Heart Circ Physiol. 2007;292:H369-377.*

Jugdutt BI, Amy RW. Healing after myocardial infarction in the dog: changes in infarct hydroxyproline and topography. *J Am Coll Cardiol. 1986 Jan;7(1):91-102.*

Karamitsos TD, Francis JM, Myerson S, Selvanayagam JB, Neubauer S. The Role of Cardiovascular Magnetic Resonance Imaging in Heart Failure. *J Am Coll Cardiol. 2009 Oct 6;54(15):1407-24.*

Khan A, Moe GW, Nili N, Rezaei E, Eskandarian M, Butany J, Strauss BH. The cardiac atria are chambers of active remodeling and dynamic collagen turnover during evolving heart failure. *J Am Coll Cardiol. 2004 Jan 7;43(1):68-76.*

Khoo CW, Krishnamoorthy S, Lim HS, Lip GY. Assessment of left atrial volume: a focus on echocardiographic methods and clinical implications. *Clin Res Cardiol. 2011 Feb;100(2):97-105.*

Kim RJ, Chen EL, Lima JA, Judd RM. Judd RM. Myocardial Gd-DTPA kinetics determine MRI contrast enhancement and reflect the extent and severity of myocardial injury after acute reperfused infarction. *Circulation. 1996 Dec 15;94(12):3318-26.*

Kim S, Iwao H. Molecular and cellular mechanisms of angiotensin II-mediated cardiovascular and renal diseases. *Pharmacol Rev. 2000 Mar;52(1):11-34.*

King TD, Gnarra D, Stanford W, Cline RE. Endocardial fibroelastosis and aneurysmal dilatation of the left atrial appendage. *Am J Dis Child 1973;125:721–723.*

Kitzman DW, Edwards WD. Age-related changes in the anatomy of the normal human heart. *J Gerontol. 1990 Mar;45(2):M33-9.*

Klein AL, Burstow DJ, Tajik AJ, Zachariah PK, Bailey KR, Seward JB. Effects of age on left ventricular dimensions and filling dynamics in 117 normal persons. *Mayo Clin Proc. 1994 Mar;69(3):212-24.*

Knowlton AA, Connelly CM, Romo GM, Mamuya W, Apstein CS, Brecher P. Rapid expression of fibronectin in the rabbit heart after myocardial infarction with and without reperfusion. *J Clin Invest. 1992 Apr;89(4):1060-8.*

Knutsen KM, Stugaard M, Michelsen S, Otterstad JE. M-mode echocardiographic findings in apparently healthy, nonathletic Norwegians aged 20–70 years Influence of age, sex and body surface area. *J Intern Med. 1989 Feb;225(2):111-5.*

Knuuti J, Bengel FM. Positron emission tomography and molecular imaging. *Heart. 2008 Mar;94(3):360-7.*

Kovacic JC, Fuster V. From treating complex coronary artery disease to promoting cardiovascular health: therapeutic transitions andchallenges, 2010-2020. *Clin Pharmacol Ther. 2011 Oct;90(4):509-18.*

Kruithof BP, van den Hoff MJ, Wessels A, Moorman AF. Cardiac muscle cell formation after development of the linear heart tube. *Dev Dyn 227: 1-13, 2003.*

Kuhl HP, Schreckenberg M, Rulands D, Katoh M, Schäfer W, Schummers G, Bücker A, Hanrath P, Franke A. High-resolution transthoracic realtime three-dimensional echocardiography: quantitation of cardiac volumes and function using semi-automated border detection and comparison with cardiac magnetic resonance imaging. *J Am Coll Cardiol. 2004 Jun 2;43(11):2083-90.*

Lang RM, Bierig M, Devereux RB, Flachskampf FA, Foster E, Pellikka PA, Picard MH, Roman MJ, Seward J, Shanewise JS, Solomon SD, Spencer KT, Sutton MS, Stewart WJ; Chamber Quantification Writing Group; American Society of Echocardiography's Guidelines and Standards Committee; European Association of Echocardiography. Recommendations for chamber quantification: a report from the American Society of Echocardiography's Guidelines and Standards Committee and the Chamber Quantification writing group, developed in conjunction with European Association of Echocardiography, a branch of the European Society of Cardiology. *J Am Soc Echocardiogr. 2005 Dec;18(12):1440-63.*

Lester SJ, Ryan EW, Schiller NB, Foster E. Best method in clinical practice and in research studies to determine left atrial size. *Am J Cardiol. 1999 Oct 1;84(7):829-32.*

Lew WYW, Chen Z, Guth B, Covell JW. Mechanisms of augmented segment shortening in nonischemic areas during acute ischemia of the canine left ventricle. *Circ Res. 1985 Mar;56(3):351-8.*

Li DS, Fareh S, Leung TK, Nattel S. Promotion of atrial fibrillation by heart failure in dogs—atrial remodeling of a different sort. *Circulation. 1999 Jul 6;100(1):87-95.*

Li HL, She Z-G, Li T-B, Wang AB, Yang Q, Wei YS, Wang YG, Liu DP. Overexpression of myofibrillogenesis regulator-1 aggravates cardiac hypertrophy induced by angiotensin II in mice. *Hypertension. 2007 Jun;49(6):1399-408.*

Lin MC, Rockman HA, Chien KR. Heart and lung disease in engineered mice. *Nat Med. 1995 Aug;1(8):749-51.*

Liu J, Yang F, Yang XP, Jankowski M, Pagano PJ. NAD(P)H oxidase mediates angiotensin II-induced vascular macrophage infiltration and medial hypertrophy. *Arterioscler Thromb Vasc Biol. 2003 May 1;23(5):776-82.*

Luepker RV, Apple FS, Christenson RH, Crow RS, Fortmann SP, Goff D, Goldberg RJ, Hand MM, Jaffe AS, Julian DG, Levy D, Manolio T, Mendis S, Mensah G, Pajak A, Prineas RJ, Reddy KS, Roger VL, Rosamond WD, Shahar E, Sharrett AR, Sorlie P, Tunstall-Pedoe H; AHA Council on Epidemiology and Prevention; AHA Statistics Committee; World Heart Federation Council on Epidemiology and Prevention; European Society of Cardiology Working Group on Epidemiology and Prevention; Centers for Disease Control and Prevention; National Heart, Lung, and Blood Institute. Case definitions for acute coronary heart disease in epidemiology and clinical research studies. A statement from the AHA Council on Epidemiology and Prevention; AHA Statistics Committee; World Heart Federation Council on Epidemiology and Prevention; the European Society of Cardiology Working Group on Epidemiology and Prevention; Centers for Disease Control and Prevention; and the National Heart, Lung, and Blood Institute. *Circulation. 2003 Nov 18;108(20):2543-9.*

Mahrholdt H, Wagner A, Judd RM, Sechtem U, Kim RJ. Delayed enhancement cardiovascular magnetic resonance assessment of nonischaemic cardiomyopathies. *Eur Heart J 2005;26:1461–74.*

Maroko PR, Kjekshus JK, Sobel BE, Watanabe T, Covell JW, Ross J Jr, Braunwald E. Factors influencing infarct size following experimental coronary artery occlusions. *Circulation. 1971 Jan;43(1):67-82.*

Matetzky S, Barbash GI, Rabinowitz B, Rath S, Zahav YH, Agranat O, Kaplinsky E, Hod H. Q-wave and non Q-wave myocardial infarction after thrombolysis. *J Am Coll Card 1995:26:1445–1451.*

Matsuda Y, Toma Y, Ogawa H, Matsuzaki M, Katayama K, Fujii T, Yoshino F, Moritani K, Kumada T, Kusukawa R. Importance of left atrial function in patients with myocardial infarction. *Circulation. 1983 Mar;67(3):566-71.*

McCormick RJ, Musch TI, Bergman BC, Thomas DP. Regional differences in LV collagen accumulation and mature cross-linking after myocardial infarction in rats. *Am J Physiol. 1994 Jan;266(1 Pt 2):H354-9.*

Milliez P, Deangelis N, Rucker-Martin C, Leenhardt A, Vicaut E, Robidel E, Beaufils P, Delcayre C, Hatem SN. Spironolactone reduces fibrosis of dilated atria during heart failure in rats with myocardial infarction. *Eur Heart J. 2005 Oct;26(20):2193-9.*

Minino AM, Smith BL. Deaths: preliminary data for 2000. *Natl Vital Stat Rep. 2001 Oct 9;49(12):1-40.*

Mitchell JH, Shapiro W. Atrial function and the hemodynamic consequences of atrial fibrillation in man. *Am J Cardiol. 1969 Apr;23(4):556-67.*

Miura T, Yellon DM, Hearse DJ, Downey JM. Determinants of infarct size during permanent occlusion of a coronary artery in the closed chest dog. *J Am Coll Cardiol. 1987 Mar;9(3):647-54.*

Morishita N, Kusachi S, Yamasaki S, Kondo J, Tsuji T. Sequential changes in laminin and type IV collagen in the infarct zone--immunohistochemical study in rat myocardial infarction. *Jpn Circ J. 1996 Feb;60(2):108-14.*

Nikitin NP, Witte KK, Thackray SD, Goodge LJ, Clark AL, Cleland JG. Effect of age and sex on left atrial morphology and function. *Eur J Echocardiogr. 2003 Mar;4(1):36-42.*

Oishi Y, Ozono R, Yano Y, Teranishi Y, Akishita M, Horiuchi M, Oshima T, Kambe M. Cardioprotective role of AT2 receptor in postinfarction left ventricular remodeling. *Hypertension. 2003 Mar;41(3 Pt 2):814-8.*

Oishi Y, Ozono R, Yoshizumi M, Akishita M, Horiuchi M, Oshima T. AT2 receptor mediates the cardioprotective effects of AT1 receptor antagonist in post-myocardial infarction remodeling. *Life Sci. 2006 Dec 3;80(1):82-8.*

Okajima K, Abe Y, Fujimoto K, Fujikura K, Girard EE, Asai T, Kwon SH, Jin Z, Nakamura Y, Yoshiyama M, Homma S. Comparative study of high-resolution microimaging with 30-MHz scanner for evaluating cardiac function in mice. *J Am Soc Echocardiogr. 2007 Oct;20(10):1203-10.*

Olivetti G, Capasso JM, Sonnenblick EH, Anversa P. Side-to-side slippage of myocytes participates in ventricular wall remodeling acutely after myocardial infarction in rats. *Circ Res. 1990 Jul;67(1):23-34.*

Ozono R, Matsumoto T, Shingu T, Oshima T, Teranishi Y, Kambe M, Matsuura H, Kajiyama G, Wang ZQ, Moore AF, Carey RM. Expression and localization of angiotensin subtype receptor proteins in the hypertensive rat heart*. Am J Physiol Regul Integr Comp Physiol. 2000;278:R781–R789.*

Pagel PS, Kehl F, Gare M, Hettrick DA, Kersten JR, Warltier DC. Mechanical function of the left atrium: new insights based on analysis of pressure-volume relations and Doppler echocardiography. *Anesthesiology. 2003 Apr;98(4):975-94.*

Patten RD, Hall-Porter MR. Small animal models of heart failure: development of novel therapies, past and present. *Circ Heart Fail. 2009 Mar;2(2):138-44.*

Peterson DJ, Ju H, Hao J, Panagia M, Chapman DC, Dixon IM. Expression of Gi-2 alpha and Gs alpha in myofibroblasts localized to the infarct scar in heart failure due to myocardial infarction. *Cardiovasc Res. 1999 Mar;41(3):575-85.*

Pfeffer MA, Braunwald E, Moyé LA, Basta L, Brown EJ Jr, Cuddy TE, Davis BR, Geltman EM, Goldman S, Flaker GC, et al. Effect of captopril on mortality and morbidity in patients with left

ventricular dysfunction after myocardial infarction. Results of the survival and ventricular enlargement trial. The SAVE Investigators. *N Engl J Med. 1992 Sep 3;327(10):669-77.*

Pfeffer MA, Braunwald E. Ventricular remodeling after myocardial infarction. Experimental observations and clinical implications. *Circulation. 1990 Apr;81(4):1161-72.*

Pfeffer MA, McMurray JJ, Velazquez EJ, Rouleau JL, Køber L, Maggioni AP, Solomon SD, Swedberg K, Van de Werf F, White H, Leimberger JD, Henis M, Edwards S, Zelenkofske S, Sellers MA, Califf RM; Valsartan in Acute Myocardial Infarction Trial Investigators. Valsartan, captopril, or both in myocardial infarction complicated by heart failure, left ventricular dysfunction, or both. *N Engl J Med. 2003 Nov 13;349(20):1893-906.*

Porter KE, Turner NA. Cardiac fibroblasts: At the heart of myocardial remodeling. *Pharmacol Ther. 2009 Aug;123(2):255-78.*

Prioli A, Marino P, Lanzoni L, Zardini P. Increasing degrees of left ventricular filling impairment modulate left atrial function in humans. *Am J Cardiol. 1998 Sep 15;82(6):756-61.*

Pritchett AM, Jacobsen SJ, Mahoney DW, Rodeheffer RJ, Bailey KR, Redfield MM. Left atrial volume as an index of left atrial size: a population-based study*. J Am Coll Cardiol. 2003 Mar 19;41(6):1036-43.*

Protti A, Dong X, Sirker A, Botnar R, Shah AM. MRI-based prediction of adverse cardiac remodeling after murine myocardial infarction. *Am J Physiol Heart Circ Physiol. 2012 Aug 1;303(3):H309-14.*

Quinn MJ, Fitzgerald DJ. Ticlopidine and clopidogrel. *Circulation 1993;100:1667–1672.*

Redfield MM, Jacobsen SJ, Borlaug BA, Rodeheffer RJ, Kass DA. Age-and gender-related ventricular-vascular stiffening: a community-based study. *Circulation. 2005 Oct 11;112(15):2254-62.*

Rehwald WG, Fieno DS, Chen EL, Kim RJ, Judd RM. Myocardial magnetic resonance imaging contrast agent concentrations after reversible and irreversible ischemic injury. *Circulation. 2002 Jan 15;105(2):224-9.*

Remme EW, Young AA, Augenstein KF, Cowan B, Hunter PJ. Extraction and quantification of left ventricular deformation modes. *IEEE Trans Biomed Eng. 2004 Nov;51(11):1923-31.*

Richeson JF, Akiyama T, Schenk E. A solid angle analysis of the epicardial ischemic TQ-ST deflection in the pig. A theoretical and experimental study. *Circ Res. 1978 Dec;43(6):879-88.*

Roger VL, Go AS, Lloyd-Jones DM, Benjamin EJ, Berry JD, Borden WB, Bravata DM, Dai S, Ford ES, Fox CS, Fullerton HJ, Gillespie C, Hailpern SM, Heit JA, Howard VJ, Kissela BM, Kittner SJ, Lackland DT, Lichtman JH, Lisabeth LD, Makuc DM, Marcus GM, Marelli A, Matchar DB, Moy CS, Mozaffarian D, Mussolino ME, Nichol G, Paynter NP, Soliman EZ, Sorlie PD, Sotoodehnia N, Turan TN, Virani SS, Wong ND, Woo D, Turner MB; American Heart Association Statistics Committee and Stroke Statistics Subcommittee. AHA Statistical Update, Executive summary: heart disease and stroke statistics - 2012 update: a report from the American Heart Association. *Circulation. 2012 Jan 3;125(1):188-97.*

Ross AJ, Yang Z, Berr SS, Gilson WD, Petersen WC, Oshinski JN, French BA. Serial MRI evaluation of cardiac structure and function in mice after reperfused myocardial infarction. *Magn Reson Med. 2002 Jun;47(6):1158-68.*

Ruff J, Wiesmann F, Hiller KH, Voll S, von Kienlin M, Bauer WR, Rommel E, Neubauer S, Haase A. Magnetic resonance microimaging for noninvasive quantification of myocardial function and mass in the mouse. *Magn Reson Med. 1998 Jul;40(1):43-8.*

Sabatine MS. Clopidogrel in ST-elevation myocardial infarction. *European Heart Journal Supplements (2006) 8 (Supplement G), G31–G34.*

Sadoshima J, Izumo S. Molecular characterization of angiotensin II induced hypertrophy of cardiac myocytes and hyperplasia of cardiac fibroblasts: critical role of the AT1 receptor subtype. *Circ Res. 1993 Sep;73(3):413-23.*

Schaefer S, Malloy CR, Katz J, Parkey RW, Buja LM, Willerson JT, Peshock RM. Gadolinium-DTPA-enhanced nuclear magnetic resonance imaging of reperfused myocardium: identification of the myocardial bed at risk. *J Am Coll Cardiol. 1988 Oct;12(4):1064-72.*

Scherrer-Crosbie M, Thibault HB. Echocardiography in translational research: Of mice and men. *J. Am. Soc. Echocardiogr. 2008;21:1083-1092.*

Schiller NB, Shah PM, Crawford M, DeMaria A, Devereux R, Feigenbaum H, Gutgesell H, Reichek N, Sahn D, Schnittger I, et al. Recommendations for quantitation of the left ventricle by two-dimensional echocardiography. *J Am Soc Echocardiogr. 1989 Sep-Oct;2(5):358-67.*

Schmieder R, Hilgers K, Schlaich M, Schmidt B. Renin–angiotensin system and cardiovascular risk. *Lancet 2007; 369:1208–1219.*

Second Chinese Cardiac Study Collaborative Group. Clopidogrel and Metoprolol in Myocardial Infarction Trial. Presented at the ACC annual conference on March 9, 2005, Orlando, Fla. *Information available at http://www.commit-ccs2.org (accessed March 2, 2009).*

Shellock FG, Crues JV. MR procedures: biologic effects, safety, and patient care. *Radiology. 2004 Sep;232(3):635-52.*

Shiota T, Jones M, Chikada M, Fleishman CE, Castellucci JB, Cotter B, DeMaria AN, von Ramm OT, Kisslo J, Ryan T, et al. Real-time three-dimensional echocardiography for determining right ventricular stroke volume in an animal model of chronic right ventricular volume overload. *Circulation. 1998 May 19;97(19):1897-900.*

Shirani J, Alaeddini J. Structural remodeling of the left atrial appendage in patients with chronic non-valvular atrial fibrillation: Implications for thrombus formation, systemic embolism, and assessment by transesophageal echocardiography. *Cardiovasc Pathol 2000;9:95–101.*

Shuttleworth CA. Type VIII collagen. *Int J Biochem Cell Biol. 1997 Oct;29(10):1145-8.*

Sick PB, Schuler G, Hauptmann KE, Grube E, Yakubov S, Turi ZG, Mishkel G, Almany S, Holmes DR. Initial worldwide experience with the WATCHMAN left atrial appendage system for stroke prevention in atrial fibrillation. *J Am Coll Cardiol. 2007 Apr 3;49(13):1490-5.*

Siri FM, Jelicks LA, Leinwand LA, Gardin JM. Gated magnetic resonance imaging of normal and hypertrophied murine hearts. *Am J Physiol. 1997 May;272(5 Pt 2):H2394-402.*

Slawson SE, Roman BB, Williams DS, Koretsky AP. Cardiac MRI of the normal and hypertrophied mouse heart. *Magn Reson Med. 1998 Jun;39(6):980-7.*

Spencer KT, Mor-Avi V, Gorcsan J 3rd, DeMaria AN, Kimball TR, Monaghan MJ, Perez JE, Weinert L, Bednarz J, Edelman K, Kwan OL, Glascock B, Hancock J, Baumann C, Lang RM. Effects of aging on left atrial reservoir, conduit, and booster pump function: a multi-institution acoustic quantification study. *Heart. 2001 Mar;85(3):272-7.*

Spigel J, Key C. Thrombosis and infarction of the left atrial appendage in an infant: A case report. *Am J Cardiovasc Pathol 1988;2:87–90.*

Spinale FG. Myocardial matrix remodeling and the matrix metalloproteinases: influence on cardiac form and function. *Physiol Rev. 2007 Oct;87(4):1285-342.*

St John Sutton, Lee D, Rouleau JL, Goldman S, Plappert T, Braunwald E, Pfeffer MA. Left ventricular remodeling and ventricular arrhythmias after myocardial infarction. *Circulation 2003;107:2577-82.*

Stanton LW, Garrard LJ, Damm D, Garrick BL, Lam A, Kapoun AM, Zheng Q, Protter AA, Schreiner GF, White RT. Altered patterns of gene expression in response to myocardial infarction. *Circ Res. 2000 May 12;86(9):939-45.*

Stefanadis C, Dernellis J, Lambrou S, Toutouzas P. Left atrial energy in normal subjects, in patients with symptomatic mitral stenosis, and in patients with advanced heart failure. *Am J Cardiol. 1998 Nov 15;82(10):1220-3.*

Steinhubl SR, Berger PB, Mann JT 3rd, Fry ET, DeLago A, Wilmer C, Topol EJ; CREDO Investigators. Clopidogrel for the Reduction of Events During Observation. Early and sustained dual oral antiplatelet therapy following percutaneous coronary intervention: a randomized controlled trial. *JAMA 2002;288:2411–2420.*

Storey JD, Tibshirani R. Statistical significance for genomewide studies. *Proc Natl Acad Sci U S A. 2003 Aug 5;100(16):9440-5.*

Studer R, Reinecke H, Müller B, Holtz J, Just H, Drexler H. Increased angiotensin-I converting enzyme gene expression in the failing human heart. Quantification by competitive RNA polymerase chain reaction. *J Clin Invest. 1994 Jul;94(1):301-10.*

Suga H. Importance of atrial compliance in cardiac performance. *Circ Res. 1974 Jul;35(1):39-43.*

Suh IW, Song JM, Lee EY, Kang SH, Kim MJ, Kim JJ, Kang DH, Song JK. Left Atrial Volume Measured by Real-Time 3-Dimensional Echocardiography Predicts Clinical Outcomes in Patients with Severe Left Ventricular Dysfunction and in Sinus Rhythm. *J Am Soc Echocardiogr 2008;21:439-45.*

Sutton MG, Sharpe N. Left ventricular remodeling after myocardial infarction: pathophysiology and therapy. *Circulation. 2000 Jun 27;101(25):2981-8.*

Tarnavski O, McMullen JR, Schinke M, Nie Q, Kong S, Izumo S. Mouse cardiac surgery: comprehensive techniques for the generation of mouse models of human diseases and their application for genomic studies. *Physiol Genomics. 2004 Feb 13;16(3):349-60.*

Taylor AA, Siragy H, Nesbitt S. Angiotensin Receptor Blockers: Pharmacology, Efficacy, and Safety. *J Clin Hypertens (Greenwich). 2011;13:677– 686. 2011 Wiley Periodicals, Inc.*

Tennant R, Wiggers CJ. 1935. The effect of coronary occlusion on myocardial contraction. *Am. J. Physiol. 112:351–36.*

The Joint European Society of Cardiology/American College of Cardiology Committee. Myocardial infarction redefined - A consensus document of the Joint European Society of Cardiology/American College of Cardiology Committee for the Redefinition of Myocardial Infarction. *Eur Heart J 2000;21:1502–1513; J Am Coll Cardiol 2000;36:959–969.*

Thomas L, Levett K, Boyd A, Leung DY, Schiller NB, Ross DL. Compensatory changes in atrial volumes with normal aging: is atrial enlargement inevitable? *J Am Coll Cardiol. 2002 Nov 6;40(9):1630-5.*

Thygesen K, Alpert JS, White HD; Joint ESC/ACCF/AHA/WHF Task Force for the Redefinition of Myocardial Infarction. Universal definition of myocardial infarction. *Eur Heart J. 2007, 28: 2525-2538.*

Timmermans PB, Wong PC, Chiu AT, Herblin WF, Benfield P, Carini DJ, Lee RJ, Wexler RR, Saye JA, Smith RD. Angiotensin II receptors and angiotensin II receptor antagonists. Pharmacol Rev 1993;45: 205-51.

Toischer K, Rokita AG, Unsold B, Zhu W, Kararigas G, Sossalla S, Reuter SP, Becker A, Teucher N, Seidler T, Grebe C, Preuss L, Gupta SN, Schmidt K, Lehnart SE, Krüger M, Linke WA, Backs J, Regitz-Zagrosek V, Schäfer K, Field LJ, Maier LS, Hasenfuss G. Differential cardiac remodeling in preload versus afterload. *Circulation. 2010;122:993-1003.*

Triposkiadis F, Tentolouris K, Androulakis A, Trikas A, Toutouzas K, Kyriakidis M, Gialafos J, Toutouzas P. Left atrial mechanical function in the healthy elderly: new insights from a combined assessment of changes in atrial volume and transmitral flow velocity. *J Am Soc Echocardiogr. 1995 Nov-Dec;8(6):801-9.*

Tsang TS, Abhayaratna WP, Barnes ME, Miyasaka Y, Gersh BJ, Bailey KR, Cha SS, Seward JB. Prediction of cardiovascular outcomes with left atrial size: is volume superior to area or diameter? *J Am Coll Cardiol. 2006 Mar 7;47(5):1018-23.*

Tsang TS, Barnes ME, Gersh BJ, Bailey KR, Seward JB. Left atrial volume as a morphophysiologic expression of left ventricular diastolic dysfunction and relation to cardiovascular risk burden. *Am J Cardiol. 2002 Dec 15;90(12):1284-9.*

Tsuchida S, Matsusaka T, Chen X, Okubo S, Niimura F, Nishimura H, Fogo A, Utsunomiya H, Inagami T, Ichikawa I. Murine double nullizygotes of the angiotensin type 1A and 1B receptor genes duplicate severe abnormal phenotypes of angiotensinogen nullizygotes. *J Clin Invest. 1998 Feb 15;101(4):755-60.*

Tsuda T, Wu J, Gao E, Joyce J, Markova D, Dong H, Liu Y, Zhang H, Zou Y, Gao F, Miller T, Koch W, Ma X, Chu ML. Loss of fibulin-2 protects against progressive ventricular dysfunction after myocardial infarction. *J Mol Cell Cardiol. 2012 Jan;52(1):273-82.*

Tsukube T, Ataka K, Taniguchi T, Yokoyama M, Hanioka K. Papillary fibroelastoma of the left atrial appendage: Echocardiographic findings. Ann Thorac Surg 2000;70:1416–1417.

Tsutsumi Y, Matsubara H, Ohkubo N, Mori Y, Nozawa Y, Murasawa S, Kijima K, Maruyama K, Masaki H, Moriguchi Y, Shibasaki Y, Kamihata H, Inada M, Iwasaka T. Angiotensin II type 2

receptor is upregulated in human heart with interstitial fibrosis, and cardiac fibroblasts are the major cell type for its expression. *Circ Res. 1998 Nov 16;83(10):1035-46.*

Tyberg JV, Forrester JS, Wyatt HL, Goldner SJ, Parmley WW, Swan HJ. An analysis of segmental ischemic dysfunction using the pressure-length loop. *Circulation. 1974 Apr;49(4):748-54.*

Ulrich MM, Janssen AM, Daemen MJ, Rappaport L, Samuel JL, Contard F, Smits JF, Cleutjens JP. Increased expression of fibronectin isoforms after myocardial infarction in rats. *J Mol Cell Cardiol. 1997 Sep;29(9):2533-43.*

Unger T. The role of the renin–angiotensin system in the development of cardiovascular disease. *Am J Cardiol 2002; 89:3–10.*

Urheim S, Edvardsen T, Torp H, Angelsen B, Smiseth OA. Myocardial strain by Doppler echocardiography. Validation of a new method to quantify regional myocardial function. *Circulation. 2000 Sep 5;102(10):1158-64.*

van Nieuwenhoven FA, Turner NA. The role of cardiac fibroblasts in the transition from inflammation to fibrosis following myocardial infarction. *Vascul Pharmacol. 2012 Aug 3.*

Vasan RS, Larson MG, Levy D, Evans JC, Benjamin EJ. Distribution and categorization of echocardiographic measurements in relation to reference limits: the Framingham Heart Study: formulation of a height- and sex-specific classification and its prospective validation. *Circulation. 1997 Sep 16;96(6):1863-73.*

Vaturi M, Sagie A, Shapira Y, Feldman A, Fink N, Strasberg B, Adler Y. Impact of atrial fibrillation on clinical status, atrial size and hemodynamics in patients after mitral valve replacement. *J Heart Valve Dis. 2001 Nov;10(6):763-6.*

Veinot JP, Harrity PJ, Gentile F, Khandheria BK, Bailey KR, Eickholt JT, Seward JB, Tajik AJ, Edwards WD. Anatomy of the normal left atrial appendage: a quantitative study of age-related changes in 500 autopsy hearts: implications for echocardiographic examination. *Circulation. 1997 Nov 4;96(9):3112-5.*

Villarreal FJ, Lew WYW, Waldman LK, Covell JW. Transmural myocardial deformation in the ischemic canine left ventricle. *Circ Res. 1991 Feb;68(2):368-81.*

Volders PG, Willems IE, Cleutjens JP, Arends JW, Havenith MG, Daemen MJ. Interstitial collagen is increased in the noninfarcted human myocardium after myocardial infarction. *J Mol Cell Cardiol 25: 1317–1323, 1993.*

Wang Y, Rossman PJ, Grimm RC, Riederer SJ, Ehman RL. Navigator-echo-based real-time respiratory gating and triggering for reduction of respiration effects in three-dimensional coronary MR angiography. *Radiology. 1996 Jan;198(1):55-60.*

Weisman HF, Bush DE, Mannisi JA, Weisfeldt ML, Healy B. Cellular mechanisms of myocardial infarct expansion. *Circulation. 1988 Jul;78(1):186-201.*

Wessels A, Sedmera D. Developmental anatomy of the heart: a tale of mice and man. *Physiol Genomics 15: 165-176, 2003.*

White HD, Aylward PE, Huang Z, Dalby AJ, Weaver WD, Barvik S, Marin-Neto JA, Murin J, Nordlander RO, van Gilst WH, Zannad F, McMurray JJ, Califf RM, Pfeffer MA; VALIANT Investigators. Mortality and morbidity remain high despite captopril and/or Valsartan therapy in

elderly patients with left ventricular systolic dysfunction, heart failure, or both after acute myocardial infarction: results from the Valsartan in Acute Myocardial Infarction Trial (VALIANT). *Circulation. 2005 Nov 29;112(22):3391-9.*

Wiesmann F, Frydrychowicz A, Rautenberg J, Illinger R, Rommel E, Haase A, Neubauer S. Analysis of right ventricular function in healthy mice and a murine model of heart failure by in vivo MRI. *Am J Physiol Heart Circ Physiol. 2002 Sep;283(3):H1065-71.*

Wiesmann F, Ruff J, Haase A. High-resolution MR imaging in mice. *MAGMA. 1998 Sep;6(2-3):186-8.*

Wilding JR, Schneider JE, Sang AE, Davies KE, Neubauer S, Clarke K. Dystrophin- and MLP-deficient mouse hearts: marked differences in morphology and function, but similar accumulation of cytoskeletal proteins. *FASEB J. 2005 Jan;19(1):79-81.*

Wright GW, Simon RM. A random variance model for detection of differential gene expression in small microarray experiments. *Bioinformatics. 2003 Dec 12;19(18):2448-55.*

Yan RT, Bluemke D, Gomes A, Burke G, Shea S, Liu K, Bahrami H, Sinha S, Wu C, Fernandes V, McClelland R, Lima JA. Regional Left Ventricular Myocardial Dysfunction as a Predictor of Incident Cardiovascular Events. *J Am Coll Cardiol. 2011 Apr 26;57(17):1735-44.*

Yang Z, Berr SS, Gilson WD, Toufektsian MC, French BA. Simultaneous evaluation of infarct size and cardiac function in intact mice by contrast-enhanced cardiac magnetic resonance imaging reveals contractile dysfunction in noninfarcted regions early after myocardial infarction. *Circulation. 2004 Mar 9;109(9):1161-7.*

Yusuf S, Peto R, Lewis J, Collins R, Sleight P. Beta blockade during and after myocardial infarction: an overview of the randomized trials. *Prog Cardiovasc Dis. 1985;27:335–71.*

Yusuf S, Wittes J, Friedman L. Overview of results of randomized clinical trials in heart disease. I. Treatments following myocardial infarction. *JAMA. 1988;260:2088–93.*

Yusuf S, Zhao F, Mehta SR, Chrolavicius S, Tognoni G, Fox KK; Clopidogrel in Unstable Angina to Prevent Recurrent Events Trial Investigators. The Clopidogrel in Unstable Angina to Prevent Recurrent Ischemic Events Trial Investigators. Effects of clopidogrel in addition to aspirin in patients with acute coronary syndromes without ST-segment elevation. *N Engl J Med 2001;345:494–502.*

Zhao Q, Ishibashi M, Hiasa K, Tan C, Takeshita A, Egashira K. Essential role of vascular endothelial growth factor in angiotensin II-induced vascular inflammation and remodeling. *Hypertension. 2004 Sep;44(3):264-70.*

Zhou R, Pickup S, Glickson JD, Scott CH, Ferrari VA. Assessment of global and regional myocardial function in the mouse using cine and tagged MRI. *Magn Reson Med. 2003 Apr;49(4):760-4.*

Zhou YQ, Foster FS, Nieman BJ, Davidson L, Chen XJ, Henkelman RM. Comprehensive transthoracic cardiac imaging in mice using ultrasound biomicroscopy with anatomical confirmation by magnetic resonance imaging. *Physiol Genomics 18: 232-244,2004.*

Zhou YQ, Foster FS, Parkes R, Adamson SL. Developmental changes in left and right ventricular diastolic filling patterns in mice. *Am J Physiol Heart Circ Physiol. 2003;285:H1563-1575.*

Zimmerman SD, Criscione J, Covell JW. Remodeling in myocardium adjacent to an infarction in the pig left ventricle. *Am J Physiol Heart Circ Physiol. 2004 Dec;287(6):H2697-704.*